UNIVERSITY OF GENOVA

PHD PROGRAM IN BIOENGINEERING AND ROBOTICS

Development of new Nanoplatforms for the treatment and prevention of Atherosclerosis

by

Valentina Di Francesco

Thesis submitted for the degree of Doctor of Philosophy (33° cycle)

March 2021

Paolo Decuzzi — Supervisor

Giorgio Cannata — Head of the PhD program

Thesis Jury:

Luca Casettari, University of Urbino — External examiner

Francesco Pasqualini, University of Pavia — External examiner

Department of Informatics, Bioengineering, Robotics and Systems Engineering

I would like to dedicate this thesis to my family…

Declaration

I hereby declare that except where specific reference is made to the work of others, the contents of this dissertation are original and have not been submitted in whole or in part for consideration for any other degree or qualification in this, or any other university. This dissertation is my own work and contains nothing which is the outcome of work done in collaboration with others, except as specified in the text and Acknowledgements. This dissertation contains fewer than 65,000 words including appendices, bibliography, footnotes, tables and equations and has fewer than 150 figures.

Valentina Di Francesco
March 2021

Acknowledgments:

I would like to thank my supervisor Prof. Paolo Decuzzi for the opportunity to develop this project. Without his knowledge and his advice, it would have not been possible to conclude this work. Also, I want to thank Prof Pasquale Maffia and his collaborator Danila Gurgone for the development of the animal studies done at the University of Glasgow. In addition, I would like to thank all the animal facility staff, the Electron Microscopy Facility, and Nikon Imaging Centre of the Italian Institute of Technology for the teaching and technical support. Special thanks to all my lab mates who, through daily scientific discussions, have contributed to my professional growth as an independent scientist. In particular, I would like to thank Dr. Sayanti Brahmachari, Roberto Palomba, Miguel Ferreira, Martina Di Francesco, and Maria Grazia Barbato.

Preface

Atherosclerosis is a pathology associated with the induction of inflammatory reactions in the vascular wall. Given the multifactorious of inflammation in atherosclerotic processes, in the last years, generic drugs, like Methotrexate (MTX) and Colchicine (COL) that have broad anti-inflammatory properties for atheroprotection, were taken in consideration. Nowadays, Nanomedicine offers many advantages in boosting the therapeutic efficacy and mitigating adverse effects compared to administering free drugs. New studies are showing the potential application of nanomedicine in controlling the progression and inducing the regression of atherosclerosis through the use of “old” chemotherapeutic drugs. In this thesis, different approaches were developed for the delivery of Methotrexate (MTX). Liposomes (LIP) and spherical polymeric nanoparticles (SPNs) were synthesized and characterized to reduce atherosclerosis inflammation. In the last part of the work, the anti-inflammatory activity was enhanced by introducing in the liposomes, together with MTX, another chemotherapeutic, Colchicine (COL).

In Chapter 1 (Introduction), the pathophysiology of atherogenesis, therapies, and the rationale of using the two drugs (MTX and COL) are introduced and explained. It is shown that, even if the clinical trial related to the MTX (CIRT) failed, several studies demonstrated the efficacy of the drug on the atherosclerosis model. Also, the clinical trials of COL are presented. Finally, it is raised an ongoing clinical trial of the use of COL and MTX to reduce the inflammation and some study that proves the excellent results on delivering the drugs through nanoparticles.

In Chapter 2 (Synthesis of Two Methotrexate Prodrugs for Optimizing Drug Loading into Liposomes), two different synthetic modifications of the methotrexate were presented (PEG-MTX and DSPE-MTX). Both prodrugs, together or alone, were loaded into liposomes. The work presents the *in vitro* chemical, physical, and biological characterizations of the three formulations.

In Chapter 3 (Modulating Lipoprotein Transcellular Transport and Atherosclerotic Plaque Formation in ApoE–/– Mice via Nanoformulated Lipid–Methotrexate Conjugates), the DSPE-MTX was loaded in two different nanoparticles: LIP and SPNs. Both nanoparticles were analyzed and tested *in vitro* for their morphological shape, stability, and release. After, they were tested on a foam cell model.

The mechanism of action of MTX was studied, confirming the anti-inflammatory effect. The MTX-LIP was selected for the *in vivo* study.

In Chapter 4 (Lipid nanoparticles encapsulating Methotrexate and Colchicine to enhance the anti-inflammatory therapy), liposomes with MTX were enriched with Col to increase the anti-inflammatory effect of the nanoparticles. Particles were synthesized by Nanossemblr, and all the chemical and physical characterization were done. Anti-inflammatory effects were evaluated on two different *in vitro* models.

In Chapter 5 (Conclusion), a summary of all the work was done, pointing out the future experiments that can be carried away to prove, *in vivo*, the capability of these particles to reduce inflammation and decrease plaque formation.

Table of Contents

List of Figures

List of Tables

Abstract

Over the last decade, many studies suggest that inflammation has an important role in atherosclerosis progression and development. In the last years, old cheaper drugs, Methotrexate (MTX) and Colchicine (COL) were considered to treat this pathology due to their anti-inflammatory effects. MTX, a conventional chemotherapeutic medicine currently representing the first-line option in inflammatory diseases like rheumatoid arthritis (RA) and psoriatic arthritis, was proposed in the clinical trial Cardiovascular Inflammation Reduction Trial (CIRT). Even though many studies have demonstrated this drug's beneficial activity on animals/patients with atherosclerosis, the clinical trial failed. Col is known for its therapeutic use in gout and Familial Mediterranean Fever (FMF). In these patients, it was noticed a reduction of myocardial infarctions after the use of Colchicine. Its effect is associated with a stronger effect in the inhibition of inflammasome activation and IL-1β secretion. These observations are at the base of different clinical trials like Low-Dose Colchicine (LoDoCo), A second Low Dose Colchicine (LoDoCo2), Low Dose Colchicine after Myocardial Infarction (LoDoCo-MI).

In general, their clinical use is limited by their several side effects and, furthermore, in MTX's case is even more difficult due to its poor bioavailability and solubility in biological fluids. Taking this into account, nanomedicine might become a valid ally in furnishing potent tools to ease combined treatment and increase drug accumulation at the target site. Thus, this work aims to propone nanoparticles, polymeric, and lipid to improve the stability and solubility of encapsulated cargos, promote transport across membranes, and prolong circulation times to increase safety and efficacy. Here, it was proposed two different strategies for modifying the methotrexate by conjugating the DSPE and PEG. The prodrugs obtained (DSPE-MTX and PEG-MTX) were used to synthesize liposomes, including one or both of them. Physiochemical features were tested. The DSPE-MTX was selected (due to the instability at pH 6.8 of the system) and delivered by liposomes (MTX-LIP) and spherical polymeric nanoparticles (MTX-SPNs). Both nanoparticle formulations presented similar features. For the lipidic nanoparticles, the size is 174±2 nm (PdI: 0.15 ± 0.0007), and Zeta Pot -48 ± 0.02 mV; for the polymeric nanocarriers, the size is 208±2 nm (PdI: 0.15 ± 0.02), and Zeta Pot 45.8 ± 0.02 mV. MTX encapsulation efficiency (EE%) 70±5% for Lip-MTX and 1.5±0.2%

for SPNs-MTX. Foam cells were obtained by treating rat bone marrow-derived monocytes (BMDM) with oxLDL. The treatment with the two nanoformulations was able to reverse foam cells maturation into macrophages. Both MTX-LIP and MTX-SPNs decreased cholesterol amounts after 24 hours in BMDM. The efficacy of the treatment was also proved by gene expression analysis. RT-PCR showed that the CD36 and SRA-1 gene expression (regulating oxLDL influx) was minimal. The reverse cholesterol transporter (ABCA1) in foam cells treated with the nanoformulations was inducing a 2-fold compare the CTRL. MTX-LIP and MTX-SPNs also reduced inflammatory gene expression (IL-6, IL-1β, and TNFα). MTX-LIP was used in vivo in a murine model of atherosclerosis. ApoE-/- mice, fed with a high-fat diet for 28 days, were treated for 4 weeks (once every three days) with MTX-LIP. Plaque burden was measured, revealing a reduction in plaque area for the treated mice. These results influenced a new line of thinking; it could be possible to boost the liposomes' anti-inflammatory effect combining in the same particles the MTX and the Colchicine (Col). Particles have a size around 100 nm with stability upon 4 days. The liposomes' encapsulation efficiency was ~ 28 % for MTX and ~ 33 % for COL with a ratio of 1:16. The anti-inflammatory effect was tested on the primary cell line (BMDM). Specifically, liposomes with MTX and Col were able to reduce the inflammation caused by the LPS. At the same time, they were able to modulate the foam cell marker (ABCA1), reflecting a reduction of the expression of IL-1β by 3-fold, IL-6 by 2-fold, and moderately of TNF-α. These results would suggest that combining the chemotherapeutic drugs in the liposomes could strongly reduce the inflammation modulating the disease progression. These data suggest that MTX and COL loaded nanoparticles could be the new strategy for the treatment of atherosclerosis.

Chapter 1

Introduction

1.1. The pathophysiology of atherogenesis

Atherosclerosis is a complex inflammatory condition developed in the intima of an arterial vessel, and it is the primary cause of cardiovascular disease (CVD) [1]. Vascular inflammation and the accumulation of lipid-laden macrophages and their products induce the maturation of the atheroma or plaque, which can rupture and lead to ischemic stroke and myocardial infarction. Atherosclerotic cardiovascular disease (ACD) is divided into two major events: cerebrovascular disease (mainly ischemic stroke) and ischemic heart disease (IHD). The stroke and ischemia are the first and the third causes of death in the world [1]. In 2015 the Global Burden of Diseases, Injuries, and Risk Factor Study reported that 422.7 million people were affected by cardiovascular diseases and were responsible for 31% of all the word deaths (17.9 million of individuals) [2, 3]. Presently, the World Health Organization estimated that by 2030, almost 23.6 million people will die from cardiovascular disease [4].

Atherosclerosis is an inflammatory disorder characterized by a gradual accumulation of lipoproteins and fibrous elements beneath the vascular wall [5]. The early stage of atherosclerosis is characterized by the sub-endothelium accumulation of cholesterol-engorged macrophages, also known as “foam cell”. The accumulated foam cells and T lymphocytes are the initial constituents of the vascular wall lesions and are denominated as “fatty streaks”. In the second step, smooth-muscle cells (SMCs) become an integral part of the lesion area. The formation of this fatty streak occurs mainly during the first decade of life of an individual. During the second decade, these formations spread to the coronary arteries, while in the third and fourth decades, the lesions are primarily located in the cerebral arteries [5].

Fatty streaks formed during the initial lesion are clinically irrelevant and, in some situations, can even regress [5]. With the passage of time, they become the precursor of more advanced lesions characterized by the accumulation of lipid-rich necrotic debris and smooth muscle cells (**Figure 1.1.**) [6]. It is well known the atherosclerosis is multifocal disease that attacks reproducible regions of the arterial tree. The vascular lesions tend to develop at sites characterized by blood flow disturbance and at regions of the wall experiencing lower shear stress [7, 8]. Specifically, regions located near the branch points and along inner curvatures, are most susceptible. Generally, the most area affected are the abdominal aorta, coronary arteries, iliofemoral arteries, and carotid bifurcations.

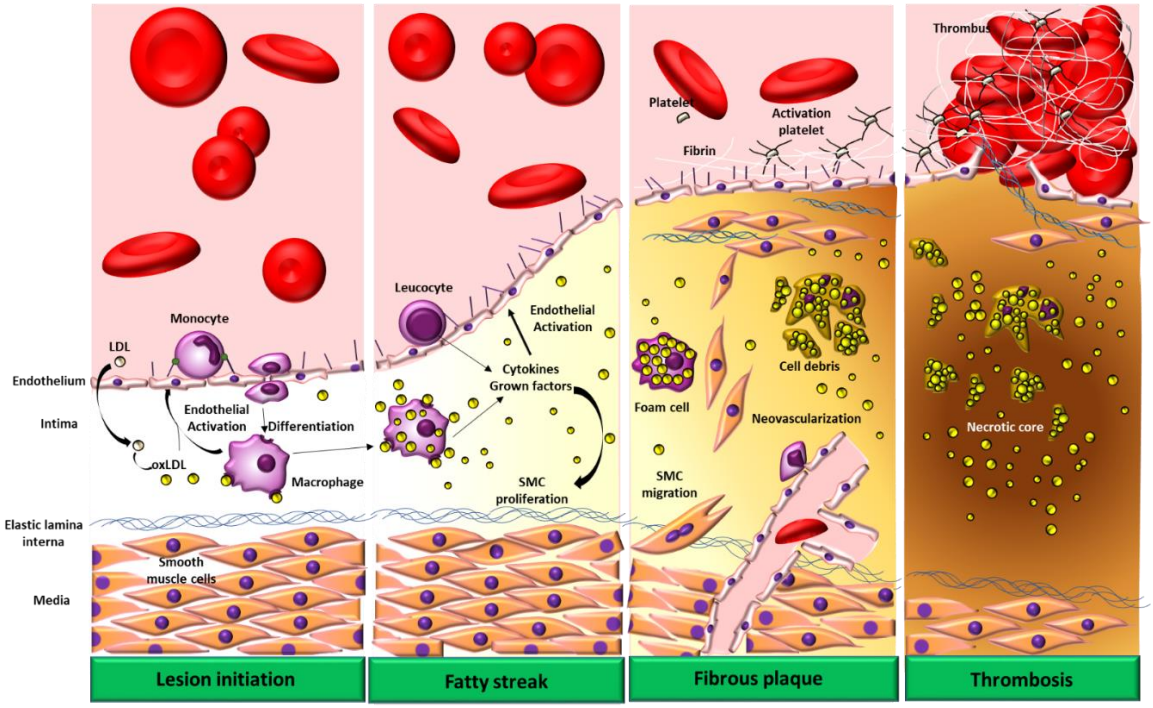

Figure 1.1. Pathogenesis of atherosclerosis. In the first step, low density lipoprotein-cholesterol (LDL) are oxidized in endothelium. OxLDL stimulate endothelium to express adhesion molecules, such as vascular cell adhesion molecule-1 (VCAM-1), P-Selectin and various chemokines. Macrophage engulf oxLDL through scavenger receptors and simultaneously, leucocytes are activated and recruited. This leads to increase the plaque volume, to promote the neovascularization and to stabilize the fibrous plaque by the proliferation of smooth muscle cells (SMCs). Foam cells can go in apoptosis releasing the debris and lipids, resulting in

necrotic core formation. The proteases secreted from foam cells can destabilize the plaque and possibly cause thrombotic events. Adapted from Gargiulo *et al* [9].

Complications might arise when the vessel lumen is obstructed, and the blood flow does not guarantee sufficient oxygen and nutrient supply to the surrounding tissue. Mainly these complications include myocardial infarction, stroke, and peripheral vascular disease; pathologies are well known for being listed among the leading causes of mortality in modern society [10].

The pathology's initial step and the inflammation involve dysfunction of the endothelium, allowing the infiltration and entrapment of Low-Density Lipoprotein (LDL) [5]. The accumulation of LDL is due to the increase in the permeability or to the disruption of the endothelium, leading to an increase in the accumulation into the intima, resulting in an increased thickness. Another factor that causes the intima's thickening is the friction of blood flow in certain points of the inner vessel surface (hemodynamic stress) [9]. In fact, spots with low or oscillatory endothelial shear stress, located near branch points and along inner curvatures, are the most susceptible to these kinds of thickening. LDL, linked by ionic bonds between their Apo-Lipoprotein B and proteoglycans in the extracellular matrix, is modified by enzymes and reactive oxygen species, turning into oxidized LDL (oxLDL) [11]. Simultaneously, conditions that stimulate the endothelium, like dyslipidemia, localized oxidation, inflammatory factors, and hypertension, promote monocyte recruitment into the vessel walls. Upon that, adhesion molecules, such as E-Selectin, P-Selectin, VCAM-1, and ICAM-1 are secreted which enable the monocytes adhesion to the endothelium [12]. Monocytes activated by growth factors, cytokines, and modified lipid species, such as oxLDL differentiate into macrophages. The accumulation of oxLDL through scavenger receptors (CD36, SRA, SRB) into the macrophages leads to the formation of foam cells. [13] This event, consequently, promotes the cytokines (TNF, interleukins, and interferon), enzymes (cysteine proteinase, serine proteinase, metalloproteinases) and growth factors (PDGF, VEGF, IGF) expression. The complex signaling cascade originated by these mediators might induce T cells activation [5]. All these events

increase the inflammatory process, the proliferation, and the migration of smooth muscle and endothelial cells within the intima.

Atherosclerosis progression ultimately leads to foam cell death and increase plaque volume. The secretion of chemokines and cytokines attracts more monocytes, turning into foam cells, further fueling the inflammation and plaque volume. Eventually, plaque destabilization and rupture induced by the foam cells' proteolytic activity might lead to athero-thrombosis and ischemic events such as myocardial infarction or stroke [10].

1.2. Therapy

Atherosclerosis is a metabolic disorder characterized by chronic inflammation and hyperlipidemia. Starting from this concept, the therapeutical approaches used for the treatment of the pathology are based on reducing of cholesterolemia, to mitigate the incidence of plaque formation, or on decreasing inflammation. The classical drugs used are:

- **Statins**: also known as hydroxy-methyl-glutaryl coenzyme A (HMG-CoA) reductase inhibitors, blocking the synthesis of endogenous cholesterol;
- **Fibrates:** activating peroxisome proliferator-activated receptors (PPAR), especially PPARα. These receptors are involved in the lipid metabolism;
- **Niacin:** a nicotinic acid, vitamin B used, alone or combined with statins, reducing the plasma VLDL, LDL, and apoB levels *in vivo*. Recent studies also demonstrated that it also increases the ABCA1 levels (a receptor involved in cholesterol efflux)[14].
- **Endoglin modulator**: also known as CD105 or TGF-β type III receptor, has a regulating the role of transforming growth factor-β (TGF-β) signaling. The action of this modulator reduces the inflammatory response [15].
- **Bile Acid Sequestrates** (BAS): polymers preventing the reabsorption of bile salts into the enterohepatic circulation pathway after binding them in the small intestine. The depletion of bile acids leads to increased cholesterol metabolism for bile salt synthesis (thereby decreasing the LDL plasma concentration) [16].

During the past years, the cardiology community has focused on treating the responsible plaque or the “culprit plaque” for coronary occlusion and death upon detecting the disease. The concept of “vulnerable plaque” recently led cardiologists into more in-depth research into the disease morphology and biochemical characteristics. This analysis increased the probability to identify plaques that could become dangerous in a short time and earlier intervention [17]. For a better understanding, imaging techniques including X-ray angiography, virtual histology intravascular ultrasound (VH-IVUS), computed tomographic (CT), single-photon emission computed tomography (SPECT), optical coherence tomography (OCT), positron emission tomography (PET), and magnetic resonance (MR) are currently being used to understand the morphological and functional aspects of the plaques [18]. However, the prevention of possible factors that cause vulnerable plaque remains a challenge. The main reason is that multiple vulnerable plaques were already developed in patients affected by ischemic heart disease, [19] and the inflammatory process is extended in the arterial tree and the myocardium [20]. The atheromatous process appears to be supported by the inflammatory one that is not localized in the culprit plaque, but it is widespread in the patients' vascular vessels.

In fact, in the last 30 years, it has been proved that inflammation is a cause and not a consequence of the disease [21, 22]. Researchers have started to dedicate their studies towards developing new-antiinflammatory therapeutical approaches. Mainly, studies were conducted with drugs commonly known for their use in other pathologies, and some of them have shown promising results in patients suffering from cardiovascular events [23]. Over the last few years, drugs such as Methotrexate (MTX) and Colchicine have received significant attention for their potential use in Cardiovascular Diseases. In this context, the anti-inflammatory action of both the drugs has been exploited in the Cardiovascular Inflammation Reduction Trial (CIRT) –Methotrexate– and the low dose Colchicine (LoDoCo) clinical trials [23].

1.3. The mechanism of action of MTX in Atherosclerosis

The inflammatory activity associated with Atherosclerosis is not confined to a small lesion but occurs throughout all vascular tree lesions. At the same time, vulnerable plaques are relatively rare, and the inflammation may play a causal role in the plaque rupture only if it is located within a thin fibrous cap [24]. Thus, Macrophages are considered key players in the whole process. They are an integral part of innate and adaptive immunity. Macrophages could assume either proinflammatory (M1) or anti-inflammatory (M2) phenotype [25]. An overproduction of the M1 phenotype causes cytokine secretion, like tumor necrosis factor (TNF)-α and is linked to the development of atherosclerosis [26]. Under these conditions, inflammation and different stress forms cause hypoxia and an increase of extracellular adenosine accumulation [27]. There is a growing evidence that adenosine receptors are crucial in anti-inflammatory response for increasing the protection from ischemic damage in several organs [27]. The agonist effect on the adenosine receptors causes the suppression of cells involved in inflammation, like natural killer cells, T cells, macrophages, monocytes, and neutrophils. The inhibition of leukocytes and platelet activation also decreases cytokine production and may have protective action against ischemic injury [28]. Simultaneously, stimulation of the adenosine receptor prevents foam cells formation, promoting the synthesis of receptors involved in the expulsion of lipoprotein from the macrophages [29]. Under normal conditions, macrophages represent the primary regulator of plasma lipoprotein metabolism and content. Specifically, they balance the lipoprotein concentration through scavenger receptors, such as CD36 and SR-A1 (for the internalization of the lipids) and ATP-Cassette (ABC) transporters, such as ABCA1, ABCG1 and SR-B1 for the expulsion of cholesterol from the cells [30]. In contrast, under inflammatory conditions, the internalization of ox-LDL and the decreased expression of ATP Cassette, gradually increase the intracellular amount of lipids, promoting foam cells formation [31].

Methotrexate (MTX), a conventional chemotherapeutic drug that currently represents the first-line option in inflammatory diseases like rheumatoid arthritis (RA) and psoriatic arthritis, was proposed for the treatment of atherosclerosis [32].

Bulgarelli *et al,* were the first to demonstrate the effect of MTX in the atherosclerotic lesions. They used an experimental rabbit model (20 animals were fed 1% cholesterol diet for 60 days)

and treated weekly by intravenous injections of MTX (4 mg/kg). The treatment produced a reduction of the lesion area by 75% and the intima-media ratio by 2%. Consequently, it led to the inhibition of macrophage migration in the intima by 50% and the reduction of apoptotic cells by 84% [33]. Also, Nishina *et al,* demonstrated the reduction of IL-6 in patients affected by RA after the use of MTX. Specifically, 49 women suffering from RA were treated for three months with the drug. At the end of their study, the levels of plasma IL-6 and TNF-α levels were measured. Data obtained showed a reduction of plasma IL-6, but not TNF-α, after MTX treatment [34]. Due to the widespread use of low dose of MTX on patients in several studies, the American College of Rheumatology collected guidelines regarding the patients' risk, doses, and regimes [35]. From the data, the use of this drug was associated with a 21% lower risk of total CVD and 18% lower risk of myocardial infarction compared to patients receiving other disease-modifying anti-rheumatic therapy [36]. These findings strongly strengthened the idea that the treatment of inflammation may reduce the risk of CVD.

Further studies confirmed that MTX reduced the inflammation in patients with RA by decreasing interleukin (IL)-1β, IL-1 receptor antagonist, IL-6, and TNF-a [37, 38]. The use of MTX for Atherosclerosis treatment is also supported by the increase in the adenosine release and subsequent agonistic effect of the adenosine on the A_{2A} receptor [39, 40]. As a result of this stimulation, an increase in the expression of proteins involved in reverse cholesterol transport, such as 27-hydroxylase and adenosine 5′-triphosphate-binding cassette transporter A1 (ABCA1) was noticed, thereby leading to a reduction of foam cells formation **figure 1.2**. [39, 40].

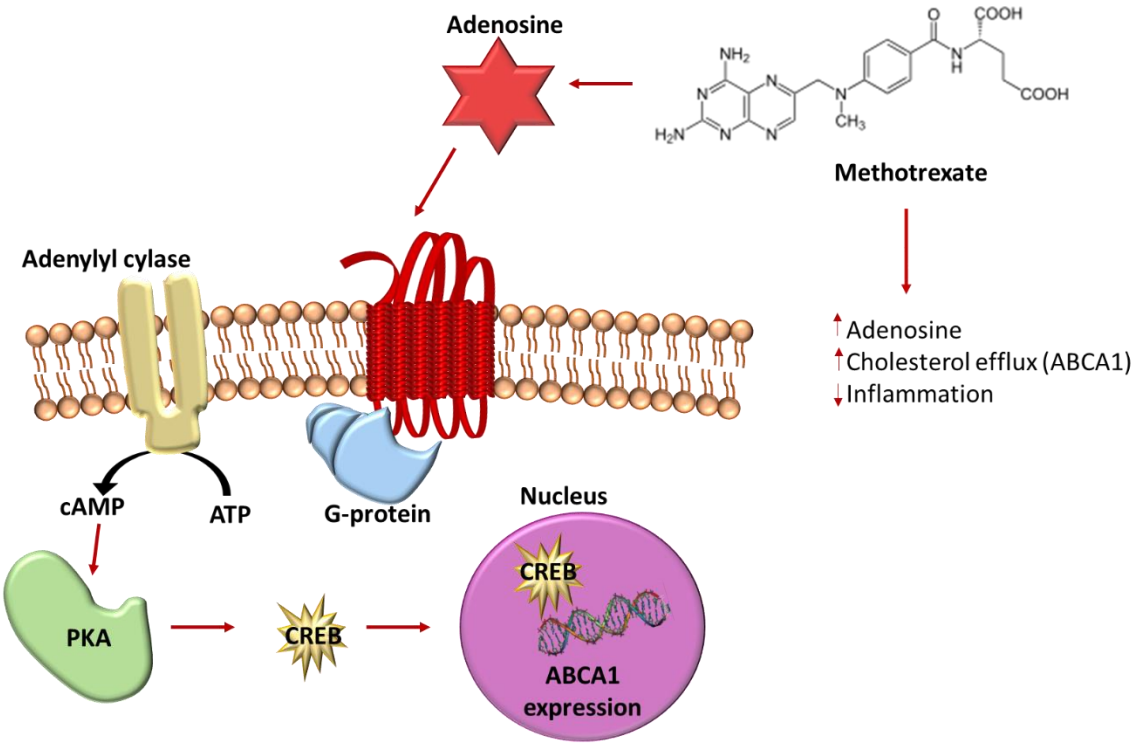

Figure 1.2. Mechanism of action of MTX. Adapted from Coomes *et al* [39].

The stimulation of A_{2A} receptor not only inhibits the early inflammatory processes but also resulted in a marked and sustained attenuation in neointimal formation [41]. Simultaneously, it reduced the expression of vascular cell adhesion molecule-1 and intercellular adhesion molecule-1, responsible for the development of atheroma [41]. As a consequence, the adenosine receptor stimulation limited foam cells formation by promoting lipoprotein expulsion from the macrophages [27].

MTX showed anti-inflammatory activity on macrophages, by lowering the production of proinflammatory cytokines; increasing the levels of adenosine monophosphate adenosine; suppressing cytokine secretion by the immune cells and protecting actions against ischemic injury [28]. All these observations formed the foundation for the clinical trial CIRT, which investigated the effect of MTX in patients affected by CVD.

1.4. CIRT/CANTOS

The Cardiovascular Inflammation Reduction Trial (CIRT) was a clinical trial conducted to investigate the impact on the reduction of strokes, heart attacks, or the death of people affected by metabolic syndrome by weekly administration of a low dose of MTX (target dose 15 to 20 mg per week) **Table 1.1**. People with a history of myocardial infarction or coronary artery disease with metabolic syndrome or type 2 diabetes were recruited as participants for the trial. From the 9321 potential participants, 6158 patients were chosen, and 4786 completed the trial. From this, 61% of the participants had a previous MI and the remaining 39% suffered from multivessel coronary disease. The results also demonstrated that a lower MTX dose did not decrease the levels of IL-1β, IL-6, or high-sensitivity C-reactive protein. MTX was not associated with a higher reduction of cardiovascular events compared to patients who were administered the placebo. Additionally, the use of MTX showed a higher incidence of non-basal-cell skin cancers, and a reduction in leukocyte counts and hematocrit levels, and elevations in liver enzyme levels [42].

Despite expected result were not met, and MTX was found not efficacious for the specific purpose, further reasoning needs to be associated to this results in order to correctly interpret it. Several studies had previously demonstrated the anti-inflammatory effect of MTX in atherosclerosis. Thornton *et al.* showed that a low dose of MTX (1 mg/kg/week) in the (NZW×BXSB)F1 murine model of inflammatory vasculopathy could add protection against cardiovascular events [43]. De Vecchis *et al,* demonstrated in his study that chronic use of MTX in patients with psoriatic or rheumatoid arthritis (RA) decreased the risk of ischemic cardiovascular events [32]. For this study, only adults receiving methotrexate at least for one year was taken into consideration. The cardiovascular endings of patients who were new users vs habitual users of MTX were evaluated. The result of this study suggested

that MTX, at low doses, was associated with a 27% decrease of the risk of ischemic cardiovascular events [32].

The development of proper nanoparticles (NPs) for the systemic introduction in the organism but aimed to a specific site constitute one of the main motives of Nanomedicine. In fact, nanoparticles have been demonstrated to be useful for systemic delivery and controlled release of therapeutic agents in a number of biomedical applications [44]. Thanks to their physic-chemical and geometrical properties, these nanovectors have the opportunity, by moving within biological systems, to transport and deliver different biomedical payloads for the treatment, prevention, and diagnosis of many diseases. They are able to efficiently to target disease sites, increasing the therapeutic efficacy and decreases the side effects in neighbor (healthy) cells [45]. Moreover, it is well known that spherical NPs with a diameter of a hundred nanometers are easily and rapidly engulfed by macrophages [46]. In another study, the delivery of MTX using nanoparticles increased the therapeutic effect on atherosclerosis. Polymeric nanoconstructs loaded with MTX, at 0.06 mg/mL, significantly reduced the production of IL-6 and TNF α *in vitro* experiments. In the $ApoE^{-/-}$ mice, fed with a high-fat diet up to 17 weeks, 4 weeks of treatment with biweekly administration of MTX-nanoparticles reduced the plaque burden by 50% [47]. Several papers showed the capability of MTX loaded nanoparticles in decreasing the side effects of the drugs [48, 49]. This mass of data not correlating with CIRT trial lead some experts to possible re-interpretations of this study.

In parallel with the CIRT, another clinical trial (Canakinumab Anti-Inflammatory Thrombosis Outcomes Study (CANTOS)) was conducted. The objective was to investigate if canakinumab, a monoclonal antibody targeting interleukin-1β, reduced the rate of recurrent cardiovascular events in patients with a history of myocardial infarction (MI) and elevated high-sensitivity C-reactive protein (hsCRP). CANTOS recruited patients that were

under stable conditions but with high cardiovascular risk and were treated with lipid-lowering therapies. Also, included patients with residual inflammatory risk (elevated high-sensitivity C-reactive protein levels – in median 4.2 mg per liter) [50]. In contrast, CIRT had recruited people suffering from metabolic syndrome with median high-sensitivity C-reactive protein level (hsCRP) that was 1.6 mg per liter. This is an important aspect because people with elevated hsCRP generally have the highest risk of cardiovascular disease. In particular, in CANTOS, significantly reduced IL-6 and hsCRP levels were observed after the canakinumab treatment, while in CIRT, MTX did not present the same result.

Before starting the CIRT, several papers had highlighted that low MTX dose reduced cardiovascular events in individuals with rheumatoid arthritis or psoriatic arthritis [36, 51, 52]. These patients had existing systemic inflammatory conditions. Also, there was evidence in patients affected by RA that the use of methotrexate reduced the C-reactive protein level. [53]. Is it possible that CIRT results were a consequence of selecting patients with low hsCRP? Is it possible that MTX could reduce hsCRP only when its levels are high? Maybe, the criteria for the patient selection were not adequate. New studies to understand these factors will be needed and specifically the influence of the hsCRP in CVD. Studies with other anti-inflammatory drugs could complement these observations.

1.5. The mechanism of action of Colchicine in Atherosclerosis

The release of cytokines in the lesions and the ability of oxLDL to activate innate and adaptive immunity leads to the classification of atherosclerosis as an immune-mediated disorder [54]. Blocking cholesterol regulating genes leads to the pathology, while the interference with the inflammatory mediators hinders the pathogenesis [55, 56]. Another component that plays an important role is the innate immunity, and therefore in

atherosclerosis, is the inflammasome. Inflammasome is a cytoplasmic multiprotein intracellular complex that is found in different forms, in which the most important segment is the leucine-rich repeat–containing receptor (NLR) family pyrin domain-containing 3 (NLRP3) [57]. Nowadays, the idea that the inflammasome is involved in lipid-driven vascular inflammation is increasing. Studies involving the NLRP3 were done in macrophages that are over recruited in the human carotid atherosclerotic plaques [58]. The activation of the NLRP3 caused the maturation and the release of the IL-1β and IL-18 (major contributors of atherogenesis) [59, 60]. There is an overexpression of these cytokines in human atherosclerotic plaques compared to the normal condition [61, 62]. Several studies demonstrated that the genetic ablation of the IL-18 modulated atherosclerosis development, while, the administration of recombinant IL-18 promotes plaque growth [62, 63]. IL-1β is a proinflammatory cytokine involved in different inflammatory disorders [64]. Its contribution in the atherogenesis was both local and systemic, and it was discussed in the review by Libby *et al*. published in the *Journal of the American College of Cardiology* [65]. IL-1β is released by different cells types involved in the atherosclerosis process, such as endothelial cells, vascular smooth muscle cells, macrophages, and the liver [66]. The NLRP3 is able to promote the release of the IL-1β and IL-18 and increases the migratory capability of the macrophages, and stimulates the lipid deposition in lysosomes. These events induce the formation of foam cells, and consequently, the formation of the plaque [67].

Colchicine is an alkaloid extracted from the plant *Colchicum autumnale*. It is known for its therapeutic use in gout and Familial Mediterranean Fever (FMF). A study following these patients noticed a reduction of myocardial infarctions after the use of Colchicine [68]. Moreover, Crittender *et al.* conducted a retrospective, cross-sectional study on gout patients (a total of 1288 patients) to evaluate if they had a reduction of the myocardial infarction

(MI) after using the drug. The result showed that patients treated with Colchicine had a significantly lower prevalence of MI [69]. Also, Langevitz *et al.*, led another study on patients affected by FMF, studying the presence of ischemic heart disease and its risk factors. The study followed 290 patients with FMF and 2 control groups (the spouses of the FMF and other patients with inflammatory diseases). This study suggested that colchicine was able to reduce the incidence of CVD. In fact, patients treated with the alkaloid had the same probability of the normal population of having ischemic heart disease [70]. Both studies demonstrated the drug's safety and effectiveness when used continuously over decades as secondary prevention of acute inflammatory flares [71, 72]. Nidorf *et al.* showed that a low dose of colchicine was able to reduce high-sensitivity C-reactive protein levels in patients with stable coronary disease [73]. In general, Colchicine has a large spectrum of effects in the cells that targets multiple aspects of the innate immune response. The administration of colchicine showed a stronger effect in the inhibition of inflammasome activation and IL-1β secretion proving a rational for its use in atherosclerosis treatment **Figure 1.3** [54, 74, 75]. All these results are the primary motivation for the studies based on the Low-Dose Colchicine (LoDoCo). They suggest that the drug may act on the prevention of cardiovascular events by inhibiting the inflammation in patients with unstable coronary plaques.

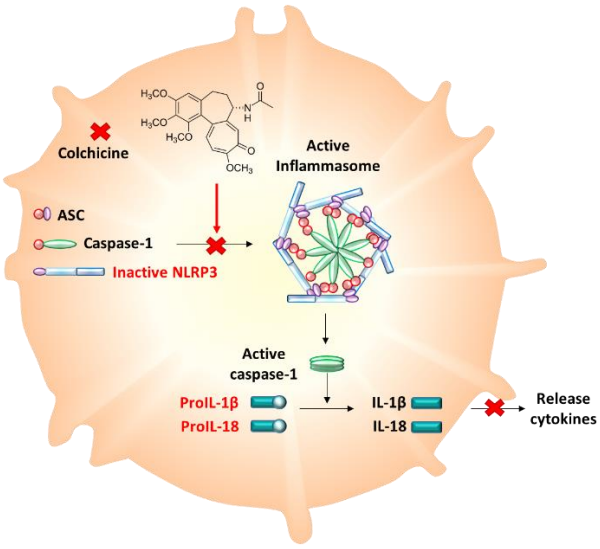

Figure 1.3. Mechanism of action of Colchicine

1.6. LoDoCo

The Low-Dose Colchicine (LoDoCo) was a clinical trial conducted by the Heart Research Institute of Western Australia that was approved in 2008 [76]. The objective of the study was to investigate whether colchicine (0.5 mg/day) reduced the risk of cardiovascular events in patients with clinically stable coronary disease. **Table 1.1**. 532 patients with angiographically proven coronary disease were recruited and they were under treatment with aspirin and/or clopidogrel (93%) and statins (95%). Colchicine or placebo was randomly assigned to them for a median of 3 years [76]. This first trial demonstrated that colchicine added to a standard therapy in patients with a stable coronary disease, decreased the cardiovascular events. These effects were reached under a scenario of wide use of effective secondary prevention strategies, such as high-dose of statins. These results also suggested that this drug may have a role in the prevention of cardiovascular problems caused by the instability of the plaque. This can be associated with the inhibition of inflammation, recognized in unstable native coronary plaques [77]. In particular, the study led to the idea that the positive effect of the drug is due to the inhibition of neutrophil

chemotaxis, ingress, and activation within a proinflammatory environment. Activated neutrophils could destabilize a plaque in patients with coronary syndromes [77]. Despite some early intolerance problems, this study suggested that colchicine (0.5 mg/daily) could be a candidate for the secondary prevention in patients with stable coronary disease.

Moreover, results from CANTOS supported the hypothesis that reducing the effects of activation of the NLRP3 inflammasome by targeting the IL-1β with the monoclonal antibody canakinumab. This led to the creation of a new clinical trial for more in depth study into the effect of the colchicine on patients with coronary disease. A second Low Dose Colchicine (LoDoCo2) started. 5522 patients, with stable coronary artery disease and already showed a tolerance for 30 days of colchicine treatment, were recruited and were randomly administered with colchicine 0.5 mg daily or matching placebo [78]. Attention was mainly focused on CV death, myocardial infarction, ischemic stroke, and ischemia-driven coronary revascularization. Colchicine has been revealed to decrease post-operative atrial fibrillation and, perhaps, improve metabolic status in diabetes. These last conditions are common inflammatory diseases affecting patients with coronary artery disease [79, 80]. Another observation that emerged from the study, was that colchicine didn't affect lipid levels and blood pressure [78]. The LoDoCo2 is ongoing and will provide data on the efficacy of low-dose colchicine administration and safety for secondary prevention in patients with stable coronary artery disease.

With the evidence that i) canakinumab reduced adverse cardiovascular events by the targeting of the IL-1 β, and ii) Colchicine decreased the responsiveness of neutrophils to inflammatory signals and the activation of NLRP3, formed the basis of the clinical trial Low Dose Colchicine after Myocardial Infarction (LoDoCo-MI). In this trial, researchers investigated the reduction of inflammation in patients following an acute MI through the use of Colchicine [81]. The objective of the study s was to investigate whether a low dose

of Colchicine in patients after a MI would decrease C-reactive protein (CRP) levels after 30 days of treatment, hence reducing the risk of recurrent vascular events [81]. With this trial, clinicians wanted to understand the effect of IL-6 (that regulate the inflammation and the hepatic CRP production [82]), and the safety and tolerability of colchicine. Their report showed that a low dose of Colchicine was well tolerated and, was safe after acute MI, but they were unable to find a significant reduction in the median level of CPR after 30 days [81].

From the LoDoCo pilot study, another clinical trial emerged, the Cardiovascular Outcomes Trial (COLCOT). This trial investigated the effect of low dose of Colchicine in individuals who had a myocardial infarction within 30 days before enrollment. A total of 4745 patients were recruited and were followed for a median of 22.6 months. The objective was to understand if a low dose of colchicine (0.5mg/daily), was able to reduce the risk of an ischemic cardiovascular event. The results of the trial highlighted a decrease of stroke, or urgent hospitalization for angina leading to coronary revascularization and death from cardiovascular causes, or cardiac arrest. Besides these, it emerged that people treated with this drug reported episodes of diarrhea and pneumonia [83].

Currently, two other ongoing randomized clinical trials “COVINCE” and “CLEAR-SYNERGY” aim to evaluate the effect of colchicine in patients with cerebrovascular disease and acute coronary syndrome **Table 1.1**. Colchicine for Prevention of Vascular Inflammation in Non-cardio Embolic Stroke (CONVINCE) evaluates the use of 0.5 mg/day of Colchicine in adults over 40 years of age that have suffered an ischemic stroke or transient ischemic attack. This study has the objective to prevent non-fatal recurrent ischemic stroke, myocardial infarction, cardiac arrest, hospitalization for unstable angina, and vascular death after ischemic stroke or transient ischemic attack (TIA) not caused by cardiac embolism or other defined causes unrelated to atherosclerosis [84]. In the

STEMI/SYNERGY (CLEAR-Synergy), a multi-international trial center 2x2 randomized placebo-controlled colchicine and spironolactone trial in patients affecting within 24 hours of ST Elevation Myocardial Infarction [85] is currently ongoing.

Table 1.1. Clinical Trials of Methotrexate and Colchicine

Trial name	Drug	Patients	Dose	Clinical trial registration
Atherosclerotic Cardiovascular Disease				
CIRT	Methotrexate	Multivessel coronary artery disease	15-20 mg po/weekly vs. placebo	NCT02576067
Treatment of Patients With Atherosclerotic Disease With Methotrexate-associated to LDL Like Nanoparticles	Methotrexate	Multivessel coronary artery disease; Aortic atherosclerosis; High-sensitivity C reactive protein (hs-CRP) levels > 2mg/L	MTX-LDE 40mg/m2 and Folic acid 5mg by mouth vs. placebo	NCT04616872
Stable coronary disease				
LoDoCo	Colchicine	Stable coronary artery disease	0.5 mg/day vs. placebo	ACTRN12610000293066
LoDoCo2	Colchicine	Stable coronary artery disease	Colchicine 0.5 mg/day vs. placebo	ACTRN12614000093684
LoDoCo-Mi	Colchicine	Acute myocardial infarction	0.5 mg/day vs. placebo	ACTRN12615001194550
Inflammation and Coronary Endothelial Function	Methotrexate Colchicine	Stable coronary artery disease	Methotrexate 15 mg weekly/vs. placebo Colchicine 0.6 mg dailyweekly/vs. placebo Methotrexate 15 mg weekly and colchicine 0.6 mg daily	NCT02366091
Acute coronary syndromes				
COLCOT	Colchicine	Acute coronary syndrome	Colchicine 0.5 mg/day vs. placebo	NCT025510 94
CLEAR-SYNERGY OASIS-9	Colchicine	Stent Registry ST elevation myocardial infarction	Colchicine 1 mg/day and/or spironolactone 25 mg/day and/or placebo and/or SYNERGY stent (2x2 factorial design)	NCT030488 25
Stroke or high-risk TIA				
CONVINCE	Colchicine	Stroke or high risk transient ischaemic attacks	Colchicine 0.5 mg/day vs. placebo	NCT028986 10

1.7. Conclusion and future prospective: combination and nanomedicine strategy.

The evidence produced from the several experimental and human studies, over the last decade, suggests that inflammation has an important role in the onset and progression of atherosclerosis and thrombosis. In particular, the chronic inflammation, immune activation, and the oxidative stress at the arterial wall characterized the atherosclerosis [86]. Besides, all cardiovascular risk factors activate these events at some stage, promoting the beginning of endothelial dysfunction and vascular damage [87]. One of the most important

endothelium roles is the release of nitric oxide (NO) under stress conditions. The relevant role of NO on the endothelium is the maintenance of vascular homeostasis. Based on these considerations, Robert G. Weiss of Johns Hopkins University, started a clinical trial where he studies the function (Inflammation and Coronary Endothelial Function) of coronary arteries, specifically the endothelium, using magnetic resonance imaging (MRI). The study will evaluate the flow and the dimension of the artery in the two conditions: normal and under stress. The researchers believed that inflammation influenced the normal function of the artery. For this reason, they will test the combinatorial effect of Methotrexate/Colchicine on the artery in order to produce a reduction in inflammation [88]. This study is ongoing. Another ongoing clinical trial follows the Treatment of Patients With Atherosclerotic Disease With Methotrexate-associated to LDL - Like Nanoparticles. The goal is to investigate the safety and efficacy of an anti-inflammatory agent, methotrexate, in a cholesterol-rich non-protein nanoparticle (MTX-LDE) in patients with stable coronary disease [89].

A work was recently published on the use of lipid modified Methotrexate, and its delivery by two types of nanosystems: spherical polymeric nanoparticles and liposomes.[90] With both formulation, *in vitro* results showed that the MTX modulated the trafficking of lipid, thereby decreasing the inflammation over time. Especially, the treatment revealed that MTX, delivered with nanoparticles, decreased the growth of the plaque in $ApoE^{-/-}$ after a brief treatment [90]. Gomes *et al.* also showed the efficient effect of MTX delivered by the nanoparticles (solid lipid particles) in atherosclerosis. In fact, in this work paclitaxel loaded nanoparticles were tested with and without nanoparticles containing MTX on thirty-eight rabbits (fed 1% cholesterol chow for 8 weeks). The results showed that the co-delivery had the ability to increase the regression of plaque areas more than the delivery of nanoparticles with only paclitaxel. They underlined that nanoparticles with paclitaxel plus nanoparticles

with MTX reduced the presence of macrophages in aortic lesions and lowered the level of TNFα, thus accelerating plaque reduction after cholesterol feeding, without any observed toxicity compared to the injection of nanoparticles with paclitaxel [49].

Zoghebi *et al.*, investigated the use of Colchicine, modified with a peptide (FDAIAEIGNQLYLFKDGKYW), on an *in vitro* model of crystal-induced inflammation. Using this peptide, they were able to target the macrophages and reduce the inflammation more than free Colchicine (also reducing the ROS generation and IL-8 secretion). They also demonstrated that the modified Colchicine reduced the cytotoxic effect of Colchicine while preserving its anti-inflammatory activity [91]. Furthermore, Chen *et al.*, developed an intramyocardial delivery system of Colchicine, using a thermo-sensitive polymer hydrogel, to treat MI. The *in vivo* study showed that this system alleviated cardiac inflammation and inhibited myocardial apoptosis and fibrosis. Moreover, the mouse survival increased compare to the free administration of Colchicine, at the same time reducing the severe systemic toxicity [92].

Atherosclerosis is a silent, progressive disease, and many times, it is very difficult to detect by current imaging methods at its early stage. Current approaches to treat the disease are systemically and this could be associated with side effects. The use of anti-inflammatory drugs combined with the nanomedicine could represent an innovative strategy to overcome this problem. Methotrexate and Colchicine are promising therapeutic agents for the clinical treatment of inflammatory disease, particularly pathologies involved in cardiovascular diseases. The use of the nanoparticles may enhance the stability and bioavailability of the drugs and improve their pharmacokinetics, improving the effect of anti-inflammatory drugs. Future studies are expected to investigate significantly deeper into the effects of Colchicine and Methotrexate. Perhaps, the combination of these two drugs, acting on

different pathways, could represent a potential strategy to strongly reduced the inflammation in atherosclerosis.

Chapter 2

Synthesis of Two Methotrexate Prodrugs for Optimizing Drug Loading into Liposomes

2.1. Abstract

Methotrexate (MTX), a compound originally used as an anticancer drug, found applications also in a broad variety of autoimmune disorders thanks to its anti-inflammation and immunomodulatory functions. The broad application of MTX is anyway limited by its poor solubility in biological fluids, its poor bioavailability, and its toxicity. In addition, encapsulating its original form in nanoformulation is very arduous due to its considerable hydrophobicity. In this work, two strategies to efficiently encapsulate MTX into liposomal particles are proposed to overcome the limitations mentioned above and to improve MTX bioavailability. MTX solubility was increased by conjugating the molecule to two different compounds: DSPE and PEG. These two compounds commonly enrich liposome formulations, and their encapsulation efficiency is very high. By using these two prodrugs (DSPE-MTX and PEG-MTX) we were able to generate liposomes comprising one or both of them and characterized their physiochemical features and their toxicity in primary macrophages. These formulations represent an initial step to the development of targeted liposomes or particles, which can be tailored for the specific application MTX is used for (cancer, autoimmune disease, or others).

2.2. Introduction

Methotrexate, 2,4-diamino-N10-methyl propylglutamic acid (MTX) is a folic acid antagonist, widely used as therapeutic agent [93, 94]. The molecule is a weak dicarboxylic acid with a molecular weight of 454.5 g/mol. It possesses pKa values of 4.7–5.5 and low permeability (Clog P = 0.53) with poor aqueous solubility (0.01 mg/mL). The first form of MTX, known as amethopterin, was originally synthesized in 1947. In the following years, after a slight modification of its chemical structure, it was first applied for the treatment of life-threatening neoplastic diseases (acute lymphoblastic leukemia, breast cancer, choriocarcinoma) [95, 96]. Being an analog and antagonist of folic acid, MTX competes for the binding site of folate on dihydrofolate reductase (DHFR), an enzyme required in the process of DNA and RNA production [97-99]. At lower dosages (1:50 – 1:100), it also found application in a series of other diseases: Rheumatoid Arthritis (RA), Multiple Sclerosis, Vasculitis, Systemic Lupus Erythematosus, Psoriasis, Inflammatory Bowel Disease, Juvenile Idiopathic Arthritis [28, 97]. It is widely accepted the positive effects in the treatment of RA depends by MTX anti-inflammatory and immunomodulatory activity. These many applications of MTX are limited by the intrinsic features of the molecule, which impede harnessing the full potential of this drug. As mentioned before, MTX possesses poor water solubility and low permeability, which determines its low bioavailability [95, 100]. Its uptake by cells is in fact extremely limited as demonstrated by in vitro assays [101]. Upon administration, MTX is rapidly excreted by the kidneys, showing a short half-life, and its plasma concentration drops rapidly upon intravenous administration, being nearly undetectable after only 4 h [94, 102, 103]. For the mentioned reasons, out of a discrete administered dose of drug, the amount effectively reaching its biological target tissues is supposed to be very low. Moreover, even when used at low dosages, MTX is not free from drug toxicity; rather than inefficacy, toxicity is the main cause of MTX treatment withdrawal [96]. MTX toxic effects can be severe and include hepatotoxicity, liver fibrosis, acute pneumonitis, neurotoxicity and kidney damage, just to cite some [104-107]. This

considered, to optimize its use, it would be beneficial to develop novel formulation and targeted therapies to maximize its therapeutic effect, reduce its dosage and thus its toxic effects.

In the recent past, various Novel Drug Delivery Systems (NDDS) such as microemulsions [108], nano-conjugates [109], nanoparticles [110], nanocapsules [111], polymeric micelles [112], pH-responsive polymersomes [113] and liposomes [101, 114] were proposed. The development of these nanoformulations allowed to the introduction of novel targeting and release strategies and to the improvement of MTX loading through some modification of the molecule. Despite these valuable advancements, MTX loading still remained suboptimal and a series of characterizations and studies are needed to approve and safely apply the majority of these novel technologies. Among the listed formulations, liposomes represent one of the most common nanocarrier for targeted and untargeted delivery [115]. They are mainly constituted by endogenous compounds, represent a very well tolerated drug delivery system, and are generally considered as pharmaCologically inactive. These formulations currently represent a more efficient and less harmful alternative to conventional chemotherapy and possess the potential to positively influence therapeutic efficacy and reduce drug toxicity [116]. Their use improves the biodistribution of therapeutics to the diseased site, increases cell uptake and stabilizes the vectored compounds by protecting them from degradation and early inactivation [117]. Their biomedical application have improved the therapy of a broad variety of pathologies, and their continued translation success is progressing over time [117, 118].

In this work we modified MTX molecule with the aim to furtherly improve it's loading into liposomes. In particular, we generated two prodrugs by covalently binding MTX to DSPE (DSPE-MTX) or polyethylene glycol (PEG-MTX). Three different liposomal formulations were obtained by loading into liposomes the two prodrugs, individually or in combination. The physio-chemical features of these MTX-Liposomal formulations, generated by loading into liposome DSPE-MTX, PEG-MTX or both were acquired and compared. The stability of the formulations was analyzed in neutral or acidic environment and the prodrug release profile was analyzed. The uptake of Cy5 loaded liposomes in primary Bone Marrow Derived Macrophages (BMDM) from rat was studied: confocal imaging, revealing liposome internalization and flow cytometry analysis calculating the percent of cells positive for liposomes uptake are shown. In addition, a

toxicity analysis was performed in BMDM, in order to assess any possible difference among the formulations.

2.3. Materials and Methods

Materials: 1-Ethyl-3-(3-dimethylaminopropyl) carbodiimide (EDC), N-Hydroxysuccinimide (NHS), Triethylamine (TEA), was purchased from Sigma-Aldrich (St. Louis, MO, USA). Methotrexate (MTX) and NH2-PEG (1K) was bought by AlfaAesar (Haverhill, MA, USA). 1,2-distearoyl-sn-glycero-3-phosphoethanolamine-N-[succinyl(polyethylene glycol)-2000] (DSPE-PEG-COOH), 1,2-distearoyl-sn-glycero-3-phosphoethanolamine (DSPE-NH2), 1,2-Dipalmitoyl-sn-glycero-3-phosphocholine (DPPC) were purchased from Avanti Polar Lipid (Alabaster, AL, USA). All reagents and solvents were used without further purification. Cy5 was purchased from Luminoprobe (Hunt Valley, MD, US).

Synthesis of DSPE-MTX.

DSPE-MTX was synthesized as reported by Ferreira and coworkers with some modifications [49]. Briefly, 30 mg of MTX was incubated with 1eq of 1-Ethyl-3-(3-dimethylaminopropyl)carbodiimide (EDC) and 1eq. of N-Hydroxysuccinimide (NHS) in 2mL Dimethyl sulfoxide (DMSO) for 30 minutes, at room temperature. 0.98 eq DSPE-NH2 dissolved in 0.5mL DMSO were added. The reaction was left to stir for 72 hours after added a catalytic amount of triethylamine (TEA). The mixture was washed three times with cold diethyl ether. Finally, the pro-drug was lyophilized and stored at -20°C.

Synthesis of PEG-MTX.

For PEG-MTX synthesis, 20 mg of NH2-PEG (1,000 Da) were dissolved in a mixture of dichloromethane (DCM) and MeOH (2:1 Ratio). 0.98 eq of MTX was dissolved in 200 mL of dimethylformamide (DMF) and added to the previous solution. A catalytic amount of triethylamine (TEA) was added to the reaction and was left to stir for 16 hours. The intended

product was precipitated with cold diethyl ether, and then washed 3 times with cold diethyl ether getting the final product with a yield of 90%. More details of this procedure can be found in previous author's literature [119].

Synthesis of DSPE-Cy5.

DSPE-Cy5 was synthetized as reported elsewhere [119]. Briefly, DSPE-NH2 (15 mg) was dissolved in dichloromethane (DCM)/Methanol (MeOH), 2:1 v/v. Cyanine-5 NHS ester (0.98 eq) was dissolved in 200 ml of dimethylformamide (DMF) and added to the previous solution. Triethylamine (TEA) was added in order to catalyze the reaction, stirring was maintained for 16 h. cold diethyl ether was used for precipitating the product which was then washed three times with cold diethyl ether obtaining the final compound with a yield equals to 90%.

Determination Log P.

DSPE-MTX and PEG-MTX Log P was determined recurring to the help of three computational software's: Biovia Draw, DASSAULT SYSTEMES, https://www.3ds.com/. VCCLAB, Virtual Computational Chemistry Laboratory, http://www.vcclab.org, 2005. ChemSketch, ACD/LABS; https://www.acdlabs.com/. Log P. is given by the following equation:

$$\log P_{oct/wat} = \log\left(\frac{[solute]_{octanol}}{[solute]_{water}}\right)$$

Synthesis of MTX liposomes (MTX-LIP) and Cy5 liposomes (Cy5-LIP).

Liposomes (LIP) were prepared by thin-layer evaporation (TLE) [31]. Briefly, DPPC, cholesterol, DSPE-PEG (6:3:1) (total amount 40 mg), and DSPE-MTX/PEG-MTX or both prodrugs (1 mg of prodrug) were dissolved in chloroform in a round-bottomed flask. After the evaporation of the organic solvent at 60° under reduced pressure, the lipid film was left under the hood overnight to remove any trace of residual solvent. The lipid film was hydrated with 2 mL of HEPES buffer (pH=7.4, 10 mM) and then subjected to three alternate cycles (3 min each) of warming at 60 °C (thermostated water bath) and vortexing at 700 rpm. The sample was dialyzed against HEPES buffer (pH=7.4, 10 mM) for 1h at 4°C.

For the preparation of Cy5-LIP, DSPE-Cy5 was used instead of the prodrugs. More in details, 0.3 mg of DSPE-CY5 were dissolved in chloroform together with lipids and cholesterol in a round-bottomed flask; the same procedure was followed. The purification step to remove the excess of Cy-5 was conducted by ultracentrifugation (1h, 45,000 rpm). All the formulation obtained were freshly used or stored at 4°C overnight as concentrated dispersions.

Liposome morphological characterization.

SEM Characterization: Liposomes were fixed for 2 h in 2% glutaraldehyde in 0.1 M cacodylate buffer. After fixation, the samples were washed twice with the same buffer and post fixed for 1h in 1% osmium tetroxide, in 0.1 M cacodylate buffer. After several washes with distilled water, samples were subsequently dehydrated in a graded ethanol series, 1:1 ethanol: hexamethyldisilazane (HMDS), and 100% HMDS and dried overnight. Samples were sputtered using gold. SEM images were Collected using JEOL JSM-7500FA (Jeol, Tokyo, JAPAN), operating at 5 kV of accelerating voltage.

TEM Characterization: Transmission electron microscopy (TEM) micrographs were acquired using JEOL JEM 1011 (Jeol, Japan) electron microscope operating with an acceleration voltage of 100 kV and recorded with a 11 MegaPixel fiber optical charge-coupled device (CCD) camera (Gatan Orius SC-1000). LIP was diluted 1:100, dropped on 150-mesh glow discharged 'Ultrathin' carbon-coated Copper TEM grids and dried. Dried TEM samples were negatively stained using 2% Uranyl Acetate aqueous solution.

Particles size, surface charge and stability characterizations.

Particle size, size distribution and ζ-Potential of all the formulations were measured using Dynamic Light scattering (DLS). For stability studies, 1 mL of each formulations was put in 9 mL of PBS (pH=7.4, 1X) or slightly acidic buffer (pH = 6.5, 1X) (final volume = 10 mL) in physiologic temperature (37 ± 2°C), under agitation. At specific time intervals of 1, 2, 3, and 4 days, samples were taken, and their physical features were examined.

Drug loading and release analysis.

To measure the MTX encapsulation efficiency (EE), samples were destroyed with cold methanol, left to dry, dissolved in acetonitrile (AcN)/H2O (1:1, v/v), and analyzed by high-performance liquid chromatography (HPLC) (Agilent 1260 Infinity, Germany) equipped with a 100 µL sample loop injector. A C18 Column (2.1× 250 mm, 5 µm particle size, Agilent, USA) was used for the chromatographic separation. MTX was eluted under isocratic conditions using a binary solvent system [H2O + 0.1% (v/v) TFA and AcN + 0.1% (v/v) TFA 43:57 v/v] pumped at a flow rate of 1.0 mL/min. The ultraviolet (UV) detection was set at 430 nm.

EE was determined using the following equation:

$$EE\ (\%) = \frac{MTX\ weight\ in\ particles}{MTX\ inizial\ feeding\ amount} \times 100$$

To study MTX and Cy5-release kinetics, 200 µL of MTX-LIP or Cy5- LIP solution were placed into Slide-A-Lyzer MINI dialysis microtubes with a molecular cutoff of 10 kDa (Thermo Scientific) and dialyzed against 4 L of PBS buffer (pH 7.4, 1X). For each time point, three samples were collected and dried. LIP samples were destroyed with cold methanol, left to dry, dissolved in AcN/H2O (1:1, v/v), and analyzed by HPLC for the MTX. The experimental data were fitted using different mathematical models: the zero-order, the first-order, the Higuchi, the square root, the two-phase Weibull, and Korsmeyer-Peppas models [37, 38].

Cy5 Loading and release analysis.

For determining DSPE-CY5 encapsulation efficiency (EE), liposomes were destroyed by adding cold methanol. After solvent evaporation the destroyed formulation was dissolved in acetonitrile (AcN) and analyzed at the spectrophotometer (ʎ=640 nm). EE was determined using the following equation:

$$EE\ (\%) = \frac{DSPE - CY5\ weight\ in\ particles}{DSPE - CY5\ initial\ feeding\ amount} \times 100$$

For studying DSPE-Cy5-release kinetic, 200 µL DSPE-Cy5-LIP suspension were placed into Slide-A-Lyzer MINI dialysis microtubes with a molecular cutoff of 10 kDa (Thermo Scientific) and dialyzed against 4 L of PBS buffer (pH 7.4, 1X). For each time point, three samples were collected and dried. Samples were subsequently destroyed with cold methanol and solvent was left to dry. The sample were than dissolved in AcN and analyzed at the spectrophotometer following the indications used for EE de-termination.

Bone Marrow Derived Macrophages harvesting.

BMDMs from rats were cultured at 37°C in 5% CO2, in high-glucose DMEM, supplemented with 15% FBS and 1% L-glutamine, according to ATCC instructions. Cells were isolated by the following procedures, also indicated elsewhere [50, 51]. After sacrificing the animal, femurs were explanted, cleaned from surrounding tissues, and washed in PBS (Thermo Fisher Scientific, USA), and a cut was performed at both ends. PBS was used for flushing the cavities to harvest cells, and the sample was centrifuged for 10' at 800 RPM at 4°C. Cells were plated in media supplemented with macrophage Colony-stimulating factor (mCSF) (10 ng mL–1) (Sigma-Aldrich, USA). Three days after media was completely replaced after one wash in PBS and the following day, cells were scraped, counted, and seeded for being furtherly processed. The procedures were conducted following the guidelines of the Institutional Animal Care and Use Commit-tee of IIT.

Confocal Fluorescent Microscopy Imaging.

Confocal images were obtained using a Nikon-A1 confocal microscope (Nikon Corporation, Japan). Cy5-DSPE was used in the fabrication step of liposomes, allowing their visualization at confocal microscope. Liposomes were suspended in HEPES Buff-er. 65000 BMDM were seeded into each well of a Nunc Lab-Tek II chamber slide system (Thermo Fisher Scientific, USA), maintaining culturing conditions, as described above. Cells were treated with 10 µL of Cy5-LIP for 30'. To favor the homogeneous distribution of the particles in the wells, all the treatments were performed by sus-pending liposomes in an adequate volume of culturing media prior of the treatment; media without liposomes was replaced by media with liposomes.

After 30', the culturing medium was removed, and cells were washed in PBS (Thermo Fisher Scientific, USA). Fixation was performed using a 3.7% solution of paraformaldehyde (Sig-ma-Aldrich, USA) for 5 min. Cell Mask was used to stain the plasma membrane and nuclei were stained using DAPI (Thermo Fisher Scientific, USA). A z-stack section was acquired using a 60× objective (12 steps of 1000 nm each were acquired). The maximum intensity profile is presented in **Figure 2.5a**. Surface reconstruction of macrophages is shown in **Figure 2.5c**.

Cell internalization studies.

Flow cytometry was performed using a FACS ARIA (Becton Dickinson, USA). 200000 BMDM were seeded into each well of a 12-well plate, maintaining culturing conditions indicated in the cell culturing section. Cells were treated for 30' with different volumes (5, 10, 15, 30 µL) of Cy5-LIP. After treatment, cells were washed using cold PBS in order to ease the scraping procedures. Cold DMEM, high glucose, no glutamine, and no phenol red (Thermo Fisher Scientific, USA) was added, and cells were harvested by gentle scraping the plastic bottom (a volume of 200 µL of was used). Samples were immediately stored in ice and vortexed right before the analysis.

Toxicity Analysis.

BMDMs were cultured according to the conditions above indicated. Cell viability was determined using MTT assay; this assay detects the reduction of MTT [3-(4,5-dimethylthiazolyl)-2,5-diphenyltetrazolium bromide] (Sigma-Aldrich, USA) by mitochondrial dehydrogenase to blue formazan product. Cells were seeded into 96-well plates at a density of 20 × 103 cells per well and incubated for 24, 48, 72 hours. Cells were treated with different concentrations of free MTX, DSPE-MTX, PEG-MTX, DSPE-MTX/PEG-MTX, DSPE-MTX-LIP, PEG-MTX-LIP and PEG-MTX/DSPE-MTX-LIP (namely, 0.0064, 0.032, 0.16, 0.8, 4, 10 and 0 µM of MTX), or empty LIP. For free MTX condition, MTX was pre-dissolved in DMSO due to the impossibility to dissolve the compound in culturing media. The MTT solution was added for 4 h, and the formed formazan crystals were dissolved in ethanol. Absorbance was measured

at 570 nm, using 650 nm as the reference wavelength (Tecan, Männedorf, Swiss). The percentage of cell viability was assessed according to the following equation:

$$Cell\ viability\ (\%) = \frac{Abs_T}{Abs_C} \times 100$$

Where, AbsT is the absorbance of treated cells and AbsC is the absorbance of untreated cells (control).

Statistical Analysis.

All the in vitro data were represented as the average ± standard deviation (SD) of 3 different measurements, unless differently specified. The statistical significant difference was assessed using ANOVA test, with Bonferroni's Multiples Comparison Test as posthoc test. All statistical in vitro analyses were performed using GraphPad Prism v.5 (GraphPad Software, USA).

2.4. Results and Discussion

MTX prodrug synthesis and characterizations.

To improve MTX solubility and loading efficiency into liposomes, two different prodrugs, DSPE-MTX and PEG-MTX, were developed (**Figure 2.1**). The two molecules were chosen since they are easily incorporated into liposomes and other nanoparticles and are commonly part of the formulations themselves. The size of the two molecules was kept similar, being PEG: 1KDa and DSPE: 0.748 KDa. For the synthesis of both DSPE-MTX and PEG-MTX, MTX was pre-activated with a mixture of EDC and NHS, before the conjugation with 0.98 eq. DSPE-NH2 or PEG-1k-NH2. A low amount of the substituent was used to avoid the conjugation on MTX second carboxylic position. TLC analysis did not show any signal of the bi-substitute product. The absence of such compound is most likely due to the steric hindrance created by the bigger size of the substituent in the vicinity of the second reaction point. Product purification was achieved through precipitation with diethyl ether. Both products were obtained with a yield >75%. A scheme of the molecules and of the above mentioned reactions is available in **Figure**

2.1. **Table 2.1** reports the formula weight, the exact mass, and the molecular formula and log P values of the three compounds.

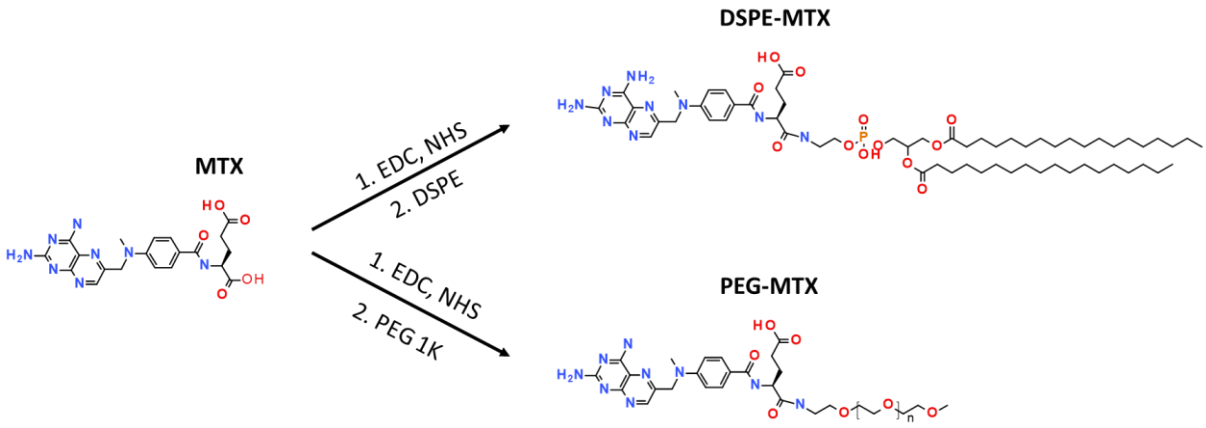

Figure 2.1. Synthesis of DSPE-MTX and PEG-MTX.

Table 2.1. Summarizes formula weight, exact Mass, Molecular Formula, Log P value (Bovia, VCClab, ACD chemsketh) of MTX and its prodrugs.

Compound	Formula Weight	Exact Mass	Mocecular Formula	Yield (%)	Log P		
					Biovia	VCClab	ACD chemsketh
MTX	4454.44	454.439	$C_{20}H_{22}N_8O_5$	---	0.11	-0.91	0.023±0.83
DSPE-MTX	1184.49	1183.73	$C_{61}H_{102}N_9O_{12}P$	81.1	13.84	7.53	16.63±1.03
PEG-MTX	1480.69	1479.80	$C_{67}H_{117}N_9O_{27}$	78.3	-0.67	0.42	-0.43±0.93

Log P is defined as the logarithm of a particular ratio of the concentrations of a solute between two solvents (for instance, for an octanol–water partition), specifically for un-ionized solutes. Three different software (Biovia, VCCLab and ACD ChemSchetch) were used to analyze this parameter for MTX and the two generated prodrugs. The software use different combination of algorithms to perform the calculatation. Biovia is based on an algorithm which considers the ionization states of the molecule [120]; log P is calculated using pKa information for each atom in the molecule. VCCLab (ALOGPs) was developed with 12908 molecules from the PHYSPROP database using 75 E-state indices. 64 neural networks were trained using 50% of

molecules selected by chance from the whole set. The logP prediction accuracy is root mean squared error rms=0.35 and standard mean error s=0.26 [121]. ACDLabs uses a consensus model for the determination of log P. Applying both Classic algorithms (Based on >12,000 experimental log P values, by using the principle of isolating carbons) and GALAS algorithms (Based on a training set of >11,000 compounds, that provides a value for log P that is adjusted with data from the most similar compounds), the consensus algorithm weights the calculation to the model best suited for each structure [122]. Results are presented in **Table 2.1** and reported here for convenience, respecting the software order indicated above. Following results were obtained for MTX: log P. = 0.11; -0.91; 0.023, for DSPE-MTX: log P. = 13.84; 7.53; 16.63 and for PEG-MTX: log P. = -0.67; 0.42; -0.43. The similar results obtained for MTX and PEG-MTX indicate that these molecules can be equally dissolved in water and organic solvents. While for MTX-DSPE, regardless the discrepancy between VCCLab software results and the two other software (to be ascribed to the different combination of algorithms used), all three programs show that MTX-DSPE is mainly soluble in organic solvents. The higher value of log P for MTX-DSPE, is due to the two aliphatic chains of the lipid. These aliphatic chains are very hydrophobic and led the software to predict MTX-DSPE to be mainly soluble in the organic phase. Instead, the amphiphilic behavior of PEG chain led the software to predict that the chain will not influence MTX solubility.

Experimentally, MTX has shown low solubility in water and organic solvents, such as Dichloromethane and Chloroform, which are commonly used to prepare Liposomes. The theoretical MTX-PEG log P (log P. = -0.67; 0.42; -0.43) could indicate similar solubility features for this compound and naïve MTX (log P. = 0.11; -0.91; 0.023). Nonetheless, MTX-PEG showed a more hybrid behavior regarding these solvents, revealing to have higher solubility in water and organic solvents with respect to MTX. This is due to the amphiphilic properties of this prodrug, which can spontaneously organize in small structures, accordingly to the solvent used. This factor is probably not taken into consideration by the software algorithms. Similar amphiphilic behavior is observed for MTX-DSPE (log P. = 13.84; 7.53; 16.63) for the same capability of self-organizing into small structures, it was possible to dissolve DSPE-MTX at low concentration in water, despite Log P. results. The observed behaviors allowed the loading of

both prodrugs into the liposomes with high yielding, conversely MTX direct loading was not successful.

MTX Liposome Assembly and Characterization.

Liposomes were synthesized via the thin layer evaporation method (TLE), using DPPC, cholesterol, carboxyl-terminated DSPE-PEG chains, and the two prodrugs: DSPE-MTX and PEG-MTX (**Figure 2.2**). The DSPE-MTX and PEG-MTX were added during the lipid film formation phase. It might be speculated that the DSPE-MTX could intercalate with the DPPC and DPSE-PEG chains, considering that the lipid part of DSPE-MTX is identical to DSPE-PEG and similar to DPPC [90]. Regarding the localization of PEG-MTX, there are two options: it could be intercalated into the lipid membranes, with a similar configuration reported for DSPE-MTX, or in the inside of the phospholipid bilayer. The loading of the combination of both prodrugs increases the complexity of the allocation, making even harder to produce hypothesis on their possible disposition inside the liposome. A schematic of the putative structures of the three liposomes is proposed in **Figure 2.2a**.

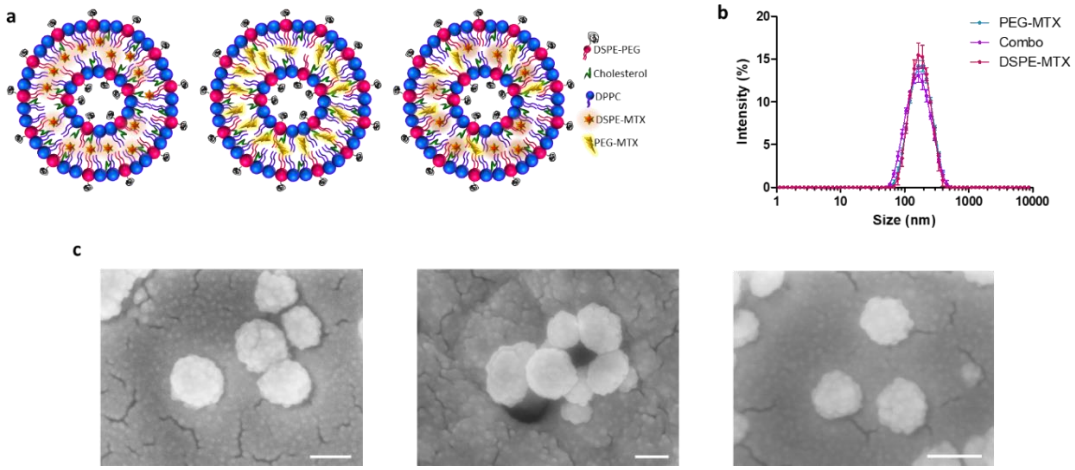

Figure 2.2. a) Schematic representation of liposomes. b) Hydrodynamic diameter of PEG-MTX-LIP, DSPE-MTX-LIP and Combo-LIP via dynamic light scattering analysis. c) Scanning electron microscopy images of PEG-MTX-LIP, DSPE-MTX-LIP and Combo-LIP, respectively (scale bar: 100 nm).

Table 2.2. Summarizes sizes, PdI, ζ-Potential and encapsulation efficiency (%EE).

Liposomes	Size (nm)	PdI	Z Pot (mV)	%EE
DSPE-MTX	159±3	0.14±0.02	-38±0.26	79.9±5.6
PEG-MTX	166±0.6	0.18±0.02	-41±0.4	82±7.5
Combo	148±1	0.18±0.01	-41.3±3	80.2±1.8
Empty	157.8±2	0.17±0.01	-41.84±1.2	---

DLS analysis showed an average hydrodynamic diameter of 159 ± 3.0 nm, 166 ± 0.6 nm, and 148 ± 1.0 nm for the DSPE-MTX-LIP, PEG-MTX-LIP, and Combo-LIP, respectively (**Figure 2.2b** and **Table 2.2**). A similar size was reported for empty liposomes (157.8 ± 2.2 nm), confirming that lipophilic drug encapsulation cannot affect particle size [123]. All the formulations are characterized by a very homogenous population: with a polydispersity index (PDI) of ~ 0.15 (**Table 2.2**). Images of the formulations were acquired by SEM (**Figure 2.2c**) and TEM analyses (**Figure 2.S3**), confirming formulations sphericity and size. Liposomes presented a negative surface electrostatic ζ-potential of -38 ± 0.26 mV, -41 ± 0.4 mV, and -41.3 ± 3 mV for the DSPE-MTX-LIP, PEG-MTX-LIP and Combo-LIP, respectively (**Table 2.2**). It is important to note that the unchanged surface electrostatic ζ-potential found for PEG-MTX-LIP supports the hypothesis of the localization of the compound between the two membranes. To evaluate the encapsulation efficiency (EE) of MTX inside liposomes, High-Performance Liquid Chromatography (HPLC) was used. The EE was calculated as the percentage ratio between the drug loaded mass and the drug input mass, used during nanoparticle synthesis. For DSPE-MTX-LIP, the encapsulation efficiency was equal to 79.9 ± 5.6 % (799 ±56 µg), while for PEG-MTX-LIP: 82 ± 7.5 % (820 ±75 µg) and the Combo-LIP: 80.2 ± 1.8 % (802±18µg) as reported in the **Table 2.2**. The direct loading of MTX unmodified molecule into liposomes was extremely difficult due to the extremely poor solubility of the compound both in water and organic solvents as also reported elsewhere [90, 124]. A series of MTX modification based strategies were pursued by other groups in the recent past. For example Guimarães et al.

produced a MTX sodium salt and loaded it into liposomes through the ethanol injection method achieving an EE% equal to 32 % [114]. In another study, Li et al. synthetized a MTX prodrug by conjugating the drug to a phospholipid (PC) achieving a EE% equal to 20.7 ± 2.4% [101]. Our results reveal that the approach proposed in this work, based on the use DSPE-MTX and PEG-MTX, led to achieve a significantly higher EE (around 80%). Such a result represents a considerable step forward in the encapsulation of MTX into liposomes.

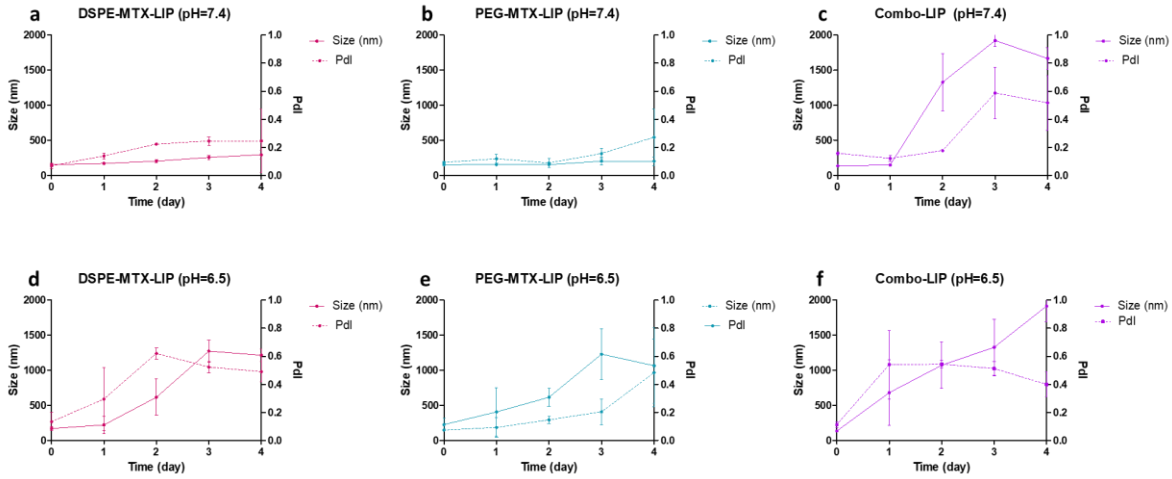

Figure 2.3. a-c) Stability of all the formulations at pH=7.4 and d-f) at pH=6.5.

In order to investigate liposomes stability under the conditions found in vivo (37°C); two buffer solutions were used to reproduce in vitro physiological condition (pH 7.4) and mildly acidic microenvironment (pH 6.5) typical of solid malignant tumors [125], and of inflamed tissues [126, 127]. Liposome size and size distribution were monitored over a period of 4 days. As reported in **Figure 2.3a-c**, both DSPE-MTX-LIP and the PEG-MTX-LIP showed to be stable at 37 ± 2 °C and pH=7.4 with a percentage change in size and PDI lower than 15% for the entire observation period. The Combo-LIP showed an increase in size and PDI already after the first day, indicating a formulation instability, which was also evident for the entire observation period. A different behavior was documented at pH = 6.5 (**Figure 2.3d-f**). All the three liposomal formulations resulted unstable under a slightly acidic environment, with a rapid size increase. DSPE-MTX formulation resulted anyway to be more stable than the other two after one day of observation. In any case, it is possible to conclude that a slight decrease in pH is able to destabilize the three formulations, possibly also leading to a faster release of the prodrugs from

the liposomes. This last consideration might be particularly relevant in vision of using these vectors for the therapy of cancer and other inflammatory diseases MTX is used for. By exploiting the slightly acidic environment, characterizing malignant tumors and inflamed areas, drug release could be fostered in those areas rather than in healthy tissues.

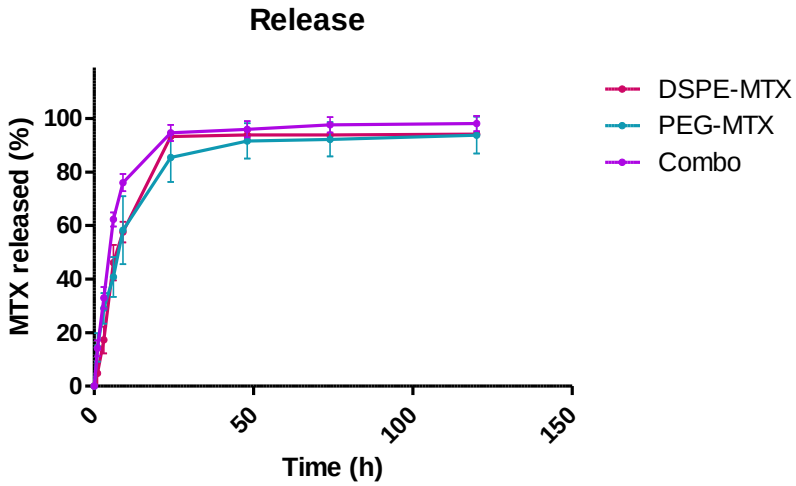

Figure 2.4. In vitro release profile of DSPE-MTX (red line), PEG-MTX (light green line) and their combinations (purple line) from liposomes (A). Data are presented as the average of 3 different experiments ± Standard deviation (SD). In vitro release profile of DSPE-MTX (red line), PEG-MTX (light green line) and their combinations (purple line) from liposomes (A). Data are presented as the average of 3 different experiments ± Standard deviation (SD).

Table 2.3. The R2 values of the zero-order, first-order kinetic, Higuchi models, Korsmeyer-Peppas and Weibull models. Kinetic parameters for the Korsmeyer-Peppas model: K represents the release rate constant; n represents the release mechanism of drug; Kinetic parameters for the Weibull model: a represents a constant based on the system, and b a constant based on the release kinetics.

R^2									
Prodrug	Zero-order	First-order	Higuchi	Korsmeyer-Peppas	Weibull	K	n	a	b
DSPE-MTX	0.9796	0.9824	0.9004	0.9830	0.8905	6.80	0.9931	0.05270	1.3510
PEG-MTX	0.9648	0.9847	0.9821	0.9931	0.9672	13.85	0.64	0.1353	0.8829
DSPE-MTX_PEG-MTX	0.9865	0.9942	0.9638	0.9966	0.9943	13.9	0.7506	0.1350	1.108

MTX-Liposome Release Profiles.

The release profiles of DSPE-MTX, PEG-MTX, and Combo liposomes were determined under infinite sink conditions (4L release volume). Briefly, the three liposomal formulations were placed in 4L of PBS buffer (1X, pH 7.4) at 37 ± 2 °C under magnetically stirring. Three samples for each time point were collected, destroyed with cold methanol, and left to dry. The obtained powder was dissolved in AcN / H2O (1:1, v/v) to release the remaining DSPE-MTX, PEG-MTX for HPLC analysis. The three liposomal formulations showed similar biphasic kinetics with different percentages of drug released (**Figure 2.4**). Specifically, DSPE-MTX and PEG-MTX formulations showed a burst drug release within the first 9 hours, with approximately 60% rapid release. The Combo formulation exhibited a faster release with 75% of DSPE-MTX/PEG-MTX after 9 hours. The faster release was also supported by stability data relative to this formulation (**Figure 2.3c**). Combo liposomes size and polydispersity index increased after 1 day confirming the lower stability of this formulation. The remaining portion of drugs was slowly and continuously released over time, yielding a ~ 95% release after 1 day for Combo and 3 days for both DSPE-MTX or PEG-MTX. The initial phase release under sink conditions is likely associated with drug molecules closer to the particle surface. These molecules diffuse out more rapidly and over a short distance upon exposure to a release medium in vitro or extracellular fluid in vivo. To better understand which kinetic model better described the three different liposomal formulation release profiles, experimental data were fitted on various mathematical models: zero order, first order, Higuchi, Korsemeyer–Peppas and Weibull [128, 129]. The cumulative % drug released versus time, the log cumulative % drug remained versus time, the cumulative % drug released versus the square root of time plot, the log cumulative % drug released versus the log time plot [129] for all the three formulations are reported in **Figure 2.S4-6**. Their correlation coefficient (R2) values are reported in **Table 2.3**. According to data, all the models provided an accurate fitting for the three release profiles, with some differences. All the three formulations followed a Korsemeyer–Peppas law (Highest correlation coefficient R2 value): DSPE-MTX showed a MTX non – Fickian diffusion (super case-II transport mechanism) ($n \geq 0.85$)[130], while PEG-MTX and DPSE-MTX/PEG-MTX a non – Fickian diffusion

(anomalous transport) ($0.43 \leq n \leq 0.85$) [130]. On the contrary, the b value obtained ($b \geq 0.75$) with the Weibull equation suggested a super case-II transport mechanism for all three formulations. Anyway, obtained data suggested that multiple mechanisms, such as diffusion and erosion [131], act simultaneously during the release study for all the three liposomal formulations. This could depend on the different interactions of prodrugs with lipids and PEG-lipids in the liposome structure previously reported for guanosine [132]. Similar non – Fickian diffusion was reported for other drugs delivered using liposomes [133-137].

Liposomes Uptake.

In order to investigate liposomes cell uptake, liposomes were loaded with the tracer molecule DSPE-Cy5. The resulting liposomes (Cy5-LIP) were found to be comparable in size and ζ-*potential* with the other formulation presented in this paper, as shown in **figure 2.S7A**. Their release profile revealed DSPE-Cy5 is slowly released over time (Fig. S7B), indicating this formulation possesses suitable characteristics for imaging purposes. BMDM were treated with Cy5-LIP. Confocal imaging showing Cy5-LIP (red signal) internalized into BMDM is reported in **Figure 2.5a** as the maximum intensity profile of a z-stack. From the figure, liposomes appeared to be within plasma membrane (green signal); the nucleus was stained by DAPI (blue signal). An image reporting each of the acquired channels is presented in **Figure 2.S8**. A high magnification image of one cell was also acquired (**Figure 2.5b**). From this image, it is possible to clearly appreciate that Cy5-LIP were quite uniformly disposed inside cell cytosol. A single cell 3D reconstruction is shown in **Figure 2.5c**. The image reports a reconstruction of the surface for each of the acquired channels. The surface reconstruction confirms Cy5-LIP internalization: in the merged image, a minor Cy5 signal was retrieved on the BMDM membrane, indicating that most of the liposomes were found inside the cell while only a minor portion is on the cell surface, possibly while being uptaken.

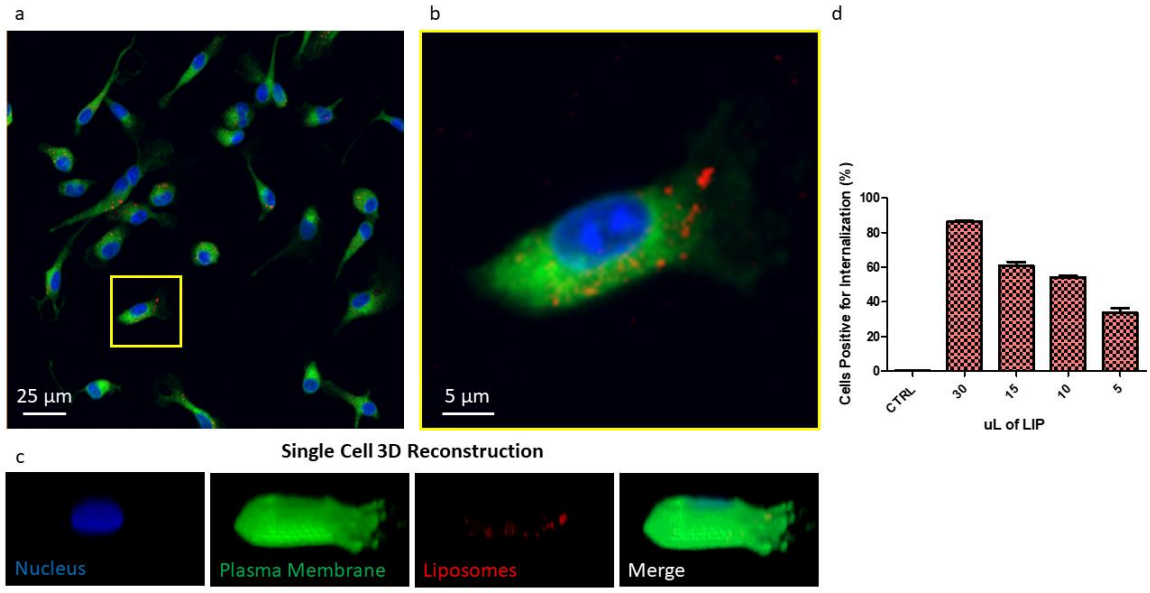

Figure 2.5. a) Image reporting a maximum intensity profile of a z-stack of BMDM treated with liposome reporting in blue the nuclei, in green the plasma membrane and in red the liposomes. b) Higher magnification inset of a single cell. c) Single cell 3D reconstruct. d) Flow Cytometry analysis of BMDM uptaking Cy5-liposomes.

Flow Cytometry analysis reveals the uptake of Cy5-LIP is dose-dependent (**Figure 2.5d**). By increasing the amount of liposomes used for BMDM treatment, also the percent of cells positive for internalization increases. Treating BMDM with 5 µL of Cy5-LIP suspension, 33% of cells were found positive for internalization; The percentage increased to 54.2% and 60.7% when BMDM were treated with 10 µL and 15 µL, reaching its maximum (86.4%) when 30 µL of liposome suspension were used. All the treatments were performed for 30 minutes.

Taken together, these data indicate that liposomes were easily uptaken by BMDM and that at the considered time point, 33% of cells are already positive for internalization when using a small amount of liposomes. Only very few liposomes were found on cell membrane, probably taken in the process of being internalized. These observations confirm that this kind of formulation can easily penetrate cell membrane to deliver its payload (in this case, represented by Cy5, which was used as a tracer). Considering the very low solubility of MTX in its naïve

forms, using a liposomal formulation is thus expected to favor its cell penetration. MTX dispersion inside body fluids, its circulation half-life (as also reported elsewhere [101, 138]) and thus its availability to the biological target [103] is supposed to be improved. Moreover, it is important to underline that liposomes can be easily functionalized with targeting ligands, imaging agents, small molecules, peptides, proteins, antibodies [117] and also aptamers [139]. This versatility should also allow to tailor our MTX liposomes basing on the specific pathology to treat.

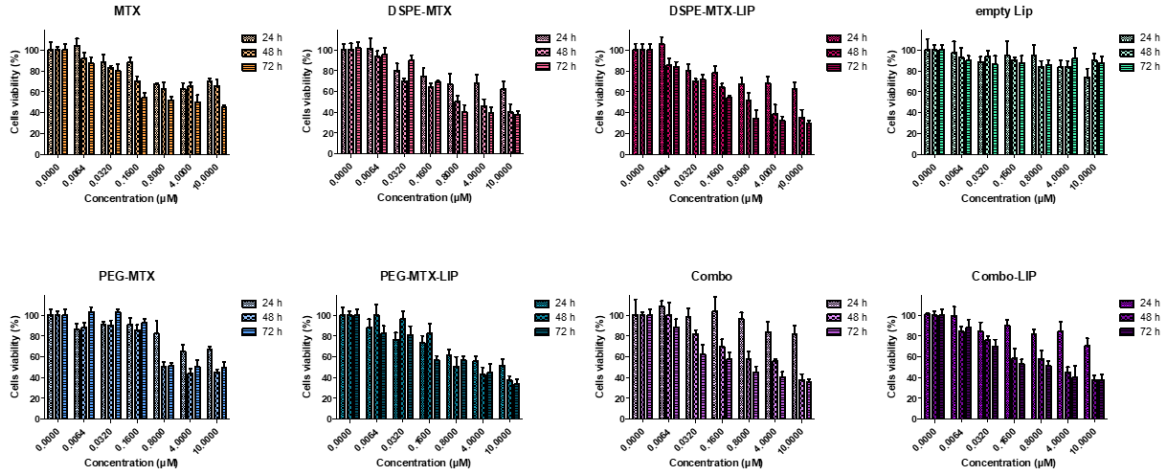

Figure 2.6. Viability of BMDM incubated with MTX, DSPE-MTX, DSPE-MTX-LIP, empty LIP, PEG-MTX, PEG-MTX-LIP, Combo and Combo-LIP a 3 different time points.

Cell cytotoxicity Analyses.

To evaluate the cytotoxicity of the prodrugs and prodrug-loaded-LIP, cell viability was measured using the MTT assay. This assay calculates the reduction of MTT by mitochondrial dehydrogenase to blue formazan product, which reflects the normal function of mitochondria. Hence, the measurement of cytotoxicity and cell viability was obtained. Different concentrations of free MTX, DSPE-MTX and/or PEG-MTX, DSPE-MTX-LIP, PEG-MTX-LIP, and Combo-LIP with a drug concentration ranging from 60 nM to 10 µM were tested on BMDM for different time points, 24, 48, 72 hours. Empty liposomes were tested as a control. For the treatment with free MTX, it is important to note that the molecule was dissolved in DMSO, considering the difficulty of dissolving it in culturing media. Viability plots are presented in **Figure 2.6**. IC_{50} values

calculated at 72 h are reported in **Table 2.4**. MTX IC_{50} was found to be equal to 2.41±0.14 µM. DSPE-MTX, free or loaded into liposomes was found to have a slightly higher toxicity (IC_{50} = 0.9±0.1 µM and 0.7±0.12 µM, respectively). A minor difference in IC_{50} was found for free or loaded PEG-MTX (IC_{50} = 2.5±0.08 µM and 1.6±0.1 µM, respectively). The co-administration of the two prodrugs and the administration of combo liposomes showed an IC_{50} very similar to DSPE-MTX: IC_{50} values for the combo were found as equal to: 0.6±0.1 µM and 0.9±0.1 µM (free prodrugs and combo-LIP, respectively). These results were in agreement with results obtained in other works produced by our group and others [90, 119, 136]. In summary, a slight difference in IC_{50} between MTX, DSPE-MTX, PEG-MTX and the liposomal formulation derived was found. This finding support the hypothesis that the activity of the molecule is possibly maintained, despite the changes operated in the structure.

Table 2.4. Table of IC_{50} showing the viability of BMDM incubated with MTX, DSPE-MTX, DSPE-MTX-LIP, empty LIP, PEG-MTX, PEG-MTX-LIP, Combo and Combo-LIP at 72h.

Sample	IC_{50} 72 h
MTX (µM)	2.41±0.14
DSPE-MTX (µM)	0.9±0.1
DSPE-MTX-LIP (µM)	0.7±0.12
PEG-MTX (µM)	2.5±0.08
PEG-MTX-LIP (µM)	1.6±0.1
Combo (µM)	0.6±0.1
Combo-Lip (µM)	0.9±0.1
Empty Lip (µM)	-

2.5. Conclusions

In the present manuscript, a strategy to efficiently load a high content of MTX into liposomes is presented. Two different prodrugs were generated by binding the compound to DSPE and PEG. The modifications operated to the molecule positively influenced MTX solubility. While the loading of the naïve molecule is particularly inefficient, the two prodrugs can be easily and directly loaded into the liposomes, singularly and in combination. The generated formulations turned out to be comparable in terms of physicochemical features, presenting a similar size of ~155 nm, a narrow size distribution, and a mean surface charge of about –40 mV. At physiologic pH, DSPE-MTX and PEG-MTX liposomes were found more stable than the formulation comprising both the prodrug. At slightly acidic pH all the formulations showed to be unstable after one day of observation. As for the release, all three liposomal formulations showed a biphasic release; both mechanisms of diffusion and erosion are involved in the process, as demonstrated by the mathematical fitting. The data acquired at confocal and by flow cytometry confirmed the suitability of liposomes in granting cell uptake. Considering that DSPE-MTX and PEG-MTX are constituents of the liposomes structure, a higher MTX uptake is expected if compared to the naïve molecule. These considerations, taken together with the benefits offered by liposomal formulations (i.e., extended circulation half-life, favored accumulation at the diseased site), support the potential advantages of MTX liposomes as a safe and efficient drug delivery system for a multitude of disease in which MTX is successfully used.

2.6. Supporting Information

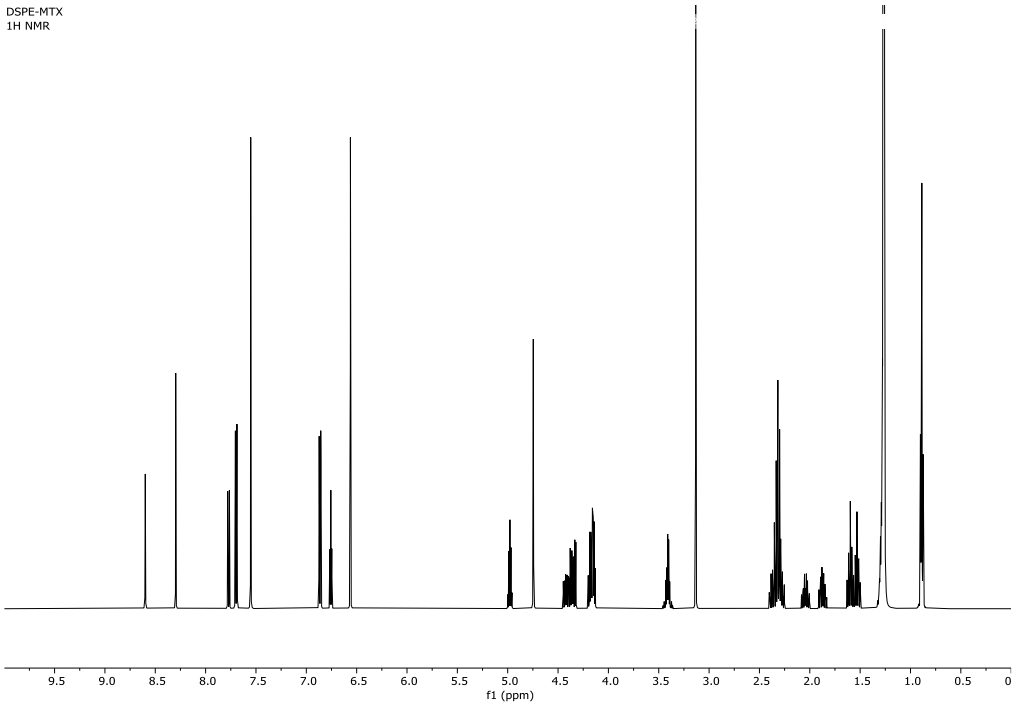

Figure 2.S1. ^{1}H NMR spectrum of DSPE-MTX in CDCl3

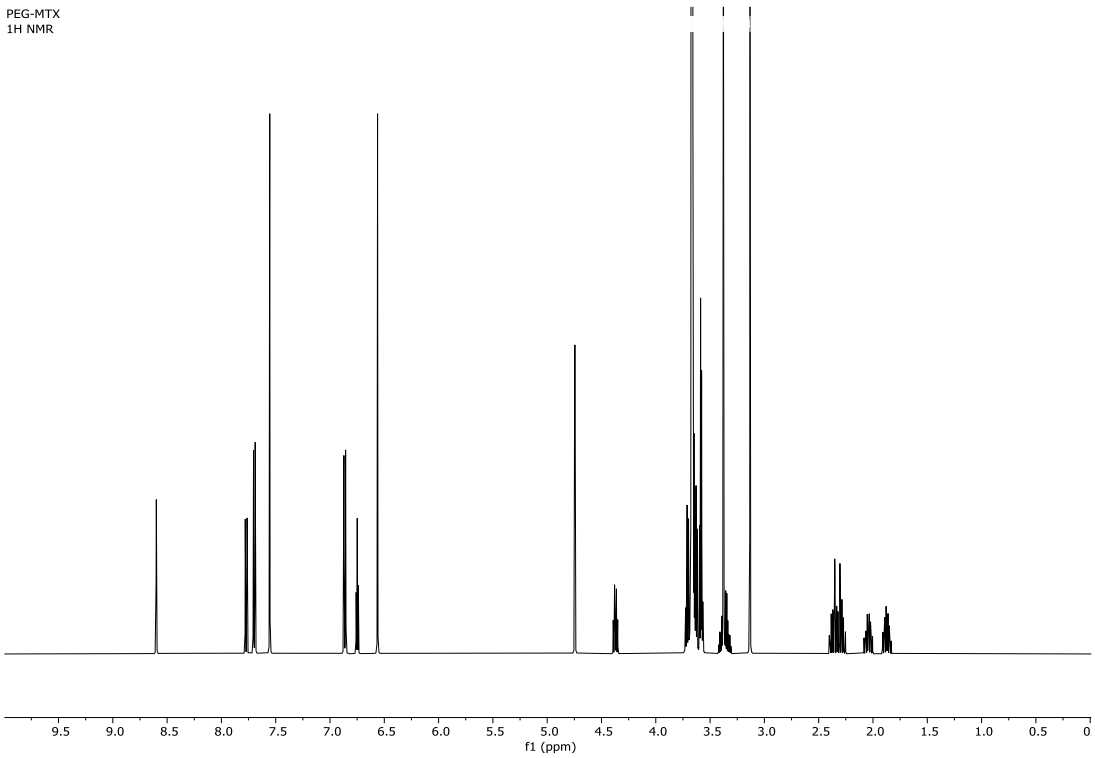

Figure 2.S2. ^{1}H NMR spectrum of $CDCl_3$

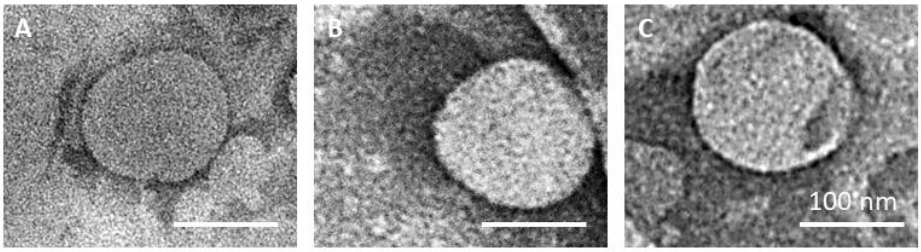

Figure 2.S3. Transmission electron microscopy images of PEG-MTX-LIP, DSPE-MTX-LIP and Combo-LIP, respectively (scale bar: 100 nm).

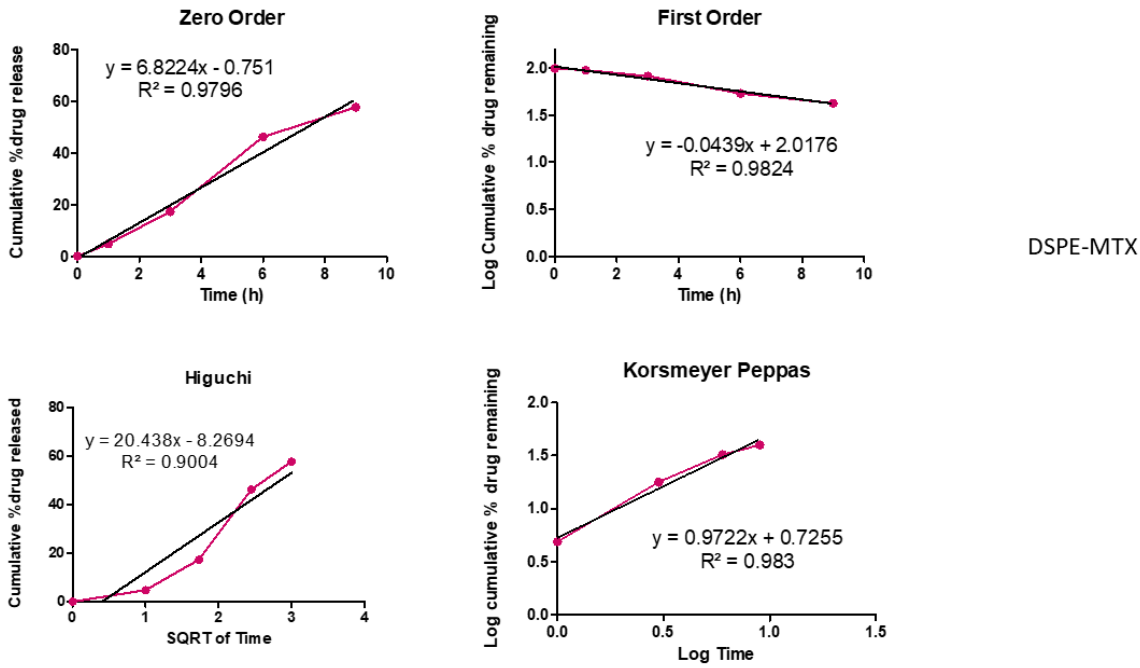

DSPE-MTX

Figure 2.S4. Mathematical models showing the fitting of DSPE-MTX-LIP. Results are representative of three independent experiments ± S.D. (n = 3).

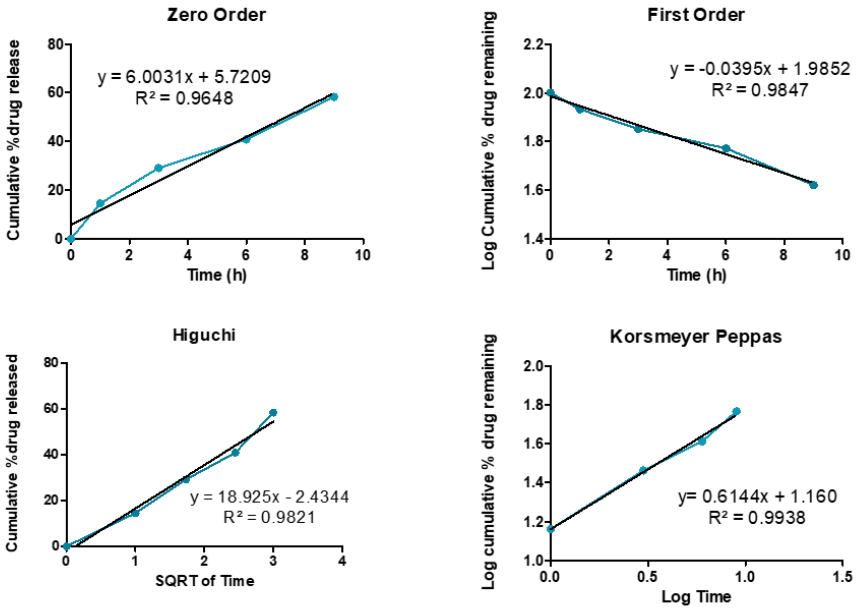

PEG-MTX

Figure 2.S5. Mathematical models showing the fitting of PEG-MTX-LIP. Results are representative of three independent experiments ± S.D. (n = 3).

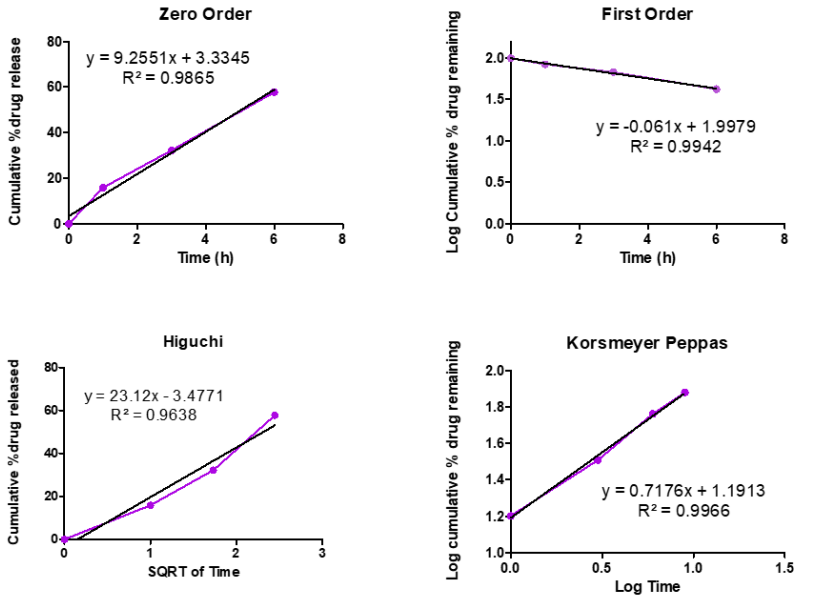

Combo-MTX

Figure 2.S6. Mathematical models showing the fitting of Combo-LIP. Results are representative of three independent experiments ± S.D. (n = 3).

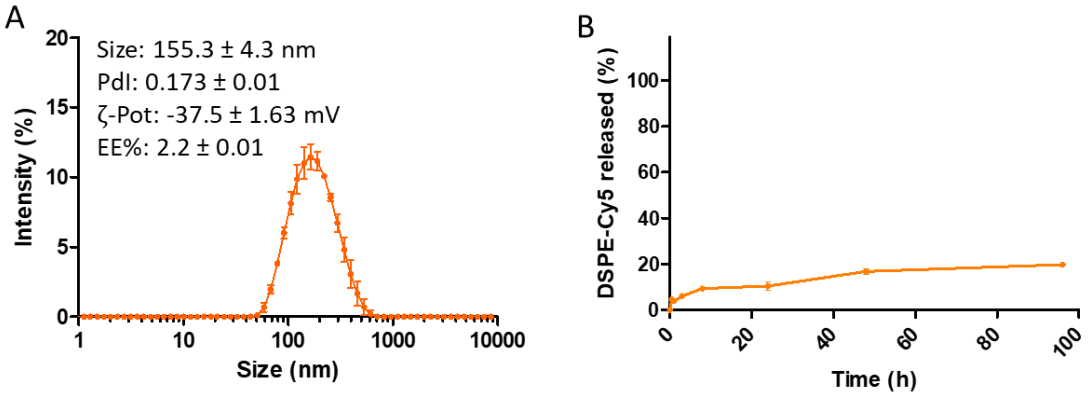

Figure 2.S7. Physico-chemical characterization of Cy5-LIP (A) and DSPE-CY5 release profile (B).

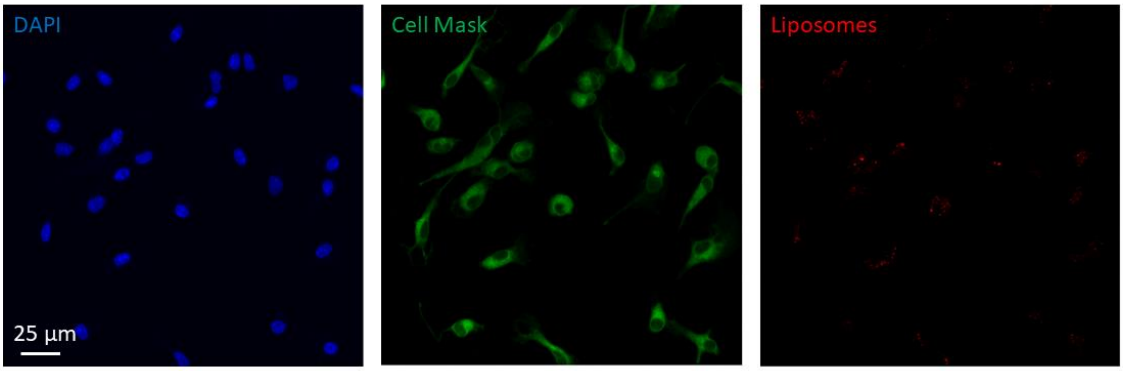

Figure 2.S8. Image reporting a maximum intensity profile of a z-stack of BMDM treated with liposome reporting in blue the nuclei, in green the plasma membrane and in red the liposomes, split channel visualization.

Chapter 3

Modulating Lipoprotein Transcellular Transport and Atherosclerotic Plaque Formation in ApoE–/– Mice via Nanoformulated Lipid–Methotrexate Conjugates

3.1. Abstract

Macrophage inflammation and maturation into foam cells, following the engulfment of oxidized low-density lipoproteins (oxLDL), are major hallmarks in the onset and progression of atherosclerosis. Yet, chronic treatments with anti-inflammatory agents, such as methotrexate (MTX), failed to modulate disease progression, possibly for the limited drug bioavailability and plaque deposition. Here, MTX-lipid conjugates, based on 1,2-distearoyl-sn-glycero-3-phosphoethanolamine (DSPE), were integrated in the structure of spherical polymeric nanoparticles (MTX-SPN) or intercalated in the lipid bi-layer of liposomes (MTX-LIP). Although, both nanoparticles were colloidally stable with an average diameter of ~ 200 nm, MTX-LIP exhibited a higher encapsulation efficiency (> 70%) and slower release rate (~50% at 10h) compared to MTX-SPN. In primary bone marrow derived macrophages (BMDM), MTX-LIP modulated the transcellular transport of oxLDL more efficiently than free MTX mostly by inducing a 2-fold overexpression of ABCA1 (regulating oxLDL efflux); while the effect on CD36 and SRA-1 (regulating oxLDL influx) was minimal. Furthermore, in BMDM, MTX-LIP showed a stronger anti-inflammatory activity than free MTX reducing the expression of IL-1β by 3-fold, IL-6 by 2-fold and also moderately of TNF-α. In 28 days of high-fat-diet fed apoE$^{-/-}$ mice, MTX-LIP reduced the mean plaque area by 2-fold and the hematic amounts of RANTES by half as compared to free MTX. These results would suggest that the nano-enhanced delivery to vascular plaques of the anti-inflammatory DSPE-MTX conjugate could effectively modulate the disease progression by halting monocytes' maturation and recruitment already at the onset of atherosclerosis.

3.2. Introduction

Atherosclerosis is an inflammatory disorder affecting large and medium size arteries and is responsible for acute cardiovascular syndromes, such as myocardial infarction (MI) and stroke. [140] Immune cells play a key role in all the stages of the pathology, from endothelial dysfunction to plaque formation and rupture. [141] Atherosclerotic vascular lesions are established by the continuous infiltration of circulating monocytes into the arterial walls and their progressive maturation into macrophages and foam cells. [142] These are lipid-rich macrophages that have up-taken large amounts of oxidized low-density lipoproteins (oxLDL), mostly through specific surface receptors such as CD36 and SRA-1. [143] Therefore, one strategy to prevent atherosclerotic plaque formation and progression relies on reducing vascular inflammation. [144, 145]

Recently, methotrexate (MTX), which is a potent chemotherapeutic and anti-inflammatory agent, was proposed for the treatment of atherosclerosis in patients affected by chronic inflammatory diseases, such as rheumatoid arthritis and psoriatic arthritis. MTX is known to possess anti-inflammatory properties and is capable to lower the production of pro-inflammatory cytokines by macrophages. [146] MTX has been shown to increase cellular levels of adenosine monophosphate and adenosine, which consequently suppress the secretion of cytokines by immune cells and may protect against ischemic injury. [28] In particular, upregulation of the adenosine receptor limits the formation of foam cells by promoting lipoprotein efflux out of macrophages. [147] Despite all these properties, in the Cardiovascular Inflammation Reduction Trial (CIRT), a low-dose MTX treatment failed to lower secondary cardiovascular event rates. [42] It is important, however, to note that the free molecule MTX is hydrophobic, suffers of low solubility in physiological environments, has a modest half-life in blood, and can induce severe adverse effects, including myelosuppression, neutropenia, infections, thrombocytopenia, and bone marrow suppression. [148]

MTX reformulation into nanoparticles could help in overcoming the above-mentioned limitations thus harnessing the full potential of this drug. Indeed, many groups have investigated the benefits associated with the encapsulation of MTX into liposomes, specifically focusing their attention on the pharmacokinetic parameters. For instance, Chen and coworkers (2019) showed that the plasma concentration of MTX drops rapidly upon intravenous administration being nearly undetectable after only 4h.[27] Conversely, MTX – loaded liposomes provided an over 5-fold increase in circulation half-life and mean residence time and a 16-fold increase in the area under the concentration−time curve (AUC 0-24), as compared to the free molecule.[149] Similar results were also reported by Alekseeva et al. (2017) documenting a 4-fold improvement in drug bioavailability for the MTX-liposomes over the free drug.[150]Also, a few studies have started to show that the atheroprotective properties of MTX can be more effectively exploited by administering nanoparticles loaded with the drug rather than the free molecule. [48, 151] For instance, MTX-loaded polymeric nanoparticles were shown by the authors to mitigate atherosclerotic progression in apolipoprotein-E (apoE)$^{-/-}$ mice, fed with a high-fat diet (HFD). [47] Indeed, accumulation of blood-borne nanoparticles into atherosclerotic plaques would increase the dose of MTX delivered specifically to the inflamed arterial wall, avoiding side effects associated with systemic exposure. Nanoparticles accumulation is supported by different and multiple mechanisms, including the direct nanoparticle uptake by phagocytic macrophages;[152-154] the deposition within the diseased tissue due to favorable, local hydrodynamic conditions (recirculation area and low wall shear stresses), hyper-permeability of a dysfunctional endothelium and increased angiogenesis; [155-159] the direct plaque localization via molecular targeting; [160-163] and the nanoparticle uptake by circulating monocytes that would eventually infiltrate the plaque. [164, 165]

In this work, two different types of nanoparticles – polymeric- and lipid-based nanoparticles – were designed, realized and tested *in vitro* and *in vivo* for the delivery of MTX. Differently from previous works, these nanoparticles were realized using a lipid-MTX conjugate, obtained by reacting MTX with the lipid chain 1,2-distearoyl-sn-glycero-3-phosphoethanolamine (DSPE). These lipid-MTX conjugates would enhance nanoparticle loading and facilitate the intracellular

delivery of the anti-inflammatory molecule. For the polymeric nanoparticles, the DSPE-MTX conjugate was dispersed as a regular payload within the hydrophobic core; whereas for the liposomes, the DSPE-MTX was integrated in the lipid by-layer thus providing both a therapeutic and a structural function. After extensive biophysical and pharmacological characterizations, MTX-loaded Spherical Polymeric Nanoparticles (MTX-SPN) and MTX-loaded Liposomes (MTX-LIP) were tested *in vitro* to demonstrate their ability to modulate oxLDL uptake by macrophages and *in vivo* to assess the atheroprotective efficacy in hyperlipidemic mice.

3.3. Materials and Methods

Materials: Poly(D, L-lactide-co-glycolide) acid terminated (PLGA, lactide:glycolide 50:50, Mw 23,000-25,000 and 38,000-54,000), 1-Ethyl-3-(3-dimethylaminopropyl) carbodiimide (EDC), N-Hydroxysuccinimide (NHS), Triethylamine (TEA), Low-density lipoproteins (LDL) and cholesterol quantitation kit were purchased from Sigma-Aldrich (St. Louis, MO, USA). Methotrexate (MTX) was bought by AlfaAesar (Haverhill, MA, USA). 1,2-distearoyl-sn-glycero-3-phosphoethanolamine-N-[succinyl(polyethylene glycol)-2000] (DSPE-PEG-COOH), 1,2-distearoyl-sn-glycero-3-phosphoethanolamine (DSPE_NH2), 1,2-Dipalmitoyl-sn-glycero-3-phosphocholine (DPPC) were purchased from Avanti Polar Lipid (Alabaster, AL, USA). All reagents and solvents were used without further purification.

Synthesis of DSPE-MTX.

DSPE-MTX was synthesized as reported by Ferreira and coworkers with some modifications. [119] Briefly, MTX was incubated with 1-Ethyl-3-(3-dimethylaminopropyl)carbodiimide (EDC) / N-Hydroxysuccinimide (NHS) in Dimethyl sulfoxide (DMSO) for 30 minutes, at room temperature. A solution of DSPE in DMSO was added to the previous solution. A catalytic amount of triethylamine (TEA) was added to the reaction and left to stir for 72 hours. The mixture was washed with cold diethyl ether. Finally, the conjugate was lyophilized and stored at -20°C. Note that free methotrexate (MTX) is soluble solely in a few organic solvents,

including DMSO and DMF, which are toxic and exhibit a very high boiling point (above 150° C). On the other hand, lipid-MTX can be efficiently separated from an original DMSO solution by using cold diethyl ether and readily used to synthesize particles without employing DMSO or DMF.

Synthesis of SPNs.

Spherical Polymeric Nanoparticles (SPNs) were synthesized by a sonication-emulsion technique method, as described elsewhere. [166] Briefly, carboxyl terminated poly(lactic-co-glycolic acid) (PLGA), DSPE-MTX and 1,2-dipalmitoyl-sn-glycero-3-phosphocholine (DPPC) were dissolved in chloroform in a 5:2:1 ratio to obtain an homogeneous solution (oil phase). The aqueous phase was prepared by dissolving 1,2-distearoyl-sn-glycero-3-phosphoethanolamine-N-[carboxy(polyethylene glycol)-2000 (DSPE-PEG-COOH) in 4% ethanol. Then, the oil phase was added drop wisely to the aqueous phase under ultrasonication (100% amplitude for 1 min and 30 sec). The obtained emulsion was then placed under magnetic stirring to facilitate solvent evaporation. SPNs were centrifuged, first, for 5 min at 1,500 rpm to settle down any possible debris, and then the supernatant was centrifuged 3 more times for 20 minutes at 12,000 rpm. The pellet were washed in water after every centrifugation step. Different SPN formulations were synthetized.

In order to label the SPNs with the near infra-red dye Cy5. A DSPE-Cy5 (0.002mg) was used instead of DSPE-MTX.

Synthesis of MTX-LIP.

Liposomes (LIP) were prepared by thin layer evaporation (TLE). [167] Briefly DPPC, cholesterol, DSPE-PEG and DSPE-MTX were dissolved in chloroform in a round bottomed flask (ratio 6:3:1:1). The thin layer lipid film was obtained with the evaporation of the organic solvent at 60° under reduced pressure. The lipid film was left under the hood overnight to remove any trace of residual solvent. For the production of the multilamellar liposomes, the lipid film was hydrated with 2 mL of HEPES and then subjected to three alternate cycles (3 min

each) of warming at 60 °C (thermostated water bath) and vortexing at 700 rpm. The sample was dialyses against HEPES for 1h. For the preparation of Cy5-LIP, DSPE-Cy5 was used instead of DSPE-MTX. The purification step to remove excess of Cy-5 was conducted by ultracentrifugation (1h, 45,000 rpm) instead of dialysis. For the preparation of ^{64}Cu-LIP, 20% w/w of DSPE-PEG was replaced with lipid-DOTA. LIP were obtained using the previous method. DOTA-LIP were then resuspended in 3 mL was water, and 200 µL of Acetate buffer (1mM, pH=6.0) and conjugated with $^{64}CuCl_2$ (1 mCi) solution for 2h at 37°C. The excess of radioactive was removed by dialyses against PBS for 1h.

Characterization of LIP and SPNs.

Liposomes were fixed for 2 h in 2% glutaraldehyde in 0.1 M cacodylate buffer. After fixation, the samples were washed twice with the same buffer and post fixed for 1h in 1% osmium tetroxide in 0.1 M cacodylate buffer. After several washes with distilled water, samples were subsequently dehydrated in a graded ethanol series, 1:1 ethanol:hexamethyldisilazane (HMDS), and 100% HMDS and dried overnight. Samples were sputtered using gold. SEM images were collected using JEOL JSM-7500FA (Jeol, Tokyo, JAPAN) operating at 5 kV of accelerating voltage. For SPNs, a drop of nanoparticle solution was deposited on a silicon wafer, dried and mounted on a stab for SEM analysis. The hydrodynamic diameter, polidispersity index and surface electron ζ-potential of LIP and SPNs were measured using dynamic light scattering (DLS, Malvern Nano ZS).

Drug loading and release.

To measure the MTX encapsulation efficiency (EE) and loading efficiency (LE), the samples were lyophilized, dissolved in acetonitrile/H2O (1:1, v/v), and analyzed by high-performance liquid chromatography (HPLC) (Agilent 1260 Infinity, Germany) equipped with a 100 µL sample loop injector. A C18 Column (2.1× 250 mm, 5 µm particle size, Agilent, USA) was used for the chromatographic separation. MTX was eluted under isocratic conditions using a binary solvent

system [H2O + 0.1% (v/v) TFA, 43:57 v/v] pumped at a flow rate of 1.0 mL/min. The ultraviolet (UV) detection was set at 430 nm.

EE and LE were determined using the following equations:

$$EE\ (\%) = \frac{MTX\ weight\ in\ particles}{MTX\ inizial\ feeding\ amount} \times 100 \qquad (1)$$

$$LE\ (\%) = \frac{MTX\ weight\ in\ particles}{Total\ weight\ of\ the\ particles} \times 100 \qquad (2)$$

To study MTX and Cy5-release kinetics, 200 µL of MTX-nanoparticle (SPN or LIP) or Cy5-nanoparticles (SPN or LIP) solution were placed into Slide-A-Lyzer MINI dialysis microtubes with a molecular cutoff of 10 kDa (Thermo Scientific) and dialyzed against 4 L of PBS buffer (pH 7.4). For each time point, three samples were collected and dried. For the SPNs, samples were then dissolved in acetonitrile/H2O (1:1, v/v) and analyzed by HPLC. For LIP samples were destroyed with cold methanol, left to dry, dissolved in acetonitrile/H2O (1:1, v/v) and analyzed by HPLC for the MTX. The experimental data were fitted by using the Ritger–Peppas model for controlled, not swellable drug-delivery systems 52 ($Y = k \times x^n$), where Y represents the drug percentage released, x is the time of observation, and k and n are the fitting parameters.

In the case of Cy-5, after LIP destruction samples were dissolved in acetonitrile and analyzed by the spectrophotometer at ʎ=640 nm. For 64Cu release, LIP were analyzed at the γ-counter. The data was normalize taking into account the decay of 64Cu.

LDL oxidation.

LDL (2 mg/ml) were incubated with 5 mM CuSO4 at 37°C for 4h without EDTA. The reaction was interrupted with the addition of EDTA (5 mM). The formed oxidized LDL molecules (oxLDL) were dialyzed against PBS containing 0.01% EDTA at 4°C for 24 h and stored at 4°C. [168] The fluorophore 1,1′-Dioctadecyl-3,3,3′,3′-tetramethylindocarbocyanine perchlorate (Dil) was

used for fluorescently tagging the lipoprotein following a previously published protoCol. [169] Briefly, Dil was pre-incubated with LDL overnight at 37°C under agitation. Dil-LDL were then oxidized and ultracentrifuged for 5 h at 45,000 rpm and 4° in order to remove unbound fluorophore. The obtained Dil-oxLDL were dialyzed against PBS containing 0.01% EDTA at 4°C for 24 h and stored at 4°C.

Bone Marrow Derived Macrophages.

For Bone Marrow Derived Macrophages (BMDM), rat femurs were explanted and the extremities were cut off. Then, the bone marrow canal was flushed four times with 500 µL of medium. The resulting cell suspension was filtered using a 70 µm cell strainers. Cells were seeded in a Petri dish and medium was changed after 3 days to remove unattached cells. BMDMs were used on the following day. BMDMs were cultured in DMEM supplemented with 15% FBS, 1% penicillin/streptomycin, and rat M-CSF (according to vendor indications). Cells were cultured under controlled environmental conditions (37°C in 5% CO2).

Foam Cell formation and Cholesterol Quantification.

BMDM/Raw 264.7 cells were cultured in DMEM containing, respectively, 15% and 10% fetal bovine serum (FBS), 1% antibiotic (penicillin/streptomycin) and 1% glutamine. Cells were seeded at a density of $1x10^5$ cells/mL. For foam cells formation different amount of oxLDL were tested (0, 20, 50 and 80 µg/mL of oxLDL). Macrophages were incubated with oxLDL overnight, the medium was removed and cells were washed twice with PBS and fixed with a solution of paraformaldehyde 3.7% (PFA). Macrophages were incubated with isopropanol and Oil Red O (ORO) working solution for 10-20 minutes. Cells were observed at the microscope (Leica 5500) and images were acquired with a 20X magnification. [170]

Confocal Fluorescent Microscopy imaging.

Confocal images of RAW 267.4 were obtained using a Nikon-A1 confocal microscope (Nikon Corporation, Japan). Free Dil or Dil-oxLDL (0.15 mg Dil: 6.5 mg LDL) were incubated with

macrophages overnight. 50,000 cells (either Raw267.4 or BMDM) were seeded into each well of a Nunc™ Lab-Tek™ II Chamber Slide™ System (Thermo Fisher Scientific, USA) maintaining culturing conditions, as described for foam cell formation and cholesterol quantification protoCol. After 14 h, the culturing media was removed and cells were washed in PBS (Thermo Fisher Scientific, USA). Fixation was performed using a 3.7% solution of PFA (Sigma Aldrich, USA) for 5 minutes. Lysosomes were stained with LysoTracker™ Green (Thermo Fisher Scientific, USA) and nuclei with DAPI (Thermo Fisher Scientific, USA) following the vendors' indications. A z-stack section was acquired using a 60X objective (≥ 12 steps of 1,000 nm each were acquired per image).

Time Lapse Microscopy Analysis.

For time lapse microscopy experiment, 20,000 BMDMs were seeded into a Nunc™ Lab-Tek™ II Chamber Slide™ System (Thermo Fisher Scientific, USA). Same experimental conditions were used: BMDMs were incubated overnight with 50 µg/mL Dil-oxLDL and an equal amount of Dil. The experiment was performed using a Nikon Eclipse-Ti-E microscope (Nikon Corporation, Japan). During the image acquisition cells were kept in controlled environmental conditions: 37 °C in a humidified 5% CO2 atmosphere. Movies were acquired at a frame rate of 80fps using a 60X objective.

Analysis of Dil-oxLDL uptake and expulsion. After inducing the transformation of BMDM in foam cells with Dil-oxLDL, cells were treated for 24 h with 0.16 µM of free MTX, empty nanoparticles and MTX-nanoparticles. At the end of the treatment, the medium was removed and cells were washed twice with PBS. Cell fixation was performed using a 3.7% solution of PFA (Sigma-Aldrich, USA) for 15 min. Actin was stained with Alexa Fluor™ 488 Phalloidin (Thermo Fisher Scientific, USA) and nuclei with DAPI (Thermo Fisher Scientific, USA), following the vendors indications. Data were analyzed with ImageJ.

Cholesterol quantification.

BMDM total cholesterol (free cholesterol and cholesteryl ester) was quantified using a Cholesterol Quantitation Kit (Sigma-Aldrich, Italy), following the manufacturer's instruction. Firstly, cells were treated with oxLDL, then with free MTX and MTX loaded-nanoparticles as described previously. Cholesterol quantification was normalized on the total amount of protein calculated using Pierce Brentford Protein Assay Kit (thermos Scientific).

TEM Characterization:

Transmission electron microscopy (TEM) micrographs were acquired using JEOL JEM 1011 (Jeol, Japan) electron microscope operating with an acceleration voltage of 100 kV and recorded with a 11 MegaPixel fiber optical charge-coupled device (CCD) camera (Gatan Orius SC-1000). LDL was diluted 1:100, dropped on 150-mesh glow discharged 'Ultrathin' carbon-coated Copper TEM grids and dried. Dried TEM samples were negatively stained using 2% Uranyl Acetate aqueous solution. In order to observe LDL uptake in foam cells, RAW 264.7 cells were cultured and treated on glass coverslips. Samples were fixed for 2 h in 1.5% glutaraldehyde in 0.1 M Sodium Cacodylate buffer (pH 7.4), post fixed in 1% osmium tetroxide in the same buffer and stained overnight with 1% uranyl acetate aqueous solution. Samples were then dehydrated in a graded ethanol series, infiltrated with series of ethanol/resin solution and finally embedded in epoxy resin (Epon 812, TAAB). Thin sections were cut with the Leica UC6 ultra-microtome (Leica Microsystems, Germany), equipped with a diamond knife (Diatome). In order to better localize the fluorescent LDL molecules inside cells, LDL uptake in foam cells was investigated by means of Correlative Light and Electron Microscopy. Foam cells were cultured and treated on grid-etched glass coverslips. After fluorescence microscopy observation, samples were fixed for 1.5 h in 4% paraformaldehyde (PFA), 0.2% Glutaraldehyde solution prepared in 0.1 M Phosphate Buffer. Fluorescence images were acquired using a Nikon-A1 confocal microscope (Nikon Corporation, Japan). Dil-oxLDL was used for the treatment. The nuclei were stained with DAPI and the lysosomes with the LysoTracker™ Green (Thermo Fisher Scientific, USA). After fluorescence observation, foam cells were processed

for TEM analysis as described above, using reference marks. Image analysis and merging were performed using the PhotoShop image processing software.

Gene expression and toxicity.

BMDMs were cultured at 37°C in 5% CO2, in high-glucose DMEM, supplemented with 15% FBS and 1% L-glutamine, according to ATCC instructions. Cells were seeded into 96-well plates at a density of 20 × 103 cells per well and incubated for 24, 48, 72 h. Cells were treated with different concentrations of free MTX, DSPE-MTX, MTX-SPNs, MTX-LIP (namely, 0.0064, 0.032, 0.16, 0.8, 4, 10 and 0 μM of MTX), or empty SPNs/LIP. The MTT solution was added for 4 h and the formed formazan crystals were dissolved in ethanol. Absorbance was measured at 570 nm, using 650 nm as the reference wavelength (Tecan, Männedorf, Swiss). The percentage of cell viability was assessed according to the following equation:

$$Cell\ viability\ (\%) = \frac{Abs_T}{Abs_C} \times 100 \qquad (3)$$

where Abs_T is the absorbance of treated cells and Abs_C is the absorbance of untreated cells (control).

The anti-inflammatory effects of MTX, MTX-SPNs and MTX-LIP was tested on foam cells at 8 and 24 h by measuring gene expression of three pro-inflammatory cytokines, namely tumor necrosis factor- α (TNF-α), interleukin-1β (IL-1β), and interleukin-6 (IL-6) in rat BMDMs.

The gene expression of foam cells markers (CD36 and SRA-1) and cholesterol expulsion ATP-binding cassette transporter 1 (ABCA1) was also assessed. Cells were cultured under controlled environmental conditions (37 °C in 5% CO2) and seeded into 6-well plates at a density of 4 × 105 cells per well. After 10 h, BMDMs were incubated with oxLDL overnight. Cells were treated with MTX-nanoparticles at 0.16 μM of MTX and incubated for 8 and 24 h. RNA was extracted using a RNAeasy Plus Mini Kit (Qiagen) and quantified by NanoDrop2000 (Thermo Scientific, Waltham, Massachusetts, USA). Three independent biological replicates were run using a Power SYBR Green RNA-to-CT 1-Step Kit (Applied Biosystems) and using

GAPDH gene expression as a housekeeping gene. Reactions were performed in a final volume of 10 µL. Primer pair sequences are listed below: GAPDH: 5′-CATCACTGCCACCCAGAAGACTG-3′ and 5′-ATGCCAGTGAGCTTCCCGTTCAG-3′; TNF-α: 5′-GGTGCCTATGTCTCAGCCTCTT-3′ and 5′-GCCATAGAACTGATGAGAGGGAG-3′; IL-1β: 5′-AACCTGCTGGTGTGTGACGTTC-3′ and 5′-CAGCACGAGGCTTTTTTGTTGT-3′; IL-6: 5′-TACCACTTCACAAGTCGGAGGC-3′ and 5′-CTGCAAGTGCATCATCGTTGTTC-3′; CD36: 5′-ATGGGCTGTGATCGGAACTG-3′ and 5′-GTCTTCCCAATAAGCATGTCTCC-3′; SRA-1: 5'-CTGAGACCTCTGGAACAGGCAT-3' and 5′-TGCACTAGCAGTGCCATCCTCT-3′; ABCA1: 5′-GGAGCCTTTGTGGAACTCTTCC-3′ and 5′- CGCTCTCTTCAGCCACTTTGAG-3′.

Internalization study.

Flow cytometry was performed using a FACS ARIA (Becton Dickinson, USA). 200,000 macrophages/foam cells were seeded into each well of a 12 well plate maintaining culturing conditions indicated in foam cell formation and cholesterol quantification protoCol. Cells were treated for 2, 8 and 24h with Cy5-LIP and Cy5-SPNs. After treatment, cells were washed using cold PBS in order to facilitate the scraping procedures. After washing, a volume of 200 µl of PBS was used to detach the cells by gentle scraping the plastic bottom. Samples were immediately stored in ice and vortexed right before the analysis. A cell population was selected setting a scatter gate that would exclude the negligible amounts of debris and aggregates while taking into account the side scatter (SSC) shift due to internal complexity changes caused by the internalized particles. The cell population positive for internalization was selected considering the basal level of fluorescence in untreated cells.

Animals.

B6.129P2-Apoe(tm1Unc)/J (apoE$^{-/-}$) mice were bred in-house (Central Research Facility, University of Glasgow). Animals were maintained on a 12/12-h light/dark cycle with free access to food and water. All the procedures were performed in accordance with local ethical and UK Home Office regulations. Twelve-week-old male apoE$^{-/-}$ mice were fed with high-fat diet (HFD)

(Western RD diet, 21% fat, 0.2% cholesterol, supplemented with 150 ppm fenbendazole, Diet code: 823963 - Special Diet Services, Essex, UK) for 28 days. Empty or MTX-LIP (2.5 mg/kg) were injected intravenously (i.v.) administered starting from day 0 every third day. Mice were culled at 28 days and samples processed as described below. At the end of the experimental protoCol mice were perfused with ice cold PBS; the heart was embedded in Tissue-Tec OCT (Tissue Tek, Sakura Finetek Europe, Zoeterwoude, The Netherlands), frozen at -80°C, and sectioned (10 μm). Aortic sinus sections were stained with oil red O counterstained with hematoxylin. Picrosirius red viewed with polarized light was used to detect Collagen. For each animal, 10 sections were analyzed to determine atherosclerotic lesion size and 4 section were analyzed to determine the Collagen content, as previously described. [171] The analyses were carried out using Image J software (National Institutes of Health Imaging; http://rsbweb.nih.gov/ij), and the results are expressed as mean lesion area and mean percentage Collagen area.

Cytokine Detection Assays.

Concentrations of eotaxin, fibroblast growth factor-basic, granulocyte-macrophage Colony-stimulating factor, IFN-γ, interleukin (IL)-1α, IL-1β, IL-2, IL-3, IL-4, IL-5, IL-6, IL-9, IL-10, IL-12 (p40), IL-12 (p70) IL-13, IL-17A, KC, monocyte chemoattractant protein-1, macrophage inflammatory protein-1α, macrophage inflammatory protein-1β, RANTES (Regulated on Activation, Normal T Cell Expressed and Secreted), tumor necrosis factor-α were assessed in serum using a Bio-Plex Pro™ Mouse Cytokine 23-plex Assay, according to the manufacturer's instructions (Bio-Rad), and analyzed using a Bio-Rad Luminex 200 Plate Reader (Hemel Hempstead, United Kingdom). Data were analyzed using Bio-Plex 6.1 software with 5PL curve fitting.

Immunohistochemical Analysis.

To determine nanoparticles distribution, apoE$^{-/-}$ mice were culled 24 h after the final injection of fluorescent Cy-5-LIP (the amount of particle used was equivalent to the one used for one injection of MTX-LIP). The aortic sinus, spleen, kidney and liver were dissected, embedded in

OCT (Tissue Tek, Sakura Finetek Europe, Zoeterwoude, the Netherlands) and snap frozen for immunohistochemical analysis. 10 µm sections were cut. For staining, sections were fixed in acetone for 10 min, air dried, and rehydrated with PBS before incubation in serum-free Protein Block (DakoCytomation, Glostrup, Denmark) for 30 min. Aortic sinus sections were incubated with FITC-conjugated anti-α-SMA antibodies. Hoechst was used to identify nuclei as previously described. [172] Images were acquired using a Zeiss Cell Observer SD confocal microscope (Zeiss, Oberkochen, Germany).

Serum lipid analysis.

Measurements of mouse blood total cholesterol levels were performed with the Cholesterol/Cholesteryl Ester Quantitation kit (ab65359, Abcam, Toronto, ON) according to the manufacturer's instructions.

Biodistribution of LIP in Naïve Mice.

LIP labeled with Cu64 were injected in 5 naïve mice (C57BL/6). At 24h post injection, the mice were sacrificed and the major organs (liver, spleen, kidneys, intestine, brain, lungs and heart) explanted and analyzed for their radioactive activity at the γ-counter. The data were then normalized for the weight of the organs.

Statistical Analysis.

All the in vitro data were represented as the average ± standard deviation (SD) of 3 different measurements, unless differently specified. The statistical significant difference was assessed using ANOVA test, with Bonferroni's Multiples Comparison Test as post-hoc test. All statistical in vitro analyses were performed using GraphPad Prism v.5 (GraphPad Software, USA). In vivo results are expressed as mean ± SEM of the number of animals. Normality distribution was tested and Student t-test was used to compare 2 groups. All statistical in vivo analyses were performed using GraphPad Prism v.7 (GraphPad Software, USA). A p value ≤ 0.05 was considered statistically significant.

3.4. Results

Physico-chemical and pharmacological characterization of MTX-loaded nanoparticles.

Methotrexate (MTX) is a potent anti-inflammatory molecule with a low solubility in physiological fluids [173] and a modest half-life in blood. [174] The formulation of MTX into nanoparticles can overcome the limitations above, thus harnessing the full potential of this drug. Two different nanotechnological platforms –Spherical Polymeric Nanoparticles (SPN) and Liposomes (LIP) – were considered for the systemic delivery of methotrexate. The MTX-SPN were realized via a single emulsion technique resulting in a PLGA hydrophobic core that is externally stabilized by a lipid monolayer, including carboxyl-terminated DSPE-PEG molecules (**Figure 3.2A**). The MTX-LIP were realized via a thin layer evaporation method (TLE) using DPPC, cholesterol and carboxyl-terminated DSPE-PEG chains (**Figure 3.2B**). The anti-inflammatory molecule MTX was included in the structure of the two nanoparticles in the form of a DSPE-MTX conjugate (**Figure 3.S1**). This was generated by reacting 1,2-distearoyl-sn-glycero-3-phosphoethanolamine-N-amino (DSPE-NH_2) with a DCC/NHS pre-activated MTX. The resulting DSPE-MTX conjugate is highly lipophilic and was included within the hydrophobic PLGA core and surface stabilizing lipid layer of SPN and, for the LIP, it was integrated naturally in the double lipid layer.

Scanning electron microscopy images of MTX-SPN and MTX-LIP are provided in **Figure 3.1C** and **1D**, respectively. The top right insets provide magnified views of the same nanoparticles. The electron microscopy analysis demonstrates the sphericity and uniform size distribution of both MTX-loaded nanoparticles exhibiting a diameter in the neighbor of 200 nm. More precisely, a Dynamic Light Scattering analysis returned an average hydrodynamic diameter of 208 $\pm$ 2 nm and 174 $\pm$ 2 nm for the MTX-SPN and MTX-LIP, respectively (**Figure 3.1E**). Both nanoparticle formulations were characterized by a moderate polidispersity index PDI $\sim$ 0.15, in agreement with the electron microscopy observations. Given the presence of carboxyl-terminated DSPE-PEG chains, both nanoformulations presented a negative surface

electrostatic ζ potential of - 45 ± 0.02 mV for the MTX-SPN and - 38 ± 0.26 mV for the MTX-LIP. These values are also listed in the table included in **Figure 3.1E**.

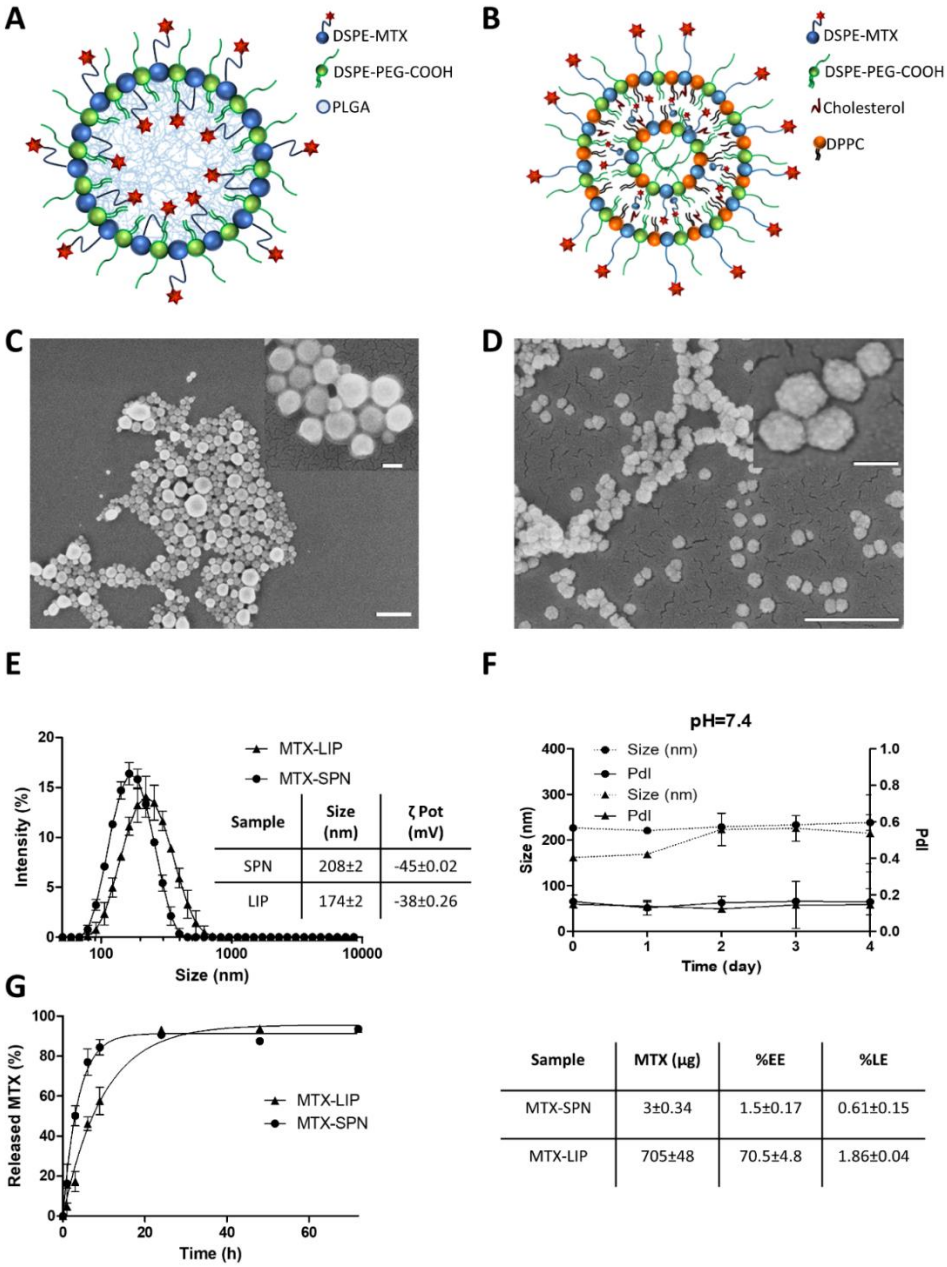

Sample	MTX (μg)	%EE	%LE
MTX-SPN	3±0.34	1.5±0.17	0.61±0.15
MTX-LIP	705±48	70.5±4.8	1.86±0.04

Figure 3.1. A., B. Schematic representation of MTX-SPN and MTX-LIP, respectively. C., D. Scanning electron microscopy images of SPN and LIP, respectively (Scale bar: 500 nm; up-right inset scale bar: 100 nm). E., F. Hydrodynamic diameter and colloidal stability of MTX-SPN and MTX-LIP via dynamic light scattering analysis. G. Release studies for MTX from MTX-SPN and MTX-LIP. The table summarizes the absolute drug mass, encapsulation efficiency (%EE), and loading (%LE) data for MTX into MTX-SPN and MTX-LIP.

For both nanoformulations, Colloidal stability tests were performed under physiological conditions at pH = 7.4 and in a slightly acidic environment with a pH = 6.5. The average hydrodynamic diameters and PDI of both nanoparticles were monitored up to 4 days. Under physiological conditions, the data in **Figure 3.1F** show very stable formulations with a percentage change in size and PDI lower than 10% through the entire observation period. Differently, at pH = 6.5, the data in **Figure 3.S2** present a steadily growing size for both MTX-LIP and MTX-SPN most likely resulting from the progressive rearrangement of the Colloidal solution. Overall, however, the MTX-LIP resulted to be more stable than the MTX-SPN. It is here important to recall that the conjugate in the MTX-LIP provides also a structural contribution in addition to the pharmacological function in that it is directly included into the double-lipid layer of the liposomes.

Next, High Performance Liquid Chromatography (HPLC) was employed to measure the loaded and released amounts of MTX from the two nanoformulations. MTX encapsulation efficiency EE was evaluated as the percentage ratio between the actual loaded mass of the drug and the input mass of the drug during nanoparticle realization. For the MTX-LIP, a significantly high EE was measured to be equal to 70.5 ± 4.8%, whereas this value dropped to only 1.5 ± 0.7% for the MTX-SPN, with a total mass of the loaded DSPE-MTX corresponding to 705 ± 48 and 3 ± 0.34 μg per single nanoparticle preparation, respectively. The MTX-loading was 1.86 ± 0.04% for LIP and 0.61 ± 0.15% for the SPN. The modest drug loading associated with the SPN is in line with previous data from the authors on other hydrophobic drug molecules.[175] Note that, in the MTX-LIP, the DSPE-MTX conjugate can intercalate with the DPPC and DPSE-PEG chains in forming the liposome double-lipid membrane. This increases significantly the amounts of drug that can be incorporated into the particles. The release profiles for MTX from SPN and LIP were determined in a 4 L PBS solution (infinite sink condition) and are plotted in **Figure 3.1G**. MTX was more rapidly released from the SPN as compared to the LIP. At 9 h post study initiation, over 80% of the drug was released out of the SPN, whereas about 50% came out of the MTX-LIP. After 1 day, almost 90% of the encapsulated MTX was released from both nanoparticles. At later time points, the release profiles reached a plateau close to 100%.

Indeed, the higher stability of MTX-LIP over MTX-SPN is also shown by the overall lower MTX release rates associated with the former particles.

It is here important to note that the EE = 1.5 ± 0.7% for the SPN results from an extensive and systematic optimization process that led to define 12 different MTX-loaded SPN formulations with the final objective of improving drug loading in these particles. From the data listed in the **Figure 3.S3**, the following parameters were changed in the synthesis of SPN: total mass of PLGA, ranging from 0.5 to 2 mg; molecular weight of PLGA, varying from low (23-35 kDa) to high (38-53 kDa); and the ratios between DPPC, DSPE-PEG and DSPE-MTX. The resulting encapsulation efficiency varied from a minimum of 0.13% to a maximum of 1.5%. In the rest of the manuscript, MTX-SPN are referred as realized with 2 mg of high molecular weight PLGA, no DPPC, 0.2 mg of DSPE-MTX and 0.11 mg of DSPE-PEG.

Macrophage Maturation to Foam Cells and Nanoparticle Uptake.

Foam cells were obtained by feeding macrophages with oxidized low-density lipoproteins (oxLDL). The continuous accumulation of these ~ 20 nm oxidized lipid particles into macrophages is responsible for their maturation into foam cells, which is a fundamental step in the progression of atherosclerotic plaques.

LDL oxidation was performed using copper salts (CuSO4) and two different cell types were exposed to oxLDL, namely the murine cell line Raw 264.7 and the primary Bone Marrow Derived Macrophages (BMDM) isolated from the femur of rats. First, the dose-dependent engulfment of oxLDL molecules into phagocytic cells was assessed. To this end, Raw 264.7 were incubated overnight with different amounts of oxLDL, namely 0, 20, 50 and 80 µg/ml, and then stained with Oil Red O (ORO). In **Figure 3.S5**, the fluorescent intensity associated with the ORO staining is shown to grow proportionally with the initial amount of oxLDL. An intermediate concentration of 50 µg/ml oxLDL was considered as appropriate for all foam cell experiments.

Then, the precise intracellular localization of oxLDL molecules was assessed via Correlative Light and Electron Microscopy (CLEM). [176] This technique allowed the authors to co-register together data from fluorescent confocal microscopy and transmission electron microscopy. For

the fluorescent microscopy experiments, the DiI dye was stably adsorbed onto oxLDL (**Figure 3.S6 and Supplementary Videos**), while macrophages were treated with 488-lysotracker and DAPI to highlight the lysosomes and nuclei, respectively. **Figure 3.2A** shows a transmission electron micrograph (left) and a confocal fluorescent image (center) of a representative foam cell, obtained by feeding RAW 264.7 cells overnight with 50 µg/ml oxLDL. In the right inset of the same image, the TEM and confocal images were registered and combined together. These figures demonstrate a massive localization of oxLDL molecule (red) into lysosomes (green) around the nucleus (blue).

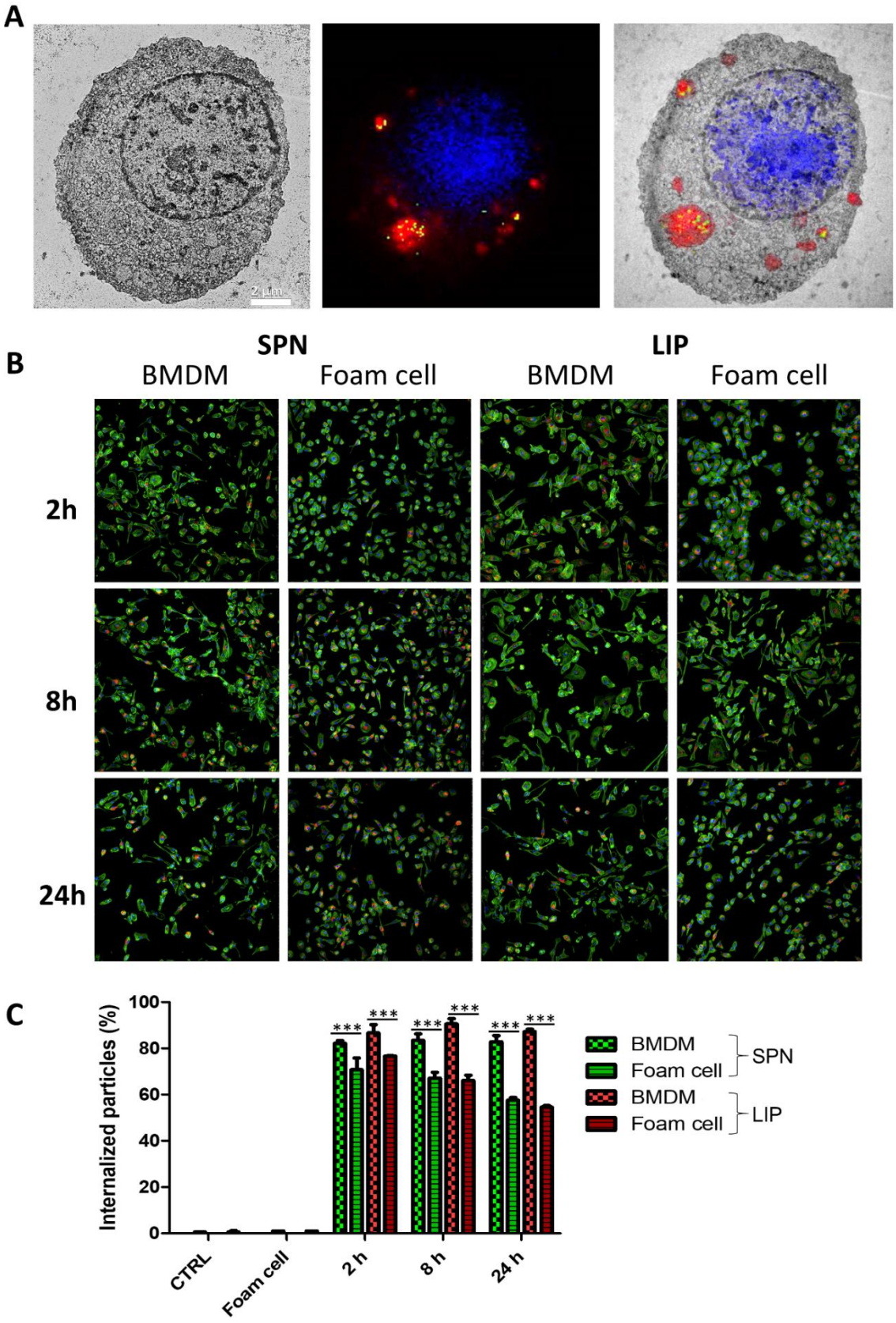

Figure 3.2. Macrophage Maturation to Foam Cells and Nanoparticle **A.** Correlative light and electron microscopy (CLEM) characterization for macrophages exposed to oxidized low density

lipoprotein (oxLDL) – Transmission electron microscopy image (left); confocal fluorescent microscopy image (center) showing the cell nucleus (blue – DAPI), the cell lysosomes (green – LysoTrackerTMGreen), oxLDL molecules (red – Dil); light and electron microscopy images overlap (right). (Scale bar: 2 µm). B. Representative confocal images of BMDM and foam cells exposed to SPN (left) and LIP (right) at different time points (2, 8 and 24 hours). C. Flow cytometry analysis BMDM and foam cells exposed to SPN and LIP at different time points (2, 8 and 24 hours). *** $p < 0.001$

Also, the TEM image shows the lysosomes as light structures due to the high lipid content and local density. Indeed, in TEM analyses of control cells (**Figure 3.S7**), lysosomes appear significantly darker. This again would support the notion that oxLDL molecules are uptaken in a dose-dependent manner by phagocytic cells and tend to localize within the lysosomes.

In order to deliver their therapeutic cargo, MTX-loaded nanoparticles should cross the plasma membrane and be uptaken by the macrophages. Therefore, the time-dependent internalization of LIP and SPN into BMDM (i.e., before exposure to oxLDL) and foam cells (i.e., after exposure to oxLDL) was assessed via confocal fluorescent microscopy and flow cytometry analysis. Figure 2B shows representative confocal fluorescent images of macrophages (BMDM) and foam cells incubated with Cy5-labeled SPN (left) and Cy5-labeled LIP (right). Both nanoparticles (red dots) were readily internalized from the two cell types. However, a significant difference was detected in uptake propensity between the BMDM (no exposure to oxLDL) and foam cells. The latter tend to engulf a smaller number of nanoparticles. This was also confirmed and quantified via flow cytometry, with the data presented in Figure 2C for both LIP and SPN. The percentage of BMDM associated with nanoparticles (i.e.: percentage of positive events) was quite constant over time for both LIP and SPN. Specifically, for the three tested time points (2, 8 and 24h), this percentage was equal to 86.66 ± 3.59; 90.60 ± 2.23 and 87.30 ± 0.96 for LIP; 82.2 ± 1.1; 83.43 ± 2.82 and 82.87 ± 2.67 for SPN. In foam cells, for the three tested time points (2, 8 and 24h), this same percentage was generally lower as compared to BMDM and equal to 76.7 ± 0.14; 66.1 ± 2.26; 54.6 ± 0.71 for LIP, and 70.8 ± 5; 67.1 ± 2.54 ; 57.65 ± 1.06 for SPN. The difference in uptake propensity between foam cells and BMDM is more evident

at the latest time point (24h). This difference could be associated with the fact that the large amounts of oxLDL stored in the lysosomes of foam cells would affect the internalization capacity of the cell. Notice also, that in agreement with the above results, other authors have documented that macrophages fed with huge amounts of lipids tend to lose their phagocytic capacity.[177-179] It is just important to highlight that the Cy5-SPN and Cy5-LIP are comparable in size and surface properties to the parent MTX-SPN and MTX-LIP. Also, the conjugation of Cy5 molecules on the particle surface was shown to be very stable (**Figure 3.S8**).

The role of Methotrexate in Macrophage Maturation to Foam Cells.

As feeding macrophages with oxLDL is responsible for the progressive transition towards foam cells, a reduction of intracellular oxLDL would restore cell homeostasis and reverse the maturation process. Indeed, this could be achieved in two different ways: limit the uptake of oxLDL and foster the efflux of oxLDL. Importantly, MTX atheroprotection has been speculated to be associated to both its anti-inflammatory effect and ability to modulate cholesterol transport. [180] Therefore, in order to assess the effect of MTX on LDL trafficking, BMDM were first treated overnight with 50 μg/ml of DiI-oxLDL to induce foam cell formation, then the same cells were treated for 24h with different interventions, namely free MTX, empty LIP, MTX-LIP, empty SPN and MTX-SPN. After 24h, fluorescent images were acquired to quantify the amounts of intracellular DiI-oxLDL. **Figure 3.3A** shows representative microscopy pics for the untreated foam cells (control experiment), free MTX and empty LIP treated foam cells; MTX-LIP treated foam cell; empty SPN treated foam cells; MTX-SPN treated foam cell; and the original BMDM, which were not exposed to oxLDL. These images clearly demonstrate the progressive decrease in fluorescent intensity associated with the cells as moving from the untreated foam cells (top) to the MTX-loaded nanoparticle treated cells (bottom). The fluorescent intensity for the different interventions is also quantified in the bar chart of **Figure 3.3B**, where the data are normalized by the number of cells within the region of interest. No statistical significant difference was observed between the three control groups – untreated foam cells (0.39 ± 0.0004/cell); empty LIP treated foam cells (0.46 ± 0.03/cell); empty SPN

treated foam cells (0.39 ± 0.03/cell); and free MTX treated foam cells (0.36 ± 0.015/cell). On the other hand, the MTX-LIP and MTX-SPN are significantly more effective than the free drug in decreasing the amounts of intracellular lipids (0.09 ± 0.009/cell and 0.09 ± 0.026/cell, respectively, vs 0.36 ± 0.015/cell – $p < 0.0001$). This should be probably ascribed to the fact that the MTX-loaded nanoparticles are more efficiently uptaken by the cells as compared to the free drug molecules. In all fluorescent images, filamentous actin was stained to highlight the cell body (green signal) and nuclei were stained using DAPI (blue signal).

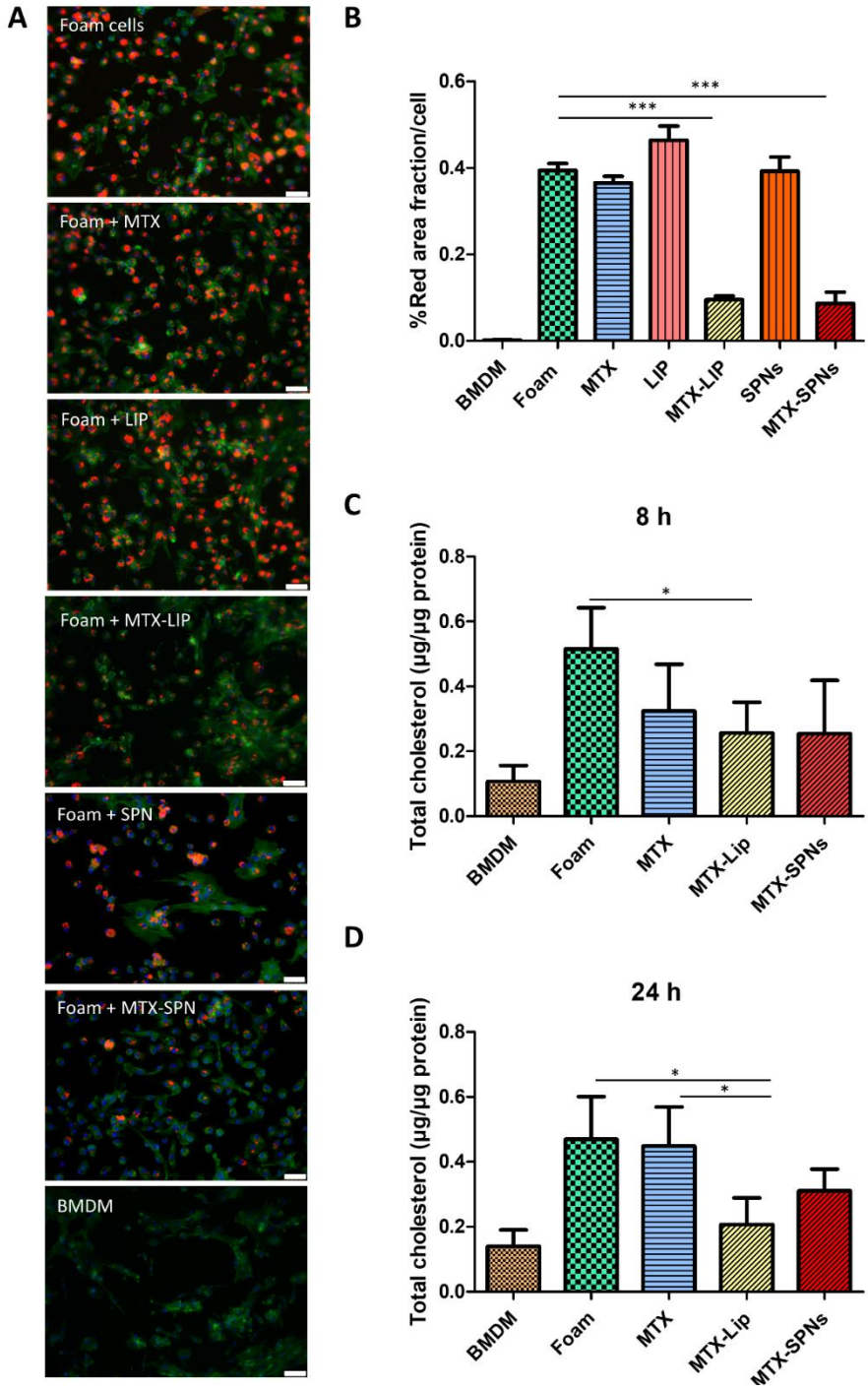

Figure 3.3. The role of Methotrexate in Macrophage Maturation to Foam Cells. A. Representative fluorescence images of different treatments conducted on BMDM forced to become foam cell following exposure to oxLDL (50 µg/ml). Red: Dil-oxLDL; blue: DAPI; green: F-Actin. From top to bottom, untreated foam cells, 24h free MTX-treated foam cells; 24h empty LIP-treated foam cells; 24h MTX-LIP treated foam cells; 24h empty SPN-treated foam cells; 24h MTX-SPN treated foam cells; and BMDM not exposed to oxLDL. (Scale bar: 50 µm) B.

Quantification of the oxLDL accumulation into cells expressed as the ratio between the size of the red area (Dil-oxLDL) and cell number. (Data are expressed as average ± SEM of n = 10 biological replicates. *** $p < 0.0001$). C., D. Quantification of the total cholesterol in macrophages treated with oxLDL (50 μg/ml) and exposed to MTX, MTX-LIP or MTX-SPN for 8 and 24h. (Data are reported as average ± SD of n = 4 biological replicates. (* $p < 0.01$, *** $p < 0.0001$).

In addition to the fluorescent signal quantification, the intracellular total cholesterol amounts were also measured, following the same treatment conditions as per the confocal microscopy analysis above. However, in this case, two different time points were considered, namely 8 and 24h, for the intervention. Data are provided in **Figure 3.3C and D** for the LIP- and SPN-based treatments at 8 and 24h, respectively. The intracellular total cholesterol analysis confirmed the trends observed via confocal fluorescent microscopy. The cholesterol content was observed to reduce as moving from untreated foam cells to free MTX-treated foam cells, MTX-LIP and MTX-SPN treated foam cells and eventually the BMDM, both at 8 and 24h. Larger differences between the control groups and the nanoparticle-treated foam cells were detected at 24h as compared to the earlier 8h time point. Notice that both MTX-LIP and MTX-SPN were able to decrease the intracellular cholesterol content at 8h, returning values of 0.25 ± 0.09 μg/μg protein and 0.25± 0.16 μg/μg protein, respectively. At 24h, the two formulations reduced the cholesterol amounts to 0.20 ± 0.08 μg/μg protein and 0.31 ± 0.07 μg/μg protein as compared to the untreated foam cells 0.44 ± 0.12 μg/μg protein. In general, MTX-LIP tended to be more effective than the MTX-SPN, especially at 24h.

Modulating the Expression of Cholesterol Transport and Inflammatory Genes in MTX-treated Foam Cells.

The expression of three foam cells markers (ABCA1, CD36 and SRA-1) and three inflammatory genes (IL-1β; IL-6 and TNF-α) was measured by real time PCR in response to different

treatment conditions, namely free MTX, empty LIP, empty SPN, MTX-LIP, MTX-SPN. Untreated foam cells and BMDM (not exposed to oxLDL) were used as control groups. The foam cell marker ABCA1 is involved in cholesterol efflux; whereas the markers CD36 and SRA-1 are known to regulate cholesterol influx. The overexpression of CD36 and SRA-1 is a landmark for the maturation of macrophages into foam cells. Specifically, it should be here recalled that CD36 recognizes the lipid moieties in the oxLDL molecules while SRA-1 binds to the oxidized portion of the lipoprotein. [181] The gene expression analysis was performed at two different time points, namely 8 and 24h. Data are presented in **Figure 3.4** and **Figure 3.S9** and **S10**, where the gene expression levels are normalized with respect to foam cells, which are arbitrarily taken as equal to 1. Importantly, a direct comparison between BMDM (not exposed to oxLDL) and foam cells reveals a 2 to 3 times increase in the expression of CD36 and SRA-1, at both 8 and 24h. Indeed, this continues to demonstrate that an overnight exposure of BMDM to 50 μg/ml of oxLDL is sufficient to trigger the maturation in to foam cells.

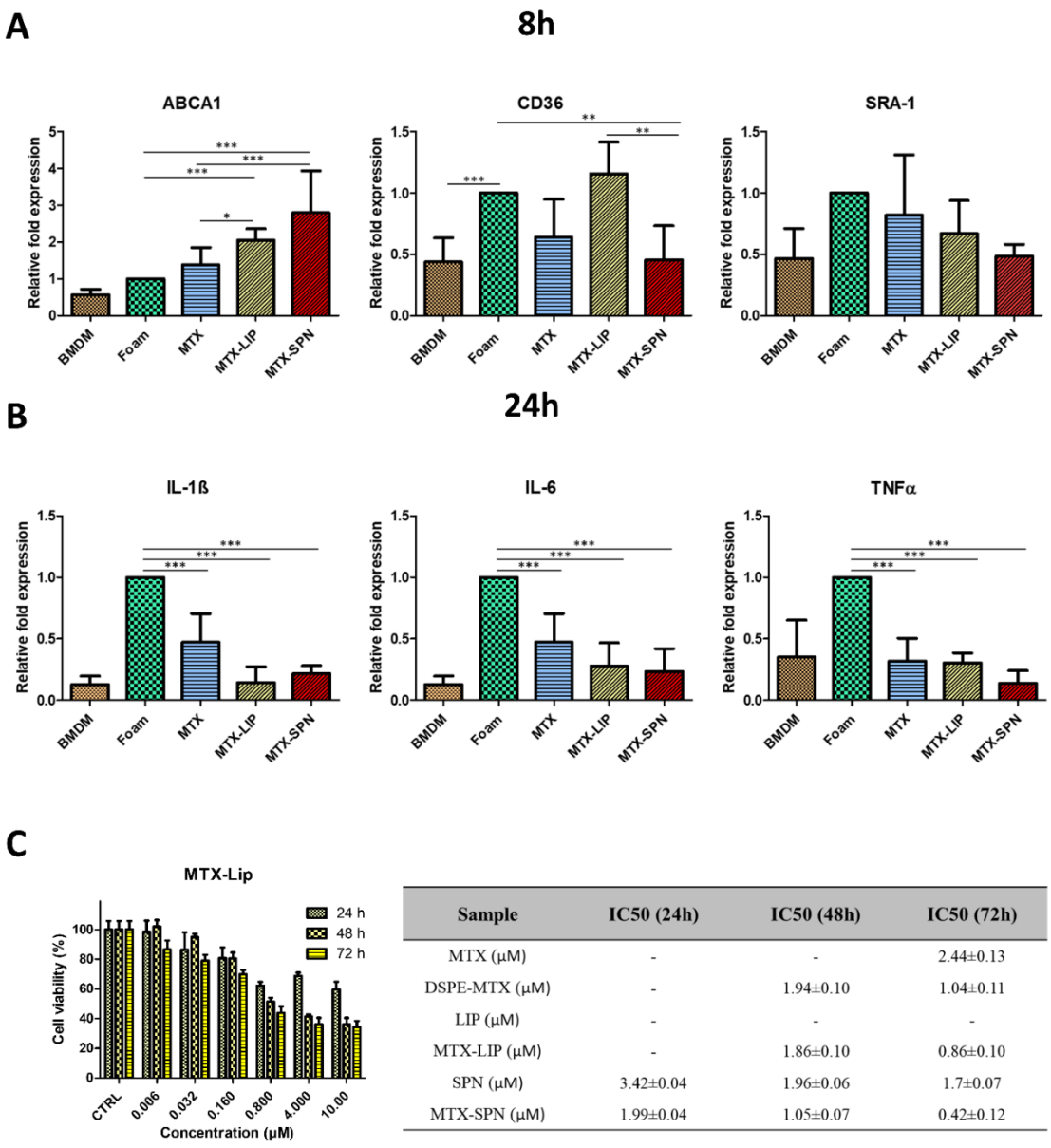

Sample	IC50 (24h)	IC50 (48h)	IC50 (72h)
MTX (µM)	-	-	2.44±0.13
DSPE-MTX (µM)	-	1.94±0.10	1.04±0.11
LIP (µM)	-	-	-
MTX-LIP (µM)	-	1.86±0.10	0.86±0.10
SPN (µM)	3.42±0.04	1.96±0.06	1.7±0.07
MTX-SPN (µM)	1.99±0.04	1.05±0.07	0.42±0.12

Figure 3.4. Expression of Cholesterol Transport and Inflammatory Genes in Macrophages and Cell Viability. A. Expression level of foam cells markers (ABCA1, CD36, and SRA-1) in macrophages treated with free MTX, MTX-LIP and MTX-SPN for 8h. B. Expression level of Pro-inflammatory cytokines (IL-1β, IL-6 and TNF-α,) in macrophages treated with free MTX, MTX-LIP and MTX-SPN for 24h. (Data are expressed as average ± SD (n = 5). *** $p < 0.0001$; ** $p < 0.001$; * $p < 0.01$). C. BMDM viability upon incubation with MTX-LIP (left). The table (right) summarizes the IC50 values on BMDM at 24, 48 and 72h post exposure to different therapeutic groups, namely free MTX, DSPE-MTX, empty LIP, MTX-LIP, empty SPN and MTX-SPN.

Figure 3.4A shows the expression of the three genes regulating the transport of cholesterol at 8h. For ABCA1, the relative fold expression increase was equal to 1.383 ± 0.468 for free MTX; 2.048 ± 0.31 for MTX-LIP; and 2.793 ± 1.14 for MTX-SPN. Indeed, an increase in ABCA1 would be mirrored into an increase in cholesterol efflux. For CD36 and SRA-1, modest variations around a relative fold expression of 1 were observed for almost all treatments, implying that MTX has lower or no significant effect on these genes. Specifically, the relative fold expression induced by LIP-MTX was 1.156 ± 0.257 for CD36 and 0.668±0.269 for SRA-1; and that induced by MTX-SPN was 0.454 ± 0.279 for CD36 and 0.485 ± 0.096 for SRA-1. This data would suggest that the treatment of foam cells with the nanoformulated MTX would induce a significant overexpression of ABCA1, thus boosting cholesterol efflux; and a moderate downregulation of CD36, which is involved in cholesterol influx. At 24h, on the other hand, a strong reduction in the expression of all three genes was recorded for the MTX-SPN (**Figure 3.S9**), whereas for the MTX-LIP a significant reduction was observed only for the SRA-1.

As per the inflammatory response, an overall decrease of all three genes was observed at both 8 and 24h upon treating the foam cells with either free MTX or MTX-loaded nanoparticles (Figure S10). However, the anti-inflammatory effect appears more clearly a 24h (Figure 4B).

For IL-1β, the relative fold expression was reduced to 0.143 ± 0.129 for the MTX-LIP and to 0.215 ± 0.065 for the MTX-SPN, which are both comparable with the level of relative expression measured in BMDM (0.127±0.067). Free MTX treatment was also able to reduce the IL-1β expression but only down to 0.470 ± 0.233. Similarly for IL-6, the level of expression reduced by 3 times in comparison to foam cells when using MTX-LIP (0.28 ± 0.18) and MTX-SPN (0.2334 ± 0.186) and by 2 times only in the case of free MTX (0.46 ± 0.20). For TNF-α, the effect of MTX-LIP and MTX-SPN, as compared to the free drug, was less significant. Specifically, the TNF-α relative fold expression levels decreased to 0.302 ± 0.080 for the MTX-LIP; 0.138 ± 0.101 for the MTX-SPN; and 0.316 ± 0.186 for the free MTX.

In the **Figure 3.S9 and S10**, data are also provided for the empty LIP and empty SPN. On the genes associated with cholesterol transport, the empty LIP induced only a modest decrease in the level of expression of ABCA1 (0.473 ± 0.162) at 24h, but in all other conditions the effect of

the liposomes was negligible. Very differently, the empty SPN were observed to downregulate the expression of ABCA1 and upregulate the expression of SRA-1, both at 8 and 24h. On the pro-inflammatory genes, both nanoparticles increased the expression of IL-1β, IL-6 and TNF-α above the levels measured for BMDM (not exposed to oxLDL). This was indeed expected for the liposomes, but the pro-inflammatory effect was much higher for the empty SPN than for the empty LIP, at all time points and for all genes. This must be related to the low encapsulation efficiency and, consequently, large number of SPN needed to administer the prescribed doses of MTX, which could eventually lead to medium acidification and local inflammation. [46, 182]

Before performing animal experiments, the viability of BMDM exposed to different concentration of MTX and MTX-loaded nanoparticles was assessed via a conventional MTT assays. **Figure 3.4C and Figure 3.S11** show the viability of cells treated with free MTX, free DSPE-MTX, MTX-LIP and MTX-SPN with a drug concentration ranging from 6 nM to 10 μM. Empty LIP and SPN were also tested using a number of particles equivalent to those needed for the delivery of a specific MTX dose. The IC50 corresponding to the different treatments are provided in the table of **Figure 3.4**. DSPE-MTX presented a slightly lower IC50 in comparison to free MTX of 1.04 ± 0.11 μM vs 2.44 ± 0.13 μM. MTX-LIP showed a similar cytotoxicity to the conjugate, with a IC50 = 0.86 ± 0.1; whereas MTX-SPN revealed a slightly higher cytotoxicity with a IC50 of 0.42 ± 0.12 μM. No significant toxicity was observed with empty LIP. Differently for the empty SPN, a toxicity similar to that of MTX-SPN was found. Again, this negative result associated with SPN should be ascribed to the low encapsulation efficiency and large number of particles needed to deliver the required amounts of MTX. Based on these observations, the following pre-clinical studies were only conducted with MTX-LIP.

Pre-clinical characterization of MTX-Liposomes.

To directly investigate the effect of MTX-loaded nanoparticles on atherogenesis, apoE$^{-/-}$ mice were subjected to 28 days High Fat Diet (HFD) to induce lesion development. Mice were concomitantly treated with MTX-LIP or empty LIP for 28 days, with a MTX dose of 2.5 mg administered systemically every three days. At the end of the treatment, mice were sacrificed. Major organs were harvested together with the aorta for ex-vivo analyses. The mice treated

with MTX-LIP presented an area of the aortic sinus plaque that was significantly smaller than that detected in control mice, which were treated with empty LIP (**Figure 3.5A**). Also, the MTX-LIP treatment had no effect on plaque Collagen content (**Figure 3.5B**). Analysis on serum samples were also conducted (**Figure 3.5C**). No significant differences in total cholesterol were noticed between the two experimental groups. It is therefore unlikely that changes in lipid levels could account for the decreased pathology observed with the MTX-nanoparticle treated mice. To determine other systemic changes that MTX-LIP may exert on atherosclerosis-driven immune responses, a Luminex analysis was performed to quantify a broad spectrum of cytokines in the serum samples (**Figure 3.5C**). A significant ($P<0.01$) decrease in RANTES (CCL5) was detected. This chemokine is expressed by many hematopoietic and non-hematopoietic cell types and plays an important role in homing and migration of immune cells. A slight increase of IL-1α ($P<0.05$) was also documented in the MTX-LIP treated mice (**Figure 3.5C**).

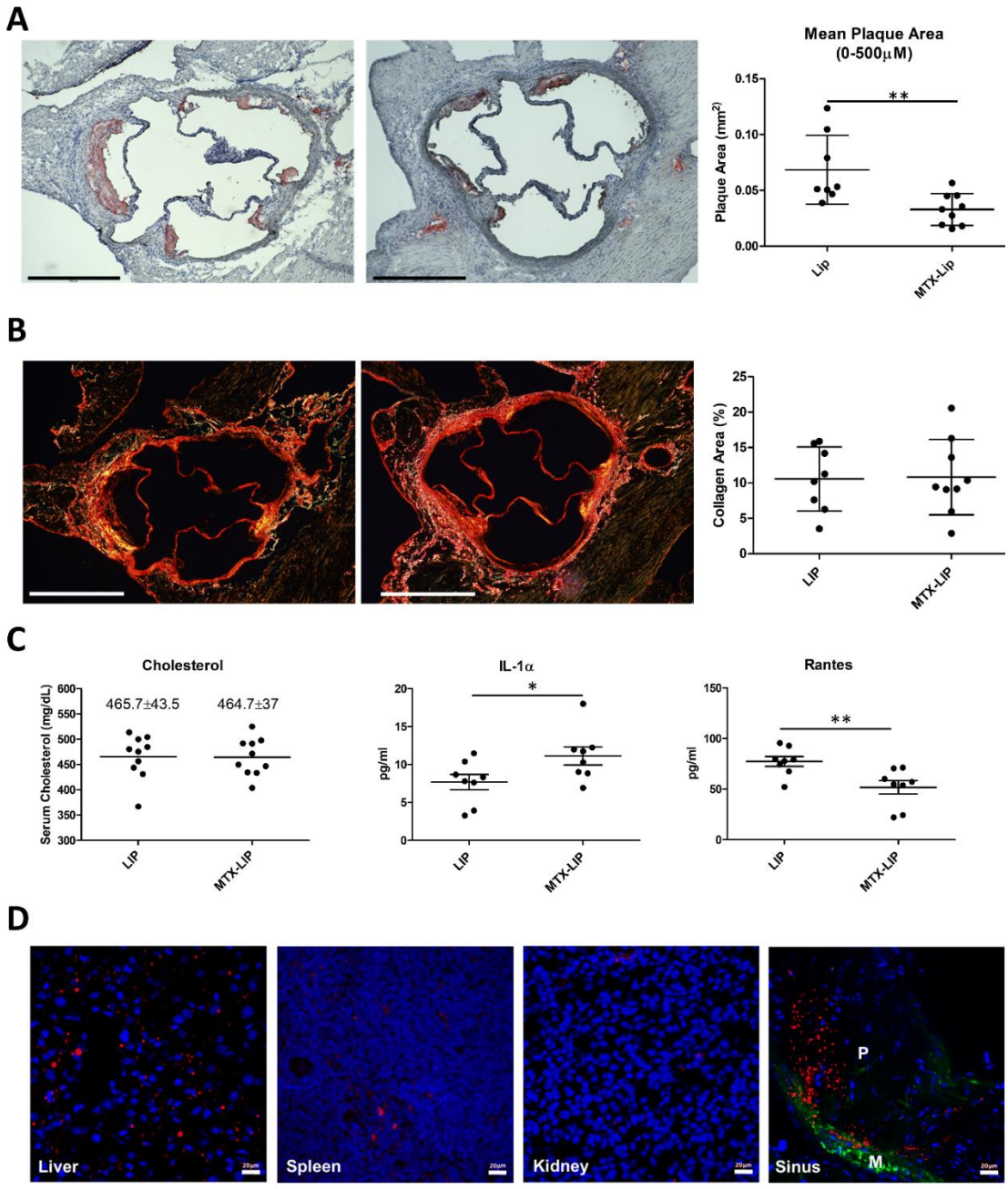

Figure 3.5. Pre-clinical characterization of MTX-Liposomes. A. Representative photomicrographs (left) of oil red O (ORO)-stained aortic sinuses (scale bar: 500 μm) and quantification of the mean lesion area (right) for empty LIP and MTX-LIP treatments. B. Representative images of plaque Collagen content (left) by picrosirius red staining (scale bar: 500 μm) and quantification of the Collagen area (right) for empty LIP and MTX-LIP treatments. For plots in (A) and (B), individual data points represent average value per mouse; horizontal bars denote mean. **p < 0.01. C. Analyses of cholesterol, IL-1α and RANTES serum content

for empty LIP and MTX-LIP treatments. Individual data points represent average value per mouse, horizontal bars denote mean. Results are presented as mean ± SEM and analyzed by Student unpaired t-test. * $p < 0.05$, ** $p < 0.01$. D. Cy5-LIP (red signal) bio-distribution in Liver, Spleen, Kidneys and aortic Sinus. Green: α-smooth muscle actin (α-SMA); Blue: cell nuclei. In the aortic sinus image: M indicates Media; P indicates Plaque (Scale bar: 20 μm).

Concentrations of eotaxin, fibroblast growth factor-basic, granulocyte-macrophage Colony-stimulating factor, IFN-γ, IL-1β, IL-2, IL-3, IL-4, IL-5, IL-6, IL-9, IL-10, IL-12 (p40), IL-12 (p70) IL-13, IL-17A, KC, monocyte chemoattractant protein-1, macrophage inflammatory protein-1α, macrophage inflammatory protein-1β and tumor necrosis factor-α did not differ significantly between the two experimental groups or were below the level of detection (**Table 3.S2**).

These data may suggest that MTX-LIP mainly exert a local anti-inflammatory effect with minor systemic implications. This consideration is in accordance with the biodistribution analysis that was performed by immunohistochemistry using Cy5-LIP. These particles maintain the same physiochemical features of the MTX-LIP in terms of size and surface charge. Twenty-four hours after i.v. injection, Cy5-LIP were detected in the spleen and kidneys (Figure 5D), whereas more particles were detected in the liver, as expected, and, more importantly, in the atherosclerotic plaque of the aortic root. A similar distribution was also observed in aged (1 year old) apoE-/- mice with Cy5-LIP clearly detectable in the plaque core and fibrous cap in the sinus and artic arch, in addition to kidney and liver (**Figure 3.S12**). It is here worth noticing that, as previously documented by the authors and other groups [47, 183-185], the percentage of injected nanoparticles accumulating in atherosclerotic plaques upon systemic administration is minimal as compared to the amounts depositing in organs of the reticuloendothelial system (RES), such as the liver and the spleen. To quantitatively assess particle biodistribution, LIP were labeled with ^{64}Cu (^{64}Cu-LIP) and injected systemically in healthy mice (C57BL/6). **Figure 3.S13.A-B** documents that the hydrodynamic size of the 64Cu-LIP is comparable to that of MTX-LIP and that the radioisotope 64Cu is firmly conjugated to the LIP surface via the chelating agent DOTA. **Figure 3.S13.C** shows the quantitative biodistribution of the 64Cu-LIP confirming a significant accumulation in the liver and spleen after 24h (**Figure 3.S13**).

3.5. Discussion

The oxLDL internalization data and the gene expression results presented in **Figure 3.2 – 4** would suggest that MTX treatments are capable to halt, and possibly reverse, the process of maturation of macrophages into foam cells, which is indeed a pivotal step in the process of atherogenesis and atherosclerosis progression. Overall, MTX treatments have been shown to lower the intracellular deposition of oxLDL in primary rat macrophages mostly by increasing the efflux rates (over expression of ABCA1) with a modest variation of the influx rates (downregulation of CD36 and SRA-1) (**Figure 3.3** and **4A**). In particular, at 8h, MTX-LIP and MTX-SPN had a different effect on the CD36: MTX-SPN induced a statistically higher reduction in CD36 expression as compared to MTX-LIP. This effect of MTX-LIP on the expression of CD36 should be ascribed to the very nature of the lipid-based particles. Indeed, liposomes do contain cholesterol that could trigger the expression of CD36, as previously reported. [186] MTX treatments appeared to have also a significant effect on modulating inflammation by reducing the production of different cytokines. Especially at 24h post MTX treatment, the expression of IL-1β, IL-6 and TNF-α went down significantly as compared to the foam cell case (**Figure 3.4B**), where inflammation was only induced by direct exposure to oxLDL molecules. Importantly, beside the CD36 expression, the effect of MTX-LIP appeared to be statistically comparable to that of MTX-SPN in most other cases. This demonstrates that the nanoformulations of MTX, even with totally different particles, leads to similar results with a general increase in the expression of genes involved in cholesterol efflux, decrease in the expression of genes involved in cholesterol influx, and mitigation of the pro-inflammatory cytokines production. Inflammation also represents a pivotal step in atherosclerosis initiation and progression, in that it favors the sustained recruitment of circulating monocytes within vascular lesions and supports their maturation in macrophages and eventually foam cells. [143] The considerable intracellular accumulation of oxLDL in macrophages reduces the ability

of the cells to metabolize cholesterol [187] and generate reactive oxygen species triggering and sustaining local inflammation. Thus, controlling both oxLDL transport in and out of cells and the local state of inflammation may have dramatic implications in halting and possibly reversing atherosclerosis.

It is here important to recall that, recently, it was demonstrated that clinical use of low-dose MTX was associated with increased ABCA1 mRNA in peripheral blood mononuclear cells (PBMC) of rheumatoid arthritis patients. [188] This change in expression in PBMC was closely related to MTX activity. [188] ABCA1 expression is regulated by the adenosine and MTX promotes adenosine release, thus causing the overexpression of ABCA1. [39] Thus, the efficient delivery of MTX to circulating monocytes and macrophages residing within arterial lesions could promote the overexpression of ABCA1 and modulate the risks of acute cardiovascular syndromes. However, a low-dose treatment with MTX was not sufficient to mitigate the occurrence of cardiovascular events as demonstrated by the recent failure of CIRT. [42] Indeed, nanoparticles could more efficiently deliver the therapeutic cargo to the biological target, as opposed to the free drug administration, reducing also the risk of adverse effects. Importantly, this work shows that even *in vitro* the nanoformulated MTX is more effective than free MTX in modulating foam cell formation and alleviating cell inflammation (see **Figure 3.3** and **4**).

3.6. Conclusions

Two MTX-loaded nanomedicines were designed, realized and characterized in vitro for their physico-chemical and pharmacological properties and in vivo for their ability to modulate atherosclerosis in high-fat fed apoE$^{-/-}$ mice. The lipid conjugate DSPE-MTX was either dispersed within the hydrophobic PLGA core of Spherical Polymeric Nanoparticles (MTX-SPN) or was integrated in the lipid by-layer of liposomes (MTX-LIP). The encapsulation of the MTX lipid conjugate into MTX-LIP was significantly more efficient than in MTX-SPN.

The ability of MTX to modulate inflammation and regulate the expression of genes involved in the transport of oxLDL was extensively demonstrated using different in vitro assays. In general, possibly because of the higher loading and encapsulation efficiency, MTX-LIP showed a larger impact in reducing the accumulation of oxLDL into macrophages as compared to MTX-SPN and free MTX. This was demonstrated both via confocal fluorescent microscopy and gene expression quantification. Finally, in apoE$^{-/-}$ mice fed on high-fat diet for 28 days, MTX-LIP were shown to accumulate in atherosclerotic plaques developing within the aortic root. This was accompanied by a significant decrease in circulating levels of RANTES (CCL5), which is an inflammatory chemokine playing a key role in homing and migration of immune cells in the vessel walls, and significant reduction in atherosclerotic plaque size.

Overall, this work would suggest that MTX-nanoparticles could resuscitate the use of this potent anti-inflammatory drug, or similar therapeutic agents, for the management of atherosclerosis.

3.7. Supporting Information

DSPE-MTX prodrug synthesis. Considering the poor solubility of the Methotrexate (MTX), a prodrug with amphiphilic properties was generated by binding MTX to 1,2-distearoyl-sn-glycero-3-phosphoethanolamine-N-amino (DSPE-NH2). In order to generate the prodrug, MTX was pre-activated *in loco* with a mixture of DCC and NHS, then conjugated with DSPE-NH_2. Compound purification was achieved by precipitation in cold diethyl ether.

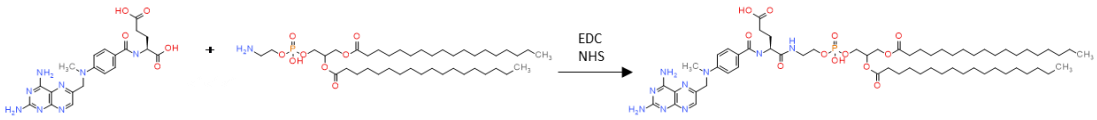

Figure 3.S1. Synthesis of prodrug.

MTX-loaded nanoparticles stability under slightly acidic conditions

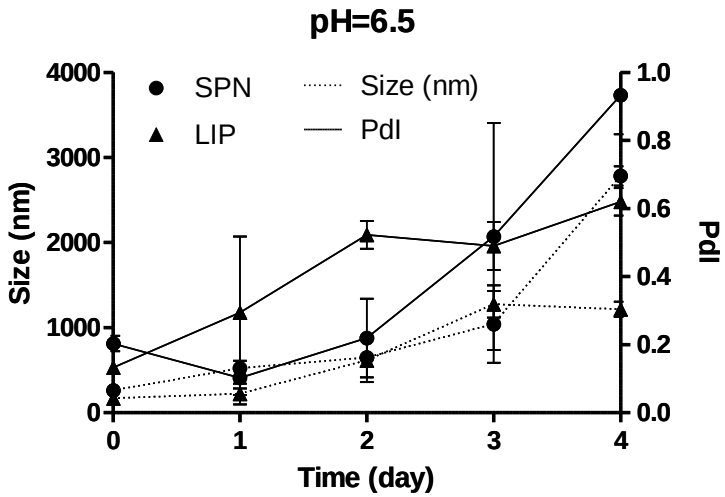

Figure 3.S2. Particle stability at pH=6.5.

MTX-SPN optimization. Optimization of SPN. To find the optimal formulation, MTX-SPNs were produced using different amounts of PLGA and DPPC and using PLGA with different molecular weights (25-35KDa or 38-53KDa) as reported in **Table S1, Figure S3**. To find the

optimal formulation, MTX-SPNs were produced using different amounts of PLGA and DPPC and using PLGA with different molecular weights (25-35KDa or 38-53KDa). All the formulations presented average sizes ranging from 200 to 225 nm and showed a negative ζ-potential ranging from - 41 to - 54 mV. With the increase of PLGA amount a relative increase on the nanoparticles size was retrieved. The negative charge is related to DSPE-PEG-COOH carboxylic groups exposed on SPNs surface. As shown in **Figure S3A** and **B** the amount of PLGA also affected DSPE-MTX encapsulation efficiency (EE%) which increases proportionally to PLGA amount, passing from about 0.2% to 0.5 % for the lowest molecular weight PLGA (25-35KDa) and from 0.4% to 1.5% for the highest (38-53kDa). EE% was also affected by the presence of DPPC, by removing DPPC the amount of internalized prodrug increased. This finding is probably related to a competition between DSPE-MTX and DPPC on the stabilization of the PLGA during the addition to the aqueous phase on the preparation of the nanoparticles. Basing on these considerations, SPNs 12 formulation was selected (**Table S1, Figure S3**). Starting from now on, we will refer to SPNs12 as MTX-SPNs.

Table 3.S1. Optimization of SPNs. The SPNs were made in triplicate (n=3) for each single experiment.

Sample	PLGA (23-35 kDa) (mg)	PLGA (38-53 kDa) (mg)	DPPC (mg)	DSPE-MTX (mg)	DSPE-PEG (mg)	Size (nm)	PdI	Z Pot (mV)	Mass of DSPE-MTX (µg)	EE(%)
SPN 1	0.5	-	0.09	0.2	0.11	200±2	0.12±0.02	-52±2.3	0.25±0.025	0.13±0.01
SPN 2	0.5	-	-	0.2	0.11	200±3	0.1±0.02	-46±5	0.26±0.06	0.13±0.03
SPN 3	1	-	0.09	0.2	0.11	201±9	0.13±0.03	-54±1	0.36±0.09	0.18±0.04
SPN 4	1	-	-	0.2	0.11	210±12	0.18±0.02	-44±15	0.52±0.02	0.26±0.01
SPN 5	2	-	0.09	0.2	0.11	223±14	0.18±0.03	-51±2	0.58±0.16	0.29±0.08
SPN 6	2	-	-	0.2	0.11	215±6	0.18±0.02	-48±3.6	0.76±0.09	0.38±0.05
SPN 7	-	0.5	0.09	0.2	0.11	200±2	0.1±0.02	-46.5±0.5	0.26±0.06	0.13±0.03
SPN 8	-	0.5	-	0.2	0.11	202±10	0.13±0.03	-41±1.5	0.41±0.04	0.21±0.02
SPN 9	-	1	0.09	0.2	0.11	215±6	0.18±0.02	-44±1.5	0.52±0.02	0.26±0.01
SPN 10	-	1	-	0.2	0.11	205±7	0.16±0.03	-46±2	0.87±0.2	0.43±0.1
SPN 11	-	2	0.09	0.2	0.11	218±1	0.19±0.02	-48±3.6	0.76±0.09	0.38±0.05
SPN 12	-	2	-	0.2	0.11	208±2	0.15±0.02	-45±0.02	3±0.34	1.5±0.17

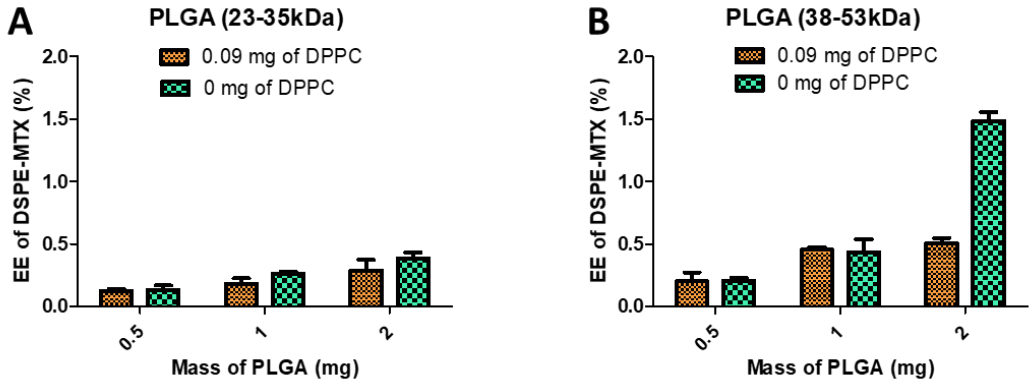

Figure 3.S3. A. and B. Different formulations with different amounts of PLGA and DPPC: EE% of DSPE-MTX.

Oxidized Low Density Lipoproteins (oxLDL)

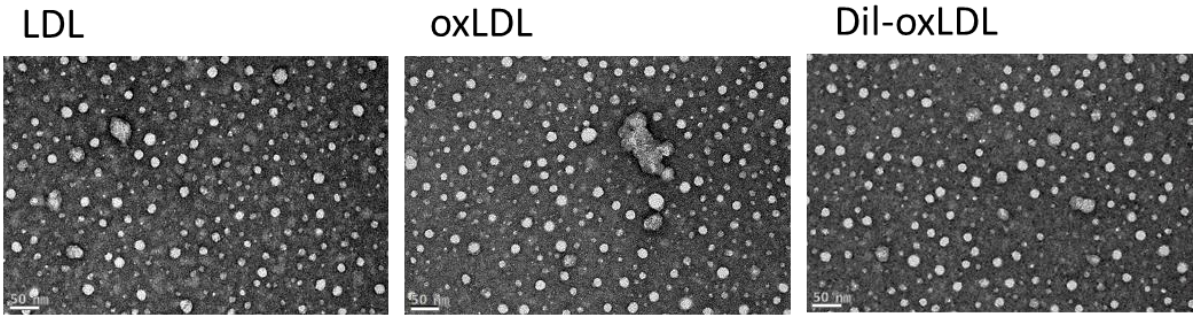

Figure 3.S4. TEM images of LDL molecules (left), oxLDL molecules (center), Dil-oxLDL (right) (scale bar = 50 μm).

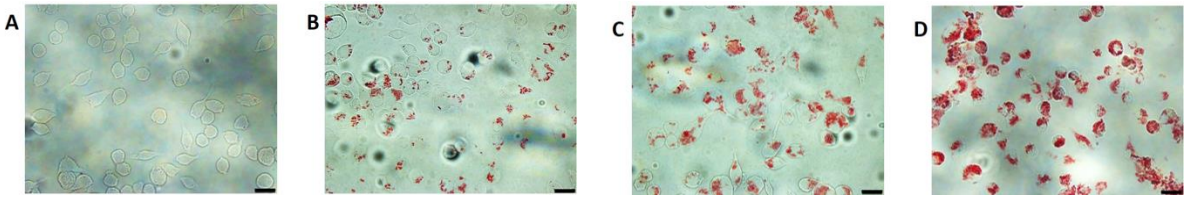

Figure 3.S5. Incubation of oxLDL with macrophages (RAW 264.7). A. 0 μg/ml oxLDL; B. 20 μg/ml oxLDL; C. 50 μg/ml oxLDL; D. 80 μg/ml oxLDL (scale bar = 25 μm).

Intracellular localization of oxLDL. To observe oxLDL intracellular distribution at confocal microscopy oxLDL were stained using DiI; for this experiment living RAW 264.7 were treated with 488-lysotracker to highlight lysosomes and with a concentration of DiI-oxLDL equivalent to 50 µg/ml of oxLDL. As it is possible to appreciate the green signal from lysosomes and the red signal from oxLDL co-localize almost completely, proving oxLDL accumulation mainly occurs into lysosomes (**Figure S6A**). Control cells were treated only with DiI (instead of DiI-oxLDL) following the same conditions, as it is possible to observe in **Figure S6B**. No co-localization at lysosomes was observed. Red signal coming from DiI was confined to plasma membrane. It is also important to underline that in cells treated with DiI-oxLDL no fluorescent signal was retrieved at plasma membrane thus proving the absence of any leakage of DiI from fluorescent oxLDL.

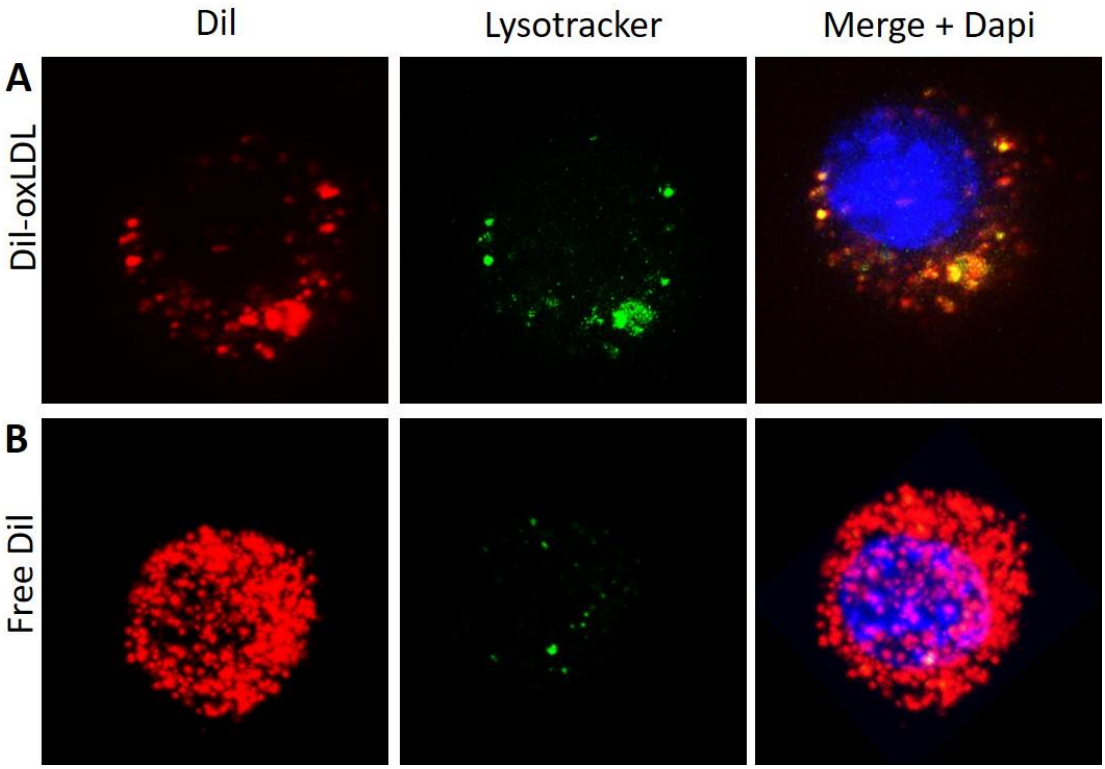

Figure 3.S6. Raw 264.7 cells treated with **A**. DiI-oxLDL and **B**. Free DiI. In red DiI and DiI-oxLDL, in green Lysotracker and in blue DAPI.

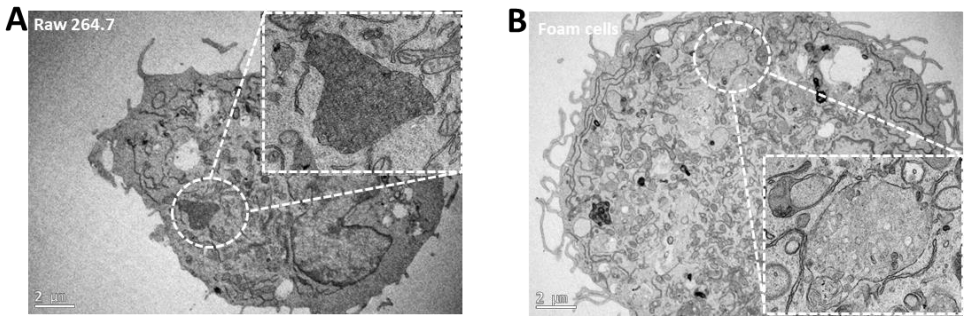

Figure 3.S7. TEM images of macrophages. A. RAW 264.7 cells not exposed to oxLDL show dark lysosomal structures. B. RAW 264.7 cells exposed to oxLDL (overnight, 50 μg/ml) show light lysosomal structures due to the high lipid content.

Stable association of DiI and oxLDL molecules. To furtherly demonstrate the stability of oxLDL and DiI a time-lapse microscopy experiment was performed (**Movie S1** and **S2**). Following the same condition living BMDM were incubated overnight with DiI-oxLDL or with DiI. 14 hours after treatment cells were observed at the microscope and movies (**Movie S1**) were recorded. In DiI-oxLDL treated cells it is possible to note particulate movement inside the cell referring to DiI-oxLDL trafficking; in free DiI treated cells, **Movie S2**, instead the fluorescent signal is revealed from firm spots most likely located in plasma membrane.

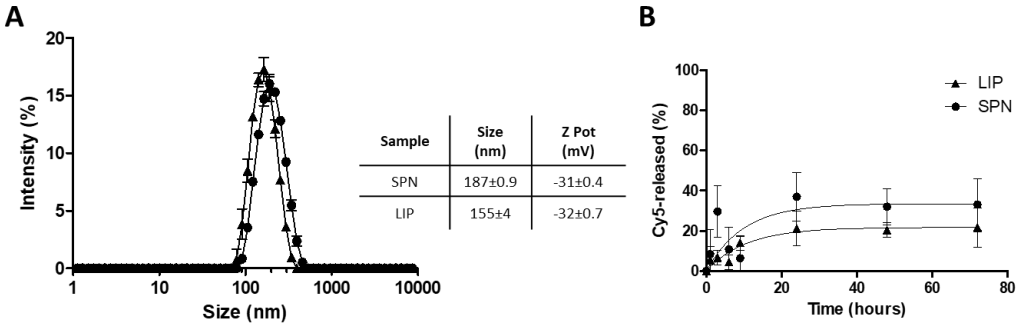

Sample	Size (nm)	Z Pot (mV)
SPN	187±0.9	-31±0.4
LIP	155±4	-32±0.7

Figure 3.S8. A. DLS analysis of Cy5-LIP and Cy5-SPN. B. Release study of Cy5 from LIP and SPN.

Expression levels for the genes regulating the cholesterol transport

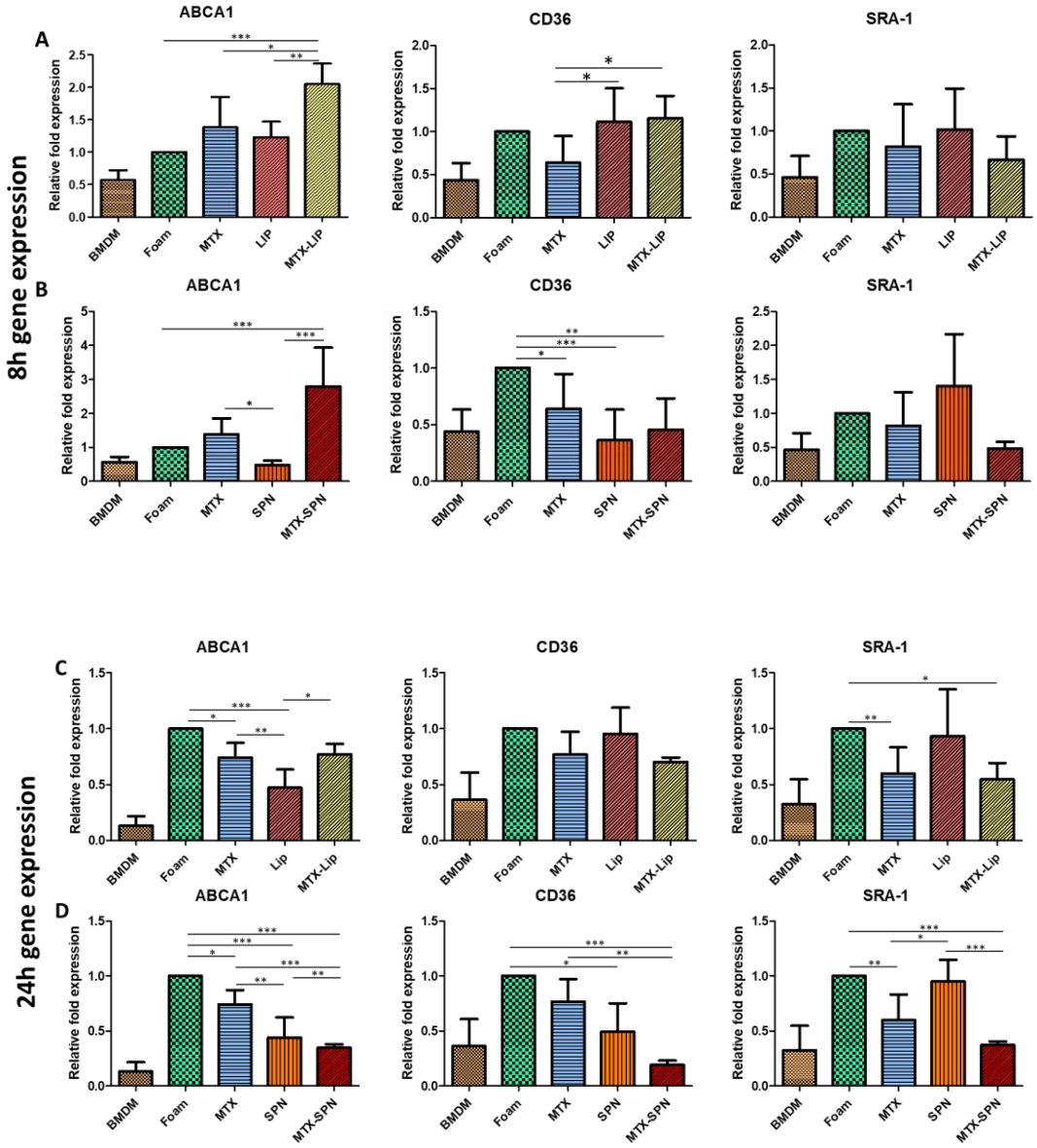

Figure 3.S9. A-D. Foam cells markers expression level (ABCA1, CD36, and SR-A1) in foam cells (treated for 8 and 24 hours with the free and empty/loaded drug in LIP and SPN). Results are expressed as average ± SD (n = 5). ***p < 0.0001; **p < 0.001; *p < 0.01

Expression levels for the genes associated with the anti-inflammatory cytokines

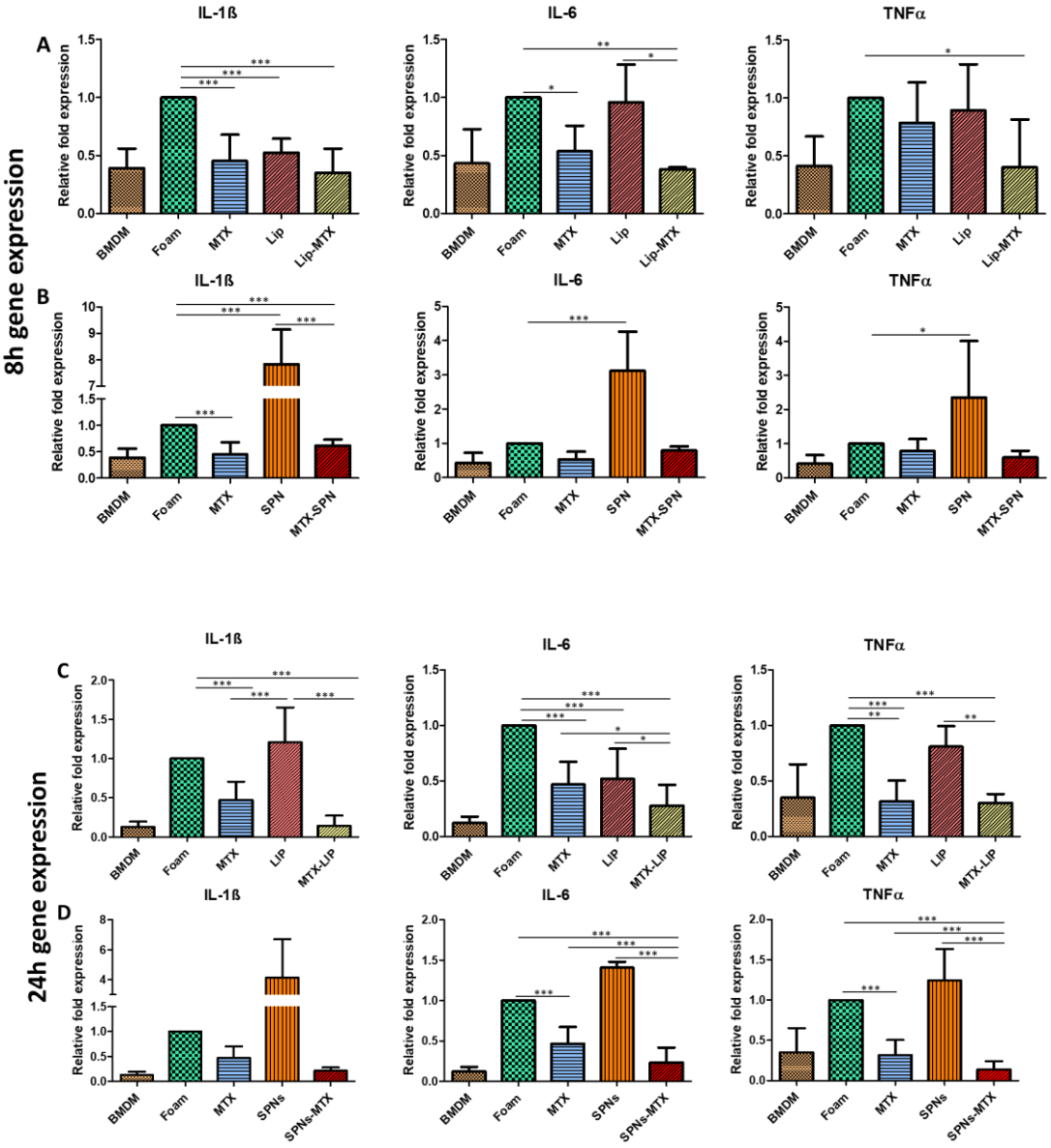

Figure 3.S10. A-D. Pro-inflammatory cytokines expression levels (TNF-α, IL-1β, and IL-6) in foam cells (treated for 8 and 24 hours with the free and empty/loaded drug in LIP and SPN). Results are expressed as average ± SD (n = 5). ***p < 0.0001; **p < 0.001; *p < 0.01

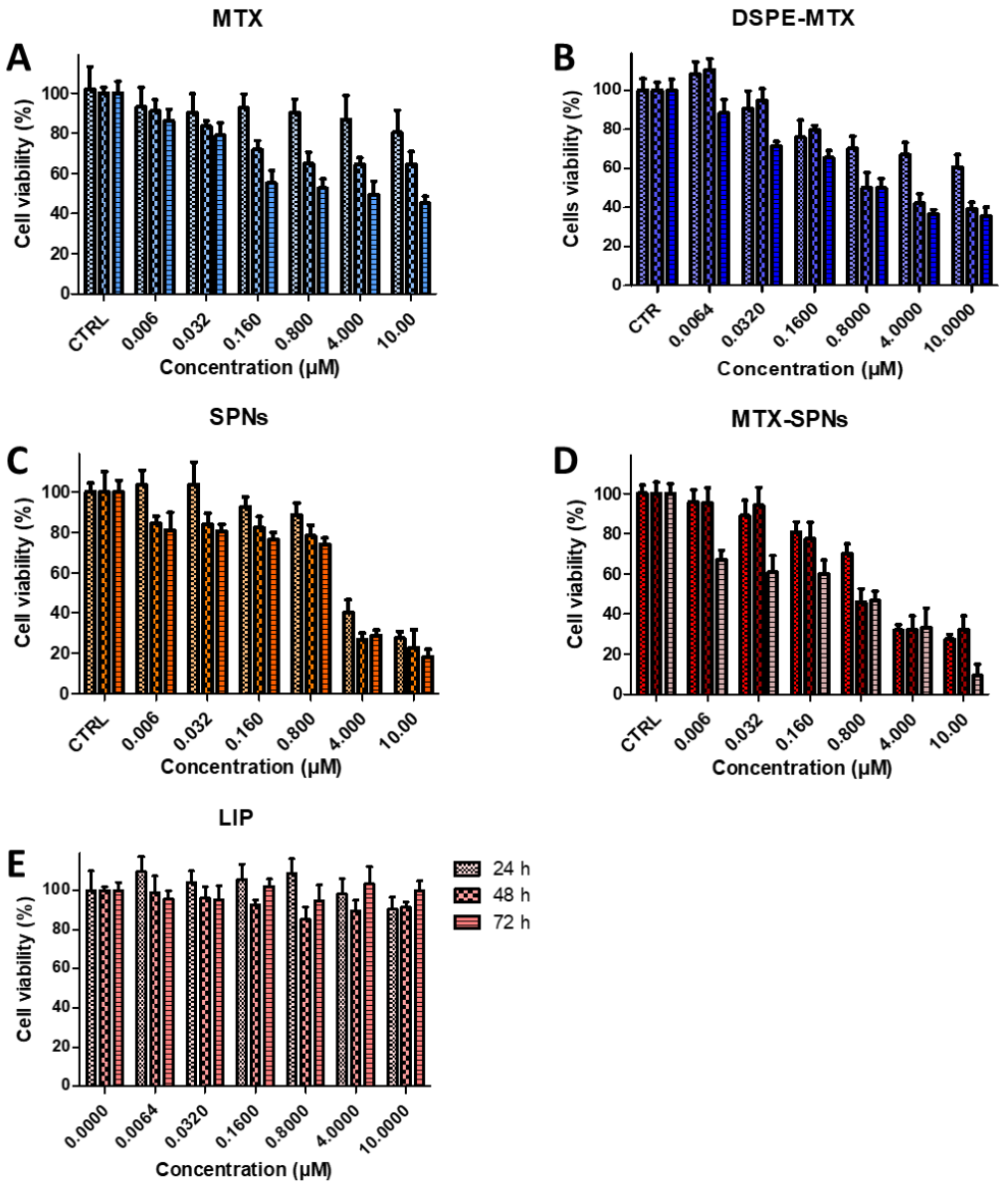

Figure 3.S11. A-E. Viability of BMDM incubated with MTX, DSPE-MTX, empty SPN, MTX-SPN and empty LIP a 3 different time points.

Table 3.S2. Luminex results.

Cytokine (pg/ml)	LIP	MTX-LIP
IL-1α	7.7±1	11.1±1.2
IL-1β	-	-
IL-2	-	-
IL-3	7.3±0.67	8.13±0.67
IL-4	2.6±0.2	2.4±0.3
IL-5	7±0.8	10.1±1.1
IL-6	11.7±3	13.6±3.75
IL-9	41.3±6.3	40.6±3.3
IL-12p40	970.8±68	930.5±72
IL-12p70	2263±98	2541.9±
IL-13	82.2±13	89±8.2
IL-17A	189.9±28	227.4±18.5
Eotaxin	2084.3±210	1866.3±160
G-CSF	308.6±85	419.6±129.5
GM-CSF	-	-
IFN-ϒ	43.8±3.4	43.8±4.9
KC	58±8.9	53.3±10
MCP-1	257.8±31.6	265.5±26.6
MIP-1α	6.2±0.2	6.29±0.4
MIP-1β	25.8±1.7	25.2±1.36
RANTES	68.6±8.44	51.84±6.6
TNF-α	1386.2±60.7	1493±108

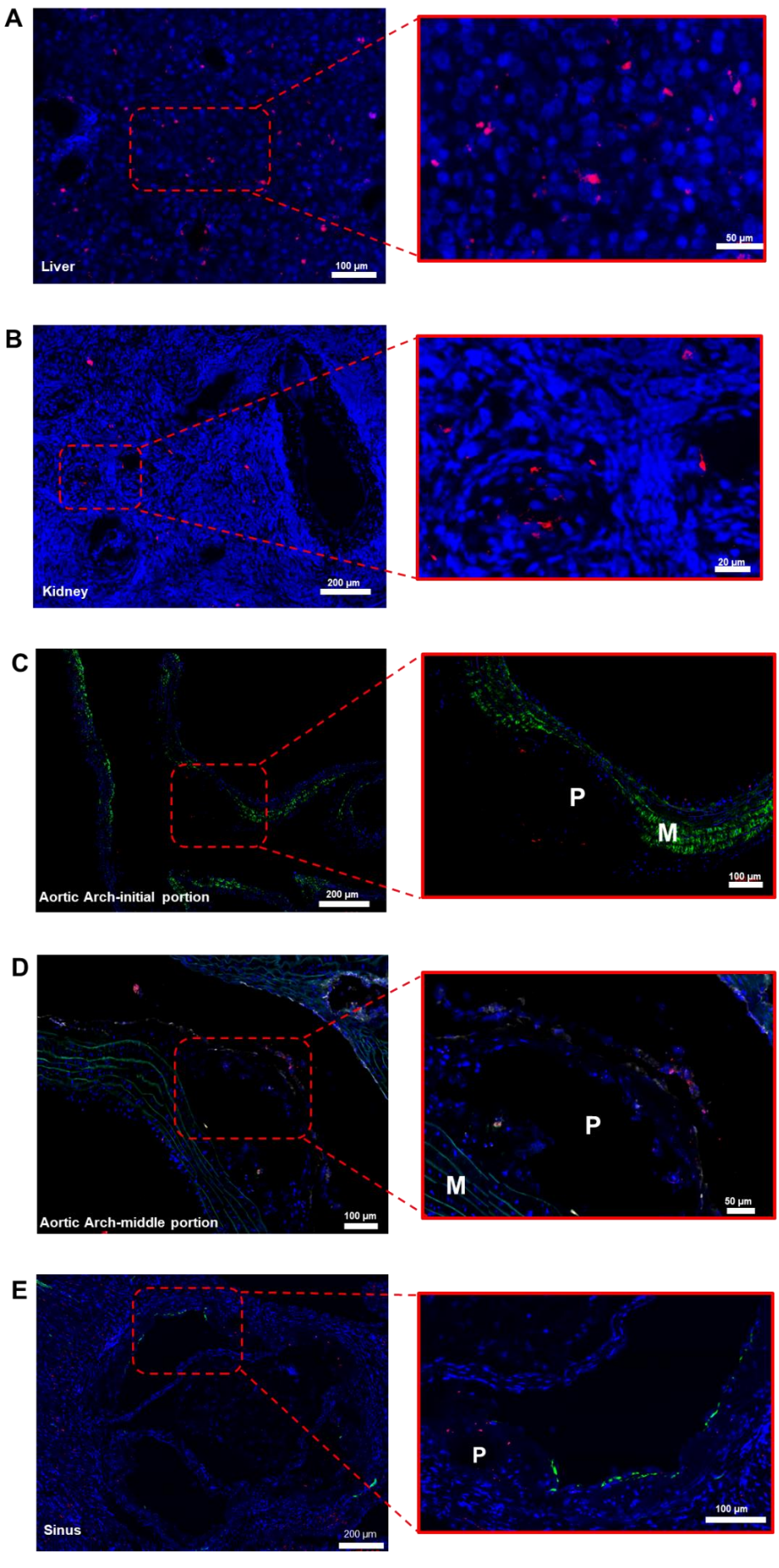
A
Liver
100 μm
50 μm
B
Kidney
200 μm
20 μm
C
Aortic Arch-initial portion
200 μm
P
M
100 μm
D
Aortic Arch-middle portion
100 μm
P
M
50 μm
E
Sinus
200 μm
P
100 μm

Figure 3.S12. Representative Bio-distribution confocal imaging after injection of Cy5-liposomes (red signal) in a one-year-old female apoE$^{-/-}$ mouse. Liver (A), and kidney (B), aortic arch: initial portion (C), middle portion (D) and aortic sinus (C). In C and D α-smooth muscle actin (α-SMA) was stained by immunofluorescence (green signal), in all of the images cell nuclei were stained using DAPI (blue signal). Insets: M= Media; P= Plaque.

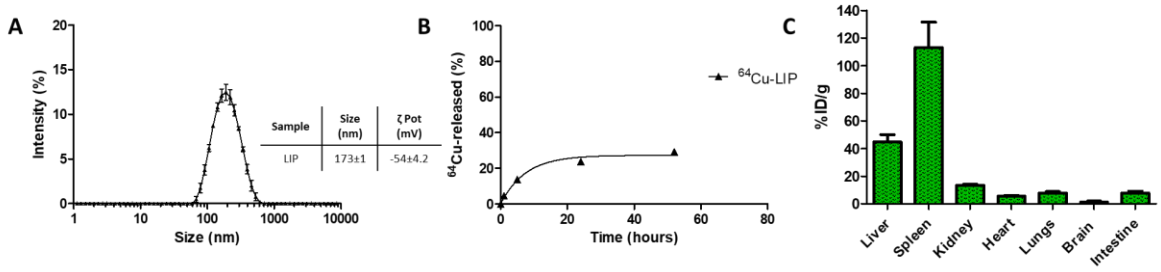

Figure 3.S13. Bio-distribution study. A. DLS analysis of ^{64}Cu-LIP. B. Release study of ^{64}Cu from LIP. C. Quantitative assessment of radioactivity distribution in selected tissues 24 h after injection (n = 5)

Chapter 4

Lipid nanoparticles encapsulating Methotrexate and Colchicine to enhance the antiiflammatory therapy

4.1. Abstract

Inflammation is one of the hallmarks in initiation, progression and in eventual thrombotic manifestations in Atherosclerosis. Hence, treatment with anti-inflammatory drugs, like methotrexate (MTX) and Colchicine (Col), could decrease the inflammation. Here, MTX-lipid conjugates, based on 1,2-distearoyl-sn-glycero-3-phosphoethanolamine (DSPE) and Col were proposed as drugs and co-loaded in the lipid bi-layer of liposomes (LipComb). The particles had an average size of 100 nm and presented a stability up to 4 days. They showed an encapsulation efficiency of ~ 28 % for MTX and ~ 33 % for Col with a ratio of 1:16. Treatment with the liposomes was found to significantly reduce LPS induced inflammation in primary BMDM cell line. At the same time, they also mitigated the overexpression of ABCA1, a gene involved in the oxLDL efflux from the cells. This also resulted in a strong reduction of the expression of IL-1β by 3-fold, IL-6 by 2-fold and also moderately of TNF-α. These results suggest that the combination of the chemotherapeutic drugs could strongly reduce the inflammation thereby modulating the disease progression.

4.2. Introduction

Atherosclerosis is a complex disease process that shows inflammation as one of the key players in its initiation, progression, and eventually thrombotic manifestations. It is characterized by the formation of complex subintimal plaques that restrict luminal blood flow, increasing the possibility of thrombotic occlusion and tissue infarction.[189] Stable plaques are characterized by chronic inflammatory infiltrate, while vulnerable plaques present active inflammation that could lead to plaque rupture [190]. Inflammation is involved in all the forms of plaque [22, 191]. In fact, van der Wall *et al.* provided evidence that there is a relationship among an inflammatory infiltrate, plaque rupture, and thrombosis [192]. These observations suggested that macrophages had a pathogenic role at the site of cap rupture in patients with fatal acute myocardial infarction [192]. The current therapies for atherosclerotic coronary artery disease (CAD), like the lipid-lowering statins, do not adequately control plaque inflammation. In the last years, the attention was focalized on alternative strategy using generic drugs with a broad anti-inflammatory properties for atheroprotection. Particularly, Methotrexate and Colchicine are currently under investigation in clinical trials. The first one is an inexpensive chemotherapeutic drug with pleiotropic upstream anti-inflammatory activity. It is used as first line therapy for conditions characterized by systemic inflammation, such as rheumatoid arthritis and psoriasis. Low dose of Methotrexate increases levels of adenosine down-regulating inflammation through several mechanisms.[193, 194] While, Colchicine is an anti-inflammatory drug used for the treatment of gout and other disorders, like familial Mediterranean fever (FMF) and recurrent pericarditis. Recently, it was discovered that it attenuated the activation of the NLR family pyrin domain containing 3 (NLRP3) inflammasome in Colchicine-treated neutrophils and macrophages as a response to monosodium urate crystals in the setting of gout. [195, 196] However, it is important to underline the various side effects on patients (e.g., neutropenia, infection, thrombocytopenia, liver and gastrointestinal toxicity, anemia, mucositis, and others) caused from both the drugs[148, 197]. To overcome the side effects, anti-inflammatory drug delivery systems with different nano-platforms have been tested. In a

previous work, the authors conjugated MTX to a lipid chain and deliver the prodrug using liposomes[90]. The authors showed that MTX-liposomes were able to increase the expulsion of cholesterol from foam cells leading to a reduction of pro-inflammatory cytokines expression compare with free drug. *In vivo* studies demonstrated that MTX-liposomes effectively reduced plaque area in ApoE-/- supporting the concept that a systemic delivery of MTX loaded particles may constitute an effective strategy to inhibit early atherogenesis.[90] In contemporaneous, other studies have shown the potency of nano-systems delivering Colchicine. [91, 198] Delivering Colchicine, by using a thermo-sensitive polymer hydrogel, resulted in a more efficient treatment than the free drug, alleviating the cardiac inflammation and inhibiting myocardial apoptosis and fibrosis. This data was reflected on the increased survival rate study on a group receiving the system compare to free administration of Colchicine in murine model. [198]

In this work, MTX and COL were co-loaded, into liposomes to improve and increase its therapeutic efficiency. In contrast to previous works, these nanoparticles were realized using a microfluidic system, Nanoassemblr. Specifically, lipid-MTX conjugate, obtained by reacting MTX with the lipid chain 1,2-distearoyl-sn-glycero-3-phosphoethanolamine (DSPE) was incorporated in the structure or in the bilayer of the liposomes while Col was encapsulated in the aqueous core. After extensive biophysical and pharmacological characterizations, MTX-COL-loaded liposomes (LipComb) were tested *in vitro* to demonstrate their ability to reduce the inflammation, modulating oxLDL uptake, on the macrophages.

4.3. Materials and Methods

Materials: 1-Ethyl-3-(3-dimethylaminopropyl) carbodiimide (EDC), N-Hydroxysuccinimide (NHS), Triethylamine (TEA), Low-density lipoproteins (LDL) and Colchicine were purchased from Sigma-Aldrich (St. Louis, MO, USA). Methotrexate (MTX) was bought by AlfaAesar (Haverhill, MA, USA). 1,2-distearoyl-sn-glycero-3-phosphoethanolamine-N-[succinyl(polyethylene glycol)-2000] (DSPE-PEG-COOH), 1,2-distearoyl-sn-glycero-3-

phosphoethanolamine (DSPE_NH2), 1,2-Dipalmitoyl-sn-glycero-3-phosphocholine (DPPC) were purchased from Avanti Polar Lipid (Alabaster, AL, USA). All reagents and solvents were used without further purification.

Synthesis of DSPE-MTX.

DSPE-MTX was synthesized as reported by Di Francesco and coworkers.[90] Briefly, 30 mg of MTX was incubated with 1-Ethyl-3-(3-dimethylaminopropyl)carbodiimide (EDC) / N-Hydroxysuccinimide (NHS) in Dimethyl sulfoxide (DMSO) for 30 minutes, at room temperature. After the dissolution of the DSPE in DMSO, it was added to the previous solution. A catalytic amount of triethylamine (TEA) was added to the reaction and left to stir for 72 hours. The mixture was washed with cold diethyl ether. Finally, the prodrug was lyophilized and stored at -20°C.

Synthesis of LipCombo.

DPPC, cholesterol, DSPE-PEG2000 (6:3:1) and DSPE-MTX (1.5mg/ml) was dissolved in EtOH, while Colchicine (0.005 mg/ml) in PBS. The organic solvent with dissolved lipids and an aqueous solution with Colchicine was injected into the two inlets of the Nanoassemblr. Aqueous dispersions of the liposomes was Collected from the outlet, resulting from the mixing of two adjacent streams and dialysed against PBS for 1h a 4°C in order to remove the excess EtOH.

Drug loading and release.

To measure the MTX and Col encapsulation efficiency (EE), the samples were lyophilized, dissolved in acetonitrile/H2O (1:1, v/v), and analyzed by high-performance liquid chromatography (HPLC) (Agilent 1260 Infinity, Germany) equipped with a 100 µL sample loop injector. A C18 Column (2.1× 250 mm, 5 µm particle size, Agilent, USA) was used for the

chromatographic separation. MTX and Col was eluted under isocratic conditions using a binary solvent system [H2O + 0.1% (v/v) TFA, 43:57 v/v] pumped at a flow rate of 1.0 mL/min.
EE was determined using the following equation:

$$EE\ (\%) = \frac{MTX/COL\ weight\ in\ particles}{MTX/COL\ inizial\ feeding\ amount} \times 100$$

To study MTX and Col-release kinetics, 200 µL of MTX-Col-nanoparticle solution was placed into Slide-A-Lyzer MINI dialysis microtubes with a molecular cutoff of 10 kDa (Thermo Scientific) and dialysed against 4 L of PBS buffer (pH 7.4). For each time point, three samples were Collected and dried. All the samples were destroyed with cold methanol, left to dry, dissolved in acetonitrile/H2O (1:1, v/v) and analyzed by HPLC for the MTX. The experimental data were fitted by using the Ritger–Peppas model for controlled, not swellable drug-delivery systems [199] ($Y = k \times x^n$), where Y represents the drug percentage released, x is the time of observation, and k and n are the fitting parameters.

LDL oxidation.

LDL (2 mg/ml) were incubated with 5 mM CuSO4 at 37°C for 4h without EDTA. The reaction was interrupted with the addition of EDTA (5 mM). The formed oxidized LDL molecules (oxLDL) were dialyzed against PBS containing 0.01% EDTA at 4°C for 24 h and stored at 4°C.

Bone Marrow Derived Macrophages.

For Bone Marrow Derived Macrophages (BMDM), rat femurs were explanted and the extremities were cut off. Then, the bone marrow canal was flushed four times with 500 µL of medium. The resulting cell suspension was filtered using a 70 µm cell strainers. Cells were seeded in a Petri dish and medium was changed after 3 days to remove unattached cells. BMDMs were used on the following day. BMDMs were cultured in DMEM supplemented with

15% FBS, 1% penicillin/streptomycin, and rat M-CSF (according to vendor indications). Cells were cultured under controlled environmental conditions (37°C in 5% CO2).

Foam Cell formation.

BMDM cells were cultured in DMEM containing, respectively, 15% fetal bovine serum (FBS), 1% antibiotic (penicillin/streptomycin) and 1% glutamine. Cells were seeded at a density of 1x105 cells/mL. Macrophages were incubated with 50 µg/ml oxLDL overnight.

Confocal Fluorescent Microscopy imaging and analysis of Aspect Ratio and Circularity.

Confocal images of BMDM were obtained using a Nikon-A1 confocal microscope (Nikon Corporation, Japan). MTX-Col-nanoparticles were incubated with macrophages for 5 hours. 50,000 cells (BMDM) were seeded into each well of a Nunc™ Lab-Tek™ II Chamber Slide™ System (Thermo Fisher Scientific, USA) maintaining culturing conditions, as described before. After 5 h, the bacterial LPS were added at a concentration of 100 ng/mL and incubated for 4 h. Macrophages with the culturing media was removed and cells were washed in PBS (Thermo Fisher Scientific, USA). Fixation was performed using a 3.7% solution of PFA (Sigma Aldrich, USA) for 5 minutes. Cytoskeletal-membrane was stained with Wheat Germ Agglutinin (WGA) (Thermo Fisher Scientific, USA) and nuclei with DAPI (Thermo Fisher Scientific, USA) following the vendors indications. For each condition 10 images were taken. Data were analyzed with ImageJ.

Gene expression and toxicity.

BMDMs were cultured at 37°C in 5% CO_2, in high-glucose DMEM, supplemented with 15% FBS and 1% L-glutamine, according to ATCC instructions. Cells were seeded into 96-well plates at a density of 20×10^3 cells per well and incubated for 24, 48, 72 h. Cells were treated with different concentrations of free DSPE-MTX and Col, free Comb, LipComb (namely,

0.0064, 0.032, 0.16, 0.8, 4, 10 and 0 µM of MTX and 0.4, 2, 10, 50, 250, 625 nM of Col), or empty Lip. The MTT solution was added for 4 h and the formed formazan crystals were dissolved in ethanol. Absorbance was measured at 570 nm, using 650 nm as the reference wavelength (Tecan, Männedorf, Swiss). The percentage of cell viability was assessed according to the following equation:

$$Cell\ viability\ (\%) = \frac{Abs_T}{Abs_C} \times 100$$

where Abs_T is the absorbance of treated cells and Abs_C is the absorbance of untreated cells (control).

The anti-inflammatory effects, namely tumor necrosis factor- α (TNF-α), interleukin-1β (IL-1β), and interleukin-6 (IL-6), on the BMDM were tested.LipComb, DSPE-MTX, COL, free Comb were incubated for 5h with cells. Then, bacterial LPS was added at a concentration of 100 ng/mL and incubated for 4 h. At the end, RNA was extracted using a RNAeasy Plus Mini Kit (Qiagen) and quantified by NanoDrop2000 (Thermo Scientific, Waltham, Massachusetts, USA). Real-time RTPCR was used to measure mRNA levels of inflammatory cytokines.

The anti-inflammatory effects of LipComb was also tested on foam cells at 8 and 24 h by measuring gene expression of three pro-inflammatory cytokines, namely tumor necrosis factor-α (TNF-α), interleukin-1β (IL-1β), and interleukin-6 (IL-6) in rat BMDMs. The gene expression of foam cells markers (CD36 and SRA-1) and cholesterol expulsion ATP-binding cassette transporter 1 (ABCA1) was also assessed. Cells were cultured under controlled environmental conditions (37 °C in 5% CO2) and seeded into 6-well plates at a density of 4×10^5 cells per well. After 10 h, BMDMs were incubated with oxLDL overnight. Cells were treated with MTX-Col-nanoparticles at 0.16 µM and 0.01 of µM of MTX and Col, respectively and incubated for 8 and 24 h. To investigate the acute inflammation, BMDM were seeded into 6-well plates and treated with MTX-Col-nanoparticles at 0.16 µM and 0.01 of µM of MTX and Col, respectively and incubated for 5 hours. Then, bacterial LPS were added at a concentration of 100 ng/mL and incubated for 4 h. RNA was extracted using a RNAeasy Plus Mini Kit (Qiagen) and

quantified by NanoDrop2000 (Thermo Scientific, Waltham, Massachusetts, USA). Three independent biological replicates were run using a Power SYBR Green RNA-to-CT 1-Step Kit (Applied Biosystems) and using GAPDH gene expression as a housekeeping gene. Reactions were performed in a final volume of 10 µL. Primer pair sequences are listed below: GAPDH: 5′-CATCACTGCCACCCAGAAGACTG-3′ and 5′-ATGCCAGTGAGCTTCCCGTTCAG-3′; TNF-α: 5′-GGTGCCTATGTCTCAGCCTCTT-3′ and 5′-GCCATAGAACTGATGAGAGGGAG-3′; IL-1β: 5′-AACCTGCTGGTGTGTGACGTTC-3′ and 5′-CAGCACGAGGCTTTTTTGTTGT-3′; IL-6: 5′-TACCACTTCACAAGTCGGAGGC-3′ and 5′-CTGCAAGTGCATCATCGTTGTTC-3′; CD36: 5′-ATGGGCTGTGATCGGAACTG-3′ and 5′-GTCTTCCCAATAAGCATGTCTCC-3′; SRA-1: 5'-CTGAGACCTCTGGAACAGGCAT-3' and 5′-TGCACTAGCAGTGCCATCCTCT-3′; ABCA1: 5′-GGAGCCTTTGTGGAACTCTTCC-3′ and 5′- CGCTCTCTTCAGCCACTTTGAG-3′.

Statistical Analysis.

All the *in vitro* data were represented as the average ± standard deviation (SD) of 3 different measurements, unless differently specified. The statistical significant difference was assessed using ANOVA test, with Bonferroni's Multiples Comparison Test as post-hoc test. All statistical *in vitro* analyses were performed using GraphPad Prism v.5 (GraphPad Software, USA).

4.4. Results

Physico-chemical and pharmacological characterization of MTX-loaded nanoparticles.

Methotrexate (MTX) and Colchicine (Col), two conventional chemotherapeutics with potent anti-inflammatory effects, were used to investigate the effect on the treatment of affected by atherosclerosis. Problems associated with drugs solubility and bioavailability could be overcome using different drug delivery systems. Liposomes represent a good candidate for

both improving their bioavailability and reducing the side effects by enhancing the pharmacokinetic and pharmacodynamic properties.

To this end, MTX and Col were co-loaded in the liposomal structure: MTX in the form of DSPE-MTX in the bilayer while Col in the aqueous core. This formulation was obtained by a systematic optimization process (**table 4.1**) in order to have a ratio between MTX: Col 16: 1. [90, 200, 201] As listed in the table, the concentration of the Colchicine was decreased from 0.5 to 0.001 mg/ml. Liposomes realized in this work were obtained with 0.005 mg/ml of Colchicine in the aqueous phase and 1.5 mg/ml of DSPE-MTX in the organic phase.

Table 4.1. Optimization of the ratio between MTX and COL

Sample	Concentration of DSPE-MTX(mg/ml)	Concentration of COL (mg/ml)	Ratio (aq.phase/org.phase)	Flow (ml/min)	Concentration total lipid (mg/ml)	Molar ratio (MTX:COLC)
DSPE-MTX+COL	1.5	0.5	3:1	1	40	0.25:1
DSPE-MTX+COL	1.5	0.25	3:1	1	40	0.8:1
DSPE-MTX+COL	1.5	0.1	3:1	1	40	1.6:1
DSPE-MTX+COL	1.5	0.05	3:1	1	40	2:1
DSPE-MTX+COL	1.5	0.01	3:1	1	40	3.2:1
DSPE-MTX+COL	1.5	0.005	3:1	1	40	16:1
DSPE-MTX+COL	1.5	0.001	3:1	1	40	47:1

Particle size and size distribution were evaluated by Dynamic Light Scattering. Particles presented an average hydrodynamic diameter of 100 ± 1 nm, with a polydispersity index (PDI) 0.16 ± 0.02 nm (**Figure 4.1A**). Given the presence of carboxyl-terminated DSPE-PEG chains, LipComb presented a negative ζ potential of -40 ± 2 mV (**Figure 4.1A**). Particle stability under physiological condition (PBS buffer pH = 7.4, 1X) was evaluated up to 4 days. The liposomal formulation appeared stable under physiological conditions showing a percentage change in size and PDI lower than 5% through the entire observation period as reported in **Figure 4.1B**. Then, the Encapsulation Efficiency (EE) and the release profile of MTX and Col from the nanoformulation was determined using HPLC. MTX and Col encapsulation efficiency was evaluated as the percentage ratio between the actual loaded mass of the drug and the input

mass of the same used during nanoparticle preparation. LipComb presented a modest EE for both drugs: 28.2 ± 1.6% and 33.8 ± 5.9 for MTX and Col, respectively with a loading 423.5 ± 24.7 μg for MTX and 1.7 ± 0.28 μg for Col (**Figure 4.1C**). The release profiles for MTX and Col from Lip were obtained in 4 L PBS buffer (pH= 7.4, 1X) in order to mimic an infinite sink condition (**Figure 4.1D**). Both drugs were rapidly released from Lip. After 9 h, over 70% of both drugs were released out from liposomes while after 1 day, almost 90% release of both encapsulated MTX and Col was reached.

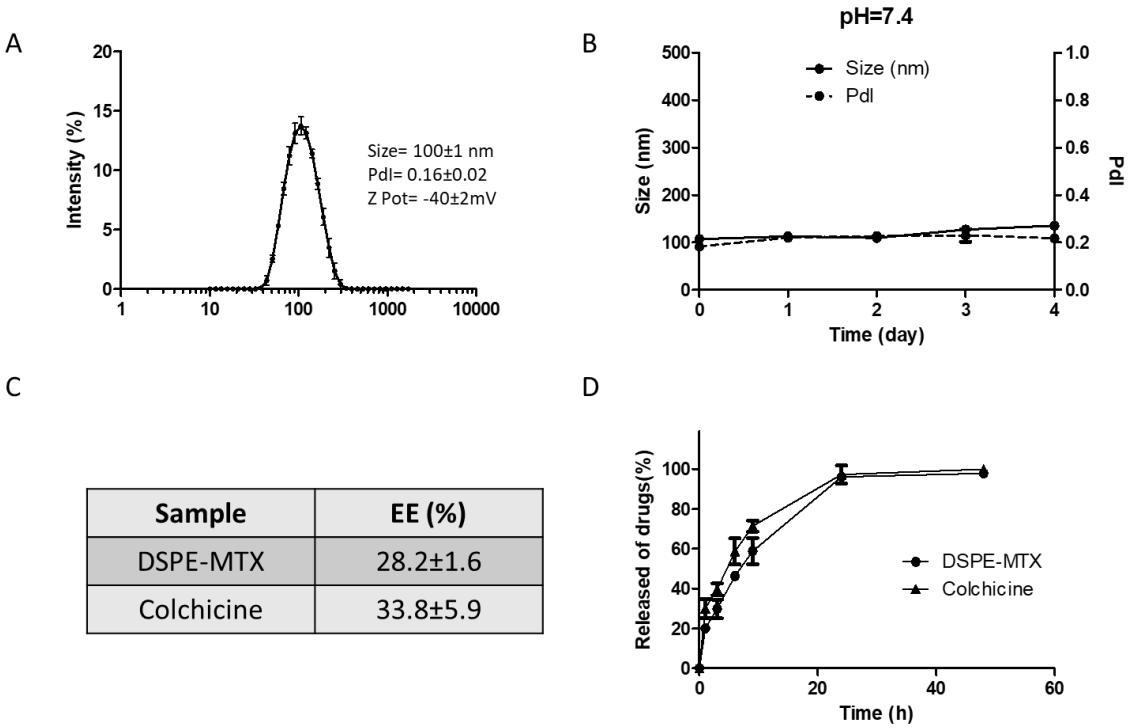

Sample	EE (%)
DSPE-MTX	28.2±1.6
Colchicine	33.8±5.9

Figure 4.1. Physico-chemical and pharmacological characterization of MTX-Col-loaded nanoparticles. A., B. Hydrodynamic diameter and Colloidal stability of LipComb via dynamic light scattering analysis. C. Encapsulation efficiency (%EE); D. release studies for MTX and COL from Lip.

Therapeutic Efficacy of MTX-Col-co-loaded Liposomes

Before studying the interaction of the liposomes with inflamed macrophages, the potential toxicity of free Col, DSPE-MTX, free Comb, and LipComb was assessed on primary phagocytic cells (BMDM). A drug concentration ranging from 60 nM to 10 µM and 0.4 to 625 nM was tested for the DSPE-MTX and for the Col, respectively. As shown in **Figure 4.2**, the cell viability was dose dependent, but time independent. For further *in vitro* experiments, a dug concentration of 160 nM for DSPE-MTX and 10 nM for the Col was used. In the previous work, it was observed that 160 nM had an anti-inflammatory effect and hence it was selected as the MTX concentration in this study.[12] In the case of COL, 10 nM was the concentration used *in vitro* as the anti-inflammatory drug concentration [200, 201].

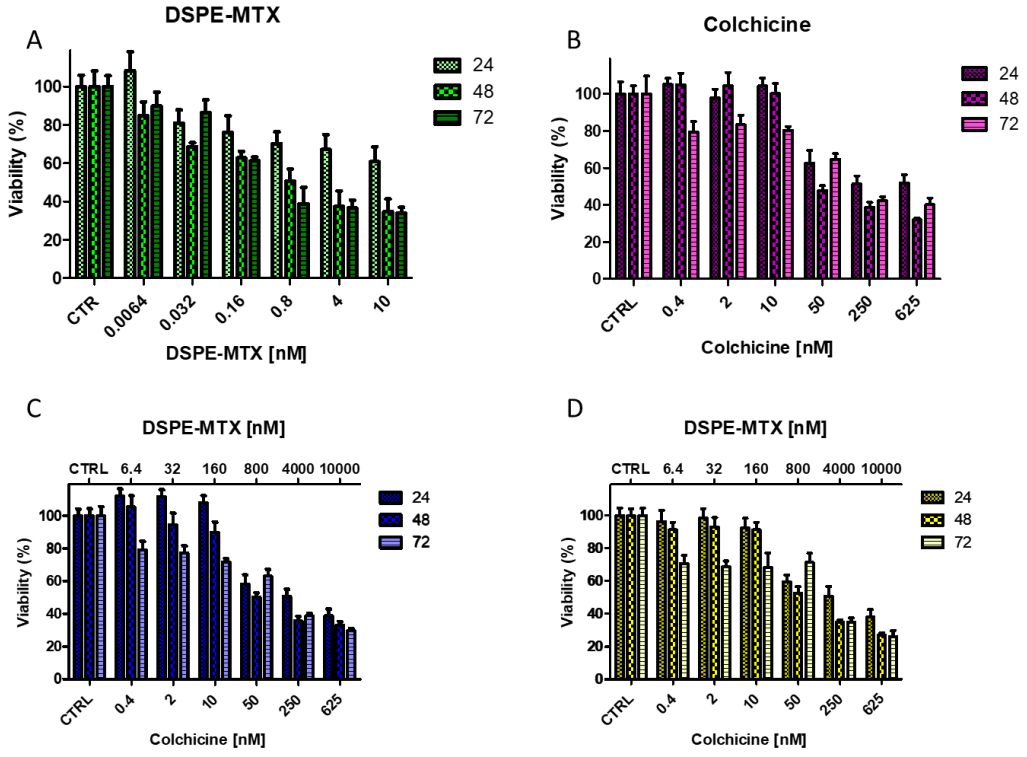

Figure 4.2. Cell Viability. BMDM viability upon incubation with DSPE-MTX (A), Colchicine (B), free Comb (C) and LipComb (D) at 24, 48 and 72h.

For demonstrating the anti-inflammatory activity of these two drugs, BMDM were incubated with Col, DSPE-MTX, free Comb, and LipComb (160 nM of DSPE-MTX and 10 nM of Col). Then, BMDM were stimulated with LPS for inducing the secretion of TNF-α, IL-1β, and IL-6. As reported in **Figure 4.3A-C**, drugs, free or co-loaded in liposomes, reduced the expression of the studied pro-inflammatory cytokines. In particular, when drugs were co-loaded inside liposomes, the inflammation was significantly reduced for all tested genes compared to the CTR and was slightly higher than the free Comb (**Figure 4.3A-C**). Results were also confirmed by morphology analysis (**Figure 4.3D-I**). Importantly, cell shape changes have been associated with different functional states of cells [202] and morphological modifications associated with inflammatory responses [203]. However, there was insufficient information about the effect of LPS and other cytokines released in its effect on the morphology of these cells[203]. In general, LPS induced a visible change of the morphology and shape of the BMDM cells. For the analysis, same treatments were done on BMDM: incubation with Col, DSPE-MTX, free Comb, and LipComb for 5h followed by LPS stimulation for 4h. At this point, cells were washed with PBS, fixed with PFA and stained. Fluorescent images were acquired to analyze cells shape. As reported in **Figure 4.3D-I**, most of the cells maintained a round shape in case of control or pretreatment with Col, DSPE-MTX, free Comb, and especially with LipComb, while stellate shapes were demonstrated in LPS-stimulated cells. Also, the aspect ratio and the circularity of macrophages pre-treated with LipComb were similar to the ones of BMDM (untreated control). The analysis suggested that treatments with drug, especially with LipComb, preserved the morphology of the cell, after the stimulation with LPS.

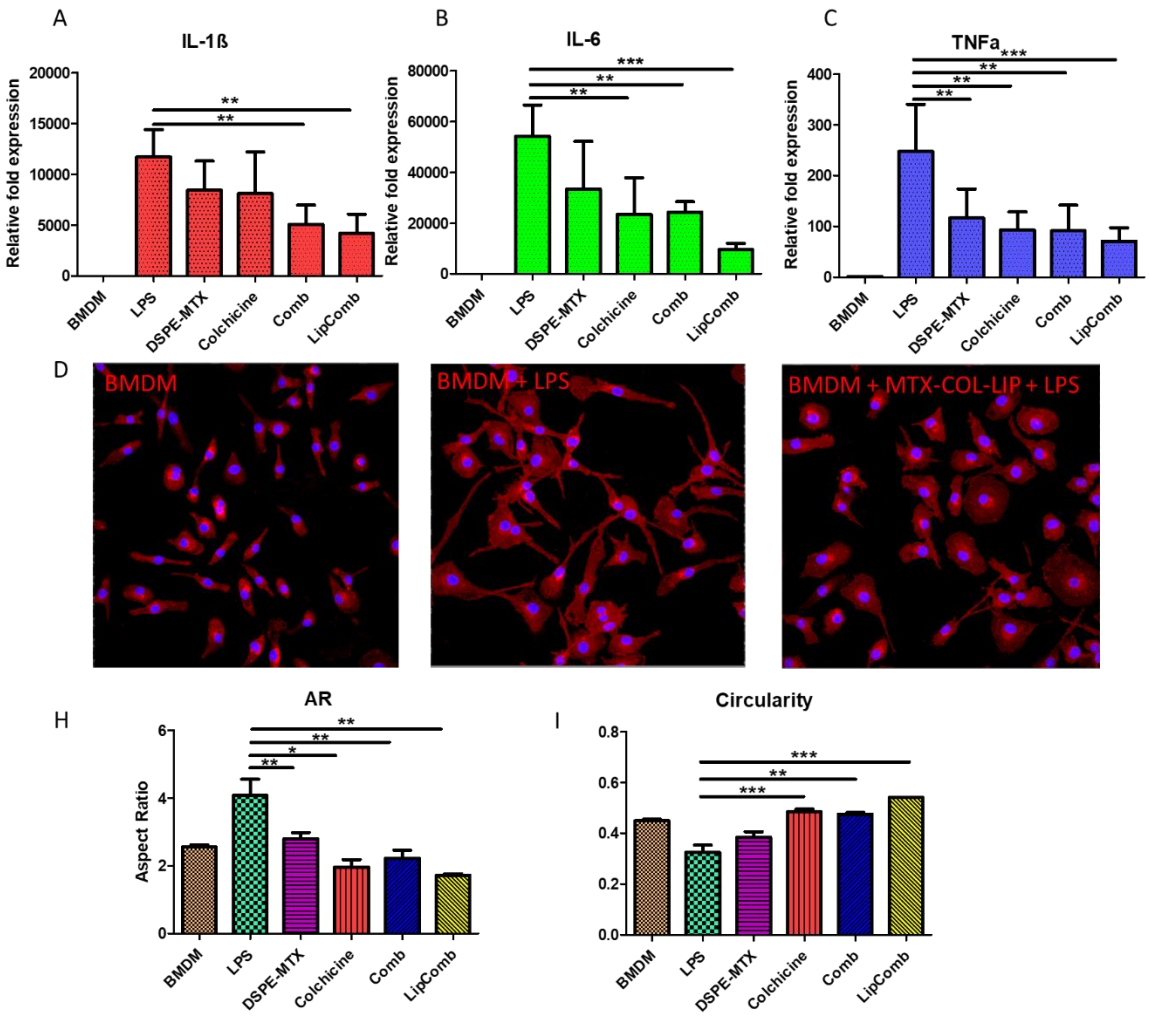

Figure 4.3. Expression of Inflammatory Genes in Macrophages. A-C. Expression level of Pro-inflammatory cytokines (IL-1β, IL-6 and TNF-α,) in macrophages pre-treated with free DSPE-MTX, COL, free Comb, LipComb for 5h and with LPS for 4h. (Data are expressed as average ± SD (n = 5). *** $p < 0.0001$; ** $p < 0.001$; * $p < 0.01$). D. Representative confocal images of BMDM pre-treated with LipComb followed by 4h of LPS treatment. H-I. Analysis of Aspect Ratio (AR) and circularity of BMDM after treatment with liposomes and LPS.

For evaluating the anti-inflammatory effect in atherosclerosis, the expression of three foam cells markers, such as ABCA1, CD36 and SRA-1, and three inflammatory genes, such as IL-1β; IL-6 and TNF-α, were taken into account. Their expression in the foam cells as a function

of different treatment conditions (free MTX and Col, free Comb,LipComb) was measured by real time PCR.

The ABCA1 is a foam cell marker involved in the cholesterol cell expulsion and its overexpression is correlated to an augmented LDL expulsion, while CD36 and SRA1 are involved in oxLDL uptake and their overexpression is considered essential in the transition from macrophage to foam cell.[90, 181] In particular, CD36 recognizes oxLDL lipid moieties and SRA1 binds the oxidized apo-lipoprotein portion. [181] Gene expression analysis was performed at two different time points, namely 8 and 24h, using untreated foam cells and BMDM (not exposed to oxLDL) as control groups presented in **Figure 3.4**. The gene expression levels were normalized with respect to foam cells, arbitrarily taken as equal to 1. Importantly, a direct comparison between BMDM (not exposed to oxLDL) and foam cells revealed an increase of 2 to 3 times of the expression of CD36 and SRA-1, at both time points. Indeed, this supports the hypothesis that an overnight exposure of BMDM to 50 μg/ml of oxLDL was sufficient to trigger the maturation into foam cells.

Figure 4.4 (top row) showed the expression of the three genes involved on cholesterol transport at 8h. For ABCA1, the relative fold expression increase with respect to untreated foam cells was equal to 1.31 ± 0.11 for free DSPE-MTX and 1.084 ± 0.334 for the free Col, 1.296 ± 0.682 for free Comb, and 1.91 ± 0.66 for LipComb, supporting the idea of an increase of cholesterol efflux. For CD36 and SRA-1, slight variations around a relative fold expression of 1 were observed for almost all treatments, except for LipComb. Specifically, in this case, the relative fold expression induced by LipComb was 0.677 ± 0.083 for CD36 and 0.803±0.0742 for SRA-1, while 0.909 ± 0.383 for CD36 and 0.854 ± 0.403 for SRA-1 in the case of free Comb. Data would suggest that the treatment of foam cells with the nanoformulated LipComb would induce a significant overexpression of ABCA1, thus boosting cholesterol efflux. Also, it induced a moderate downregulation of CD36, involved in cholesterol influx. On the other hand, after 24h, a reduction in the expression of all three genes was recorded for all the treatment conditions (**Figure 4.4**).

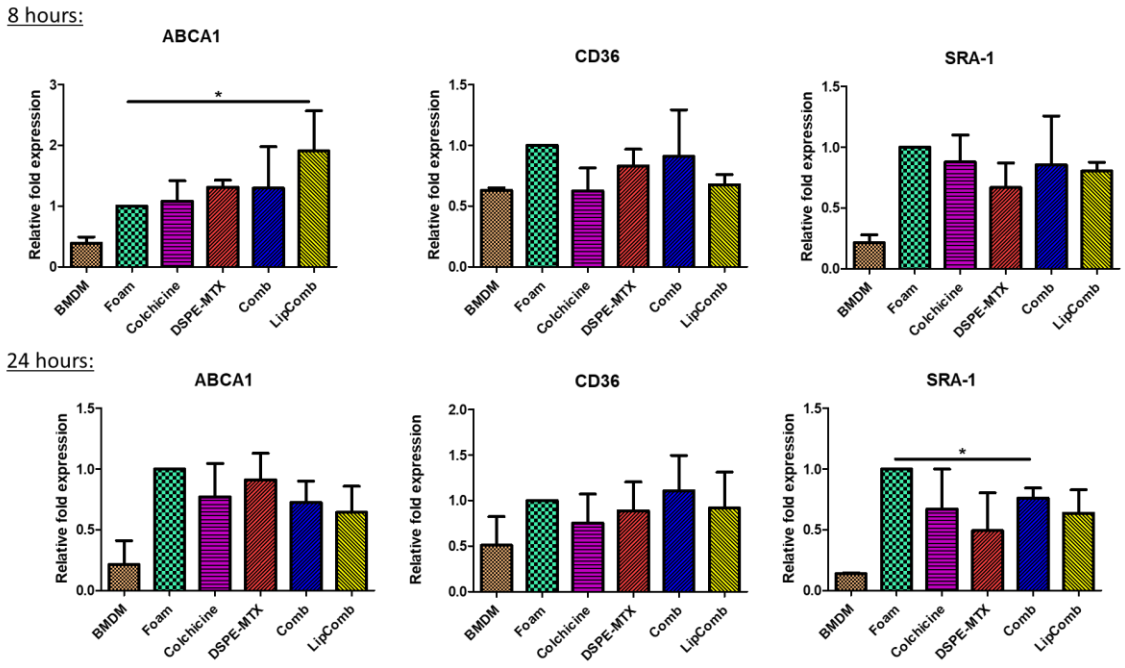

Figure 4.4. Expression of Cholesterol Transport Genes in Macrophages. A. Expression level of foam cells markers (ABCA1, CD36, and SRA-1) in macrophages treated with free DSPE-MTX, COL, free Comb, LipComb for 8h and 24h. (Data are expressed as average ± SD (n = 5). * $p < 0.01$).

As per the inflammatory response, an overall decrease of all three genes expression was observed at both 8 and 24h upon treating the foam cells with either free MTX, COL or free Comb or MTX-COL-loaded nanoparticles. However, the efficacy of the drug combination on the inflammation was clear after 24h (**Figure 4.5.**).

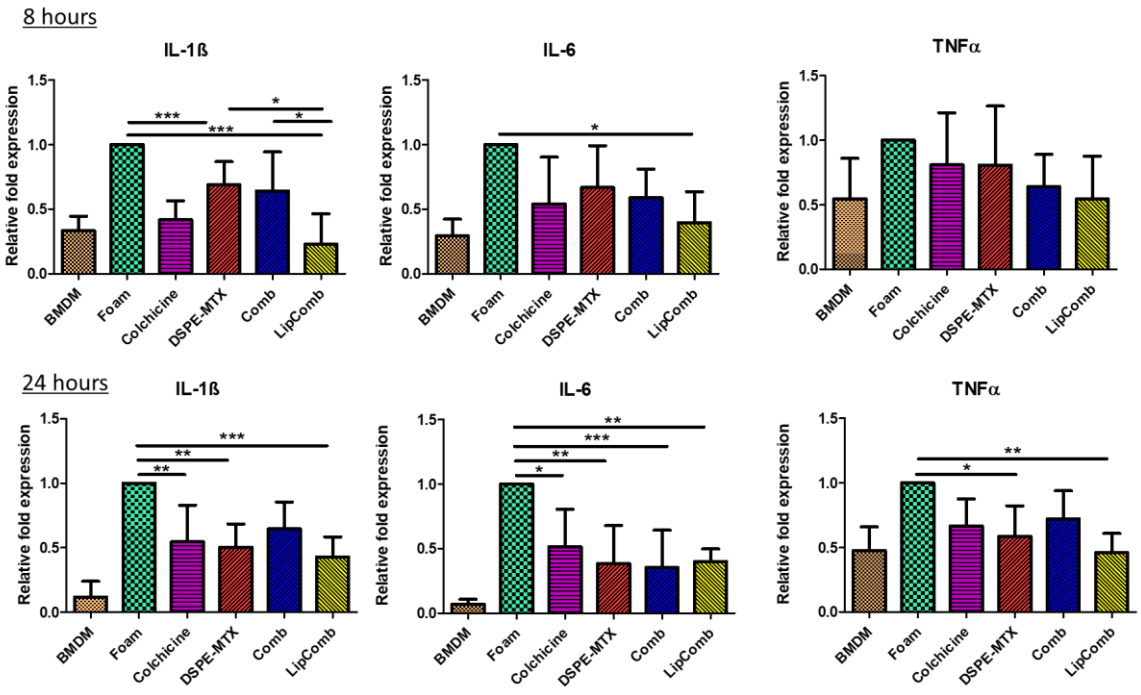

Figure 4.5. Expression of Cholesterol Transport and Inflammatory Genes in Macrophages and Cell Viability. Expression level of Pro-inflammatory cytokines (IL-1β, IL-6 and TNF-α) in macrophages treated with free DSPE-MTX, COL, free Comb, LipComb for 8h and 24h. (Data are expressed as average ± SD (n = 5). *** $p < 0.0001$; ** $p < 0.001$; * $p < 0.01$).

For IL-1β, the relative fold expression was reduced to 0.429 ± 0.154 for the LipComb and to 0.645 ± 0.211 for the free Comb. Free MTX and Col treatments were also able to reduce the IL-1β expression down to 0.504 ± 0.180 and 0.545 ± 0.284, respectively. Similar behavior was reported for IL-6. Its expression reduced by 2 times in comparison to foam cells when using LipComb (0.400 ± 0.097) and free Comb (0.353 ± 0.289), but also a reduction was observed in the case of free DSPE-MTX (0.384 ± 0.295) and free COL (0.514 ± 0.291). For TNF-α, the effect of LipComb and free Comb, as compared to the free drugs alone was not significant. Specifically, the relative fold expression levels of TNF-α decreased to 0.460 ± 0.148 for the LipComb, 0.721 ± 0.217 for the free Comb, and 0.586 ± 0.236 and 0.666 ± 0.210 for the free MTX and COL, respectively.

4.5. Discussion

Inflammation represents a key process at the basis of atherosclerosis development and progression. In order to target this, MTX and Col were loaded in liposomal formulation with a mass ratio of 1: 16 Col: DSPE-MTX. This ratio was selected because, in the previous work, authors demonstrated that 160 nM of MTX in liposomes was optimum to obtain important results in preventing and reverting the foam cells formation, and so on the inflammation[90].In case of Colchicine, Yang *et al*. demonstrated that 10 nM of the drug inhibited endothelial cell inflammation and pyroptosis induced by cholesterol crystals, suggesting its potential use in atherosclerosis[201]. The selected ratio between the two drugs was also reflected on their EE%. In the previous work[90], authors synthesized, by thin layer evaporation (TLE), liposomes-MTX with a size of ~ 150 nm and an EE% ~ 70%. Here, liposomes were obtained using a microfluidic device – Nanoassemblr, with different features. These nanoparticles presented a hydrodynamic size of 100 nm and an EE% of ~28% for DSPE-MTX and ~34% for Colchicine. The lower EE% observed in this case, compared to the previous one, was linked to the precise ratio that was chosen. As for the MTX-LIP, the obtained formulation appeared stable under physiological conditions up to 4 days (**Figure 4.1.**) and it resulted in a strong anti-inflammatory effect on a primary cell line (BMDM). In fact, as reported in **Figure 4.3.** the combination MTX-Col treatment, as free or co-loaded in liposomes, were able to reduce the inflammation by decreasing the expression of different cytokines. In particular, after the pre-treatment of MTX-Col treatment, the expression of IL-1β, IL-6 and TNF-α decreased significantly after the stimulation of LPS. In addition, MTX-Col combination treatments, as free or co-loaded in liposomes, were capable of stopping, and perhaps reverse, the progression of maturation of macrophages into foam cells, the pivotal step in the process of atherogenesis and atherosclerosis progression. LipComb increased significantly the expression of ABCA 1 in foam cells, the gene involved in the efflux of cholesterol from the cell (**Figure 4.4**). Consequently, a reduction of inflammatory cytokines expression over time was demonstrated

as compared to the foam cell, especially after 24h (**figure 4.5.**). It is important to underline that in the foam cell model, inflammation was only induced by exposure to oxLDL molecules.

These results highlight the ability of LipComb to reduce the expression of inflammatory cytokines, to act, both on the genes involved in cholesterol influx (MTX) and on inflammasome (Col). These effects were investigated in two different types of inflammation, one induced by LPS, and the other induced in foam cells by oxLDL. In our previous work, [90] we demonstrated the role of the MTX on the foam cell maturation and the progression of inflammation. Inflammation recalls the recruitment of monocytes in the vascular lesion, promoting their differentiation in macrophages and eventually foam cells.[143] As already reported, inflammation has an important role in the onset and progression of atherosclerosis and thrombosis. In particular, the chronic inflammation, immune activation, and oxidative stress of the arterial wall characterize atherosclerosis. [86] Moreover, all the cardiovascular risks start with the promotion of endothelial dysfunction and vascular damage. [87] The hypothesis that combined the effect of MTX and Col could be a good strategy for the reduction of the inflammation was also investigated by Robert G. Weiss at the Johns Hopkins University. He started a clinical trial for exploring the therapeutic efficacy of Methotrexate, Colchicine and/or their combination on coronary arteries function (Inflammation and Coronary Endothelial Function), more specifically on the inner lining of the arteries called the endothelium (ClinicalTrials.gov Identifier: NCT02366091). He is currently investigating the effect of inflammation on the artery's normal function using magnetic resonance imaging (MRI). This study is still ongoing, but MTX and Col anti-inflammatory effect, as a combination, needs to be investigated in detail. This study, also, highlights the synergic effect that these drugs could have when combined, supporting the idea/results of this work. Again, inflammation has an important role in the atherosclerosis and acting on it could reduce the progression of the pathology. Many authors investigated the effect of single drugs in atherosclerosis. It was demonstrated that Methotrexate loaded liposomes acts consistently on intracellular accumulation of oxLDL in macrophages reducing the inflammation[90], while Colchicine, when

delivered using thermos-sensitive polymer hydrogel, alleviated cardiac inflammation and inhibited myocardial apoptosis and fibrosis.[198] Indeed, the use of a drug delivery system could more efficiently deliver the two chemotherapeutic drugs to the target reducing the risk of adverse effects. Notably, this is the first work which demonstrated *in vitro* that liposomes co-loaded MTX and Col reduced the inflammation in a better way compared to free MTX, Col or their combination, modulating the foam cell formation and the release of pro-inflammatory cytokines.

4.6. Conclusions

Liposomes were synthesized with a microfluidic system (Nanoassemblr). This formulation was optimized for the co-loading of potent chemotherapeutic molecules, such as Methotrexate (conjugated a lipid chain) and Colchicine. Obtained particles were stable in the physiological environment up to 4 days, with a hydrodynamic average size of 100 nm. They were characterized and loaded with potent chemotherapeutic molecules, Methotrexate (conjugated a lipid chain), and Colchicine. MTX, conjugated with a lipid chain, was intercalated in the bilayer (becoming a part of the liposome structure) while the COL was loaded in the aqueous core. They were characterized *in vitro* for their Physico-chemical and pharmacological properties. The potency in reducing the inflammation was strongly demonstrated in the gene expression analysis underlining the influence in the foam cell formation.

Chapter 5

Conclusion

Methotrexate (MTX) has played an important role in the treatment of several diseases [96, 204]. However, its application is limited by its poor solubility, toxic side effects, and nonspecific accumulation in the target site [124]. One of the first outcomes of this experimental work was to establish strategies for increasing MTX efficacy and decreasing side effects by combining chemistry and nanomedicine. In this attempt, chemical modifications were performed in order to improve MTX solubility in common organic solvents used for particle synthesis, such as chloroform and Dichloromethane. Two different compounds, DSPE and PEG, were selected for developing MTX-prodrugs (DSPE-MTX and PEG-MTX). These modifications had an impact on the solubility of the original molecule. Three different software (Biovia, VCCLab and ACD ChemSchetch) were used to analyze the partition coefficient (Log P) of MTX and the two developed prodrugs. The mathematical analysis revealed that MTX and PEG-MTX could be equally dissolved both in water and organic solvents (MTX: log P. = 0.11; -0.91; 0.023; PEG-MTX: log P. = -0.67; 0.42; -0.43), while DSPE-MTX was mainly soluble in organic solvents (DSPE-MTX: log P. = 13.84; 7.53; 16.63). On the contrary, experimentally, MTX had shown a very low solubility both in water and organic solvents. Although the PEG-MTX featured a similar theoretical solubility, experimentally, it presented a more hybrid behavior, revealing a higher solubility in water and organic solvents compared to MTX. The reason for this behavior might be related to the amphiphilic properties of this prodrug, which could spontaneously organize in small structures. This factor was probably not taken into consideration by the software algorithms. Similar amphiphilic behavior was observed for MTX-DSPE. Due to this behavior, DSPE-MTX, PEG-MTX or both compounds were loaded successfully into liposomes.

The three formulations, DSPE-MTX/Lip, PEG-MTX/Lip and Combo-Lip, presented a similar physio-chemical feature but different stability over time in the acidic microenvironment (pH=6.5). In this environment, liposomes with PEG-MTX showed stability up to 3 days compared to the liposomes with DSPE-MTX or both prodrugs. All three formulations showed a biphasic release profile under infinite sink conditions (v = 4L). Specifically, DSPE-MTX and PEG-MTX formulations showed a burst drug release within the first 9 hours, with approximately 60% of the drug released, while the combo exhibited a faster release with 75% of DSPE-MTX/PEG-MTX after 9 hours. The remaining portion of drugs was slowly and continuously released over time, yielding a ~ 95% release after 1 day for Combo and 3 days for both DSPE-MTX or PEG-MTX. In general, multiple mechanisms, such as diffusion and erosion, act simultaneously during the release study for all the three liposomal formulations, as demonstrated by fitting the release data in various mathematical models. These might be related to the different interactions of the prodrugs with lipids and PEG-lipids in the liposomal structure.

In the last decade, MTX was proposed as an anti-inflammatory agent for treating atherosclerosis in patients affected by chronic inflammatory diseases [32]. Considering this, we suggested the use of MTX for reducing or reverting foam cell formation (mainly responsible for the plaque formation). The prodrug DSPE-MTX was loaded in two different nanoplatforms, the previously synthesized liposomes (LIP), and new polymeric nanoparticles (SPNs), to study their efficacy for the treatment of atherosclerosis. An *in vitro* comparative study was effectuated to assess the effectivity of the platforms. While LIP are spherical vesicles composed of a phospholipid bilayer, SPNs are spherical particles characterized by a hydrophobic core of PLGA stabilized by a lipid monolayer.

Particles with an average size of around 200 nm for both lipidic and polymeric formulations were obtained. Both formulations were characterized by a moderate polydispersity index (PDI) ~ 0.15, and a negative surface electrostatic ζ potential. They presented similar stability under physiological conditions (pH = 7.4) and an instability in a slightly acidic environment (pH = 6.5). However, a significant difference in the encapsulation efficiency of the two particles was noted. In the case of

MTX-LIP an encapsulation efficiency equal to 70.5 ± 4.8% was achieved, whereas this value dropped to only 1.5 ± 0.7% for the MTX-SPN. Their anti-inflammatory activity was evaluated *in vitro* on foam cells. Both formulations were actively uptaken by Bone Marrow-Derived Monocytes (BMDM). Results showed that the percentage (86.66 ± 3.59; 90.60 ± 2.23 and 87.30 ± 0.96 for LIP; 82.2 ± 1.1; 83.43 ± 2.82 and 82.87 ± 2.67 for SPN) of BMDM (used as control) associated with nanoparticles (i.e., percentage of positive events) was quite constant over time for both LIP and SPN for the three tested time points (2, 8 and 24h). The same study was realized on foam cells. It emerges from this study that the uptake was slightly lower when compared with BMDM (76.7 ± 0.14; 66.1 ± 2.26; 54.6 ± 0.71 for LIP, and 70.8 ± 5; 67.1 ± 2.54; 57.65 ± 1.06 for SPN), probably due to the large amounts of oxLDL stored in their lysosomes that could affect the cells' internalization capacity.

The variation of cholesterol on the cells before and upon the treatment was also quantified. Results showed that total intracellular cholesterol reduced as we moved from untreated foam cells to free MTX-treated foam cells, to MTX-LIP (0.20 ± 0.08 µg/µg) or MTX-SPNs (0.31 ± 0.07 µg/µg) treated foam cells (0.44 ± 0.12 µg/µg protein), and eventually to the BMDM, at 24h. In general, MTX-LIP was found to be more effective than the MTX-SPN. These results were in agreement with the expression of three foam cell markers (ABCA1, CD36, and SRA-1) and three inflammatory genes (IL-1β; IL-6, and TNF-α). In fact, MTX treatments, at 8h, appeared to have a significant effect on modulating inflammation by increasing the production of ABCA1, especially MTX-nanoparticles (1.383 ± 0.468 for free MTX; 2.048 ± 0.31 for MTX-LIP; and 2.793 ± 1.14 for MTX-SPN) and modest variations around a relative fold expression of 1 were observed for the CD36 and SRA-1. At 24h post MTX treatment, the expression of IL-1β, IL-6, and TNF-α went down significantly as compared to the case of foam cells. Both formulations were also tested for their biocompatibility on BMDM. Results showed that polymer formulation, empty or loaded MTX (IC_{50} of 1.7 ± 0.07 and 0.42 ± 0.12 µM, respectively) has a slightly higher cytotoxicity than LIP one (IC50 = 0.86 ± 0.1 µM). No significant toxicity was observed with empty LIP. Based on these observations, the following pre-clinical studies on $ApoE^{-/-}$ atherosclerosis mouse model were conducted with MTX-LIP. Results

demonstrated that the mice treated with MTX-LIP presented a reduction of the aortic sinus plaque compared with the control mice treated with empty LIP. No significant differences in total cholesterol and Luminex analysis were noticed between the two experimental groups. These data may suggest that MTX-LIP mainly exerted a local anti-inflammatory effect with minor systemic implications, as supported by the biodistribution study.

Based on these results and the new evidence on the impact of inflammation on arteriosclerosis, a strategy was envisaged to increase the anti-inflammatory effect of the previously developed liposomal formulation. In particular, the anti-inflammatory effect of MTX in combination with Colchicine, a chemotherapeutic drug, was investigated. Colchicine (COL) is generally used as an anti-inflammatory drug to treat gout and other disorders [68]. Recently, it was discovered that it attenuated the activation of the NLRP3 inflammasome. Based on this evidence, both drugs, COL and DSPE-MTX, were co-loaded in liposomal constructs to boost the anti-inflammatory effect by acting in different pathways of the inflammatory cascade. For this purpose, the nanoformulation was developed with the help of a microfluidic system, Nanoassemblr. With the use of the microfluidic system, particles presented an average size of around 100 nm, slightly lower than the liposomes from the previous study, a narrow size distribution (0.16 ± 0.02), and a negative ζ potential -40 ± 2 mV. A molar ratio between the two drugs of 16:1 MTX: COL was fixed after systematic optimization. MTX-Col-LIP presented an EE of 28.2 ± 1.6% and 33.8 ± 5.9 for MTX and Col, respectively. The developed formulation was stable under a physiological environment (pH=7.4) within 4 days. After evaluating their cytotoxicity activity, particles were tested for their anti-inflammatory effect *in vitro* on foam cells. Results showed that drug co-loaded liposomes reduced the inflammation significantly compared to the CTR for all the genes taken into account (TNF-α, IL-1β, and IL-6), as also confirmed by the morphological analysis. Combo-lip treatment for 8 h induced higher production of ABCA1 than the single drugs, either alone or in combination. However, the anti-inflammatory effect of the drug combination loaded liposomes appears more clearly after 24h of treatment. These are only preliminary results, and further investigations are needed to better understand the anti-inflammatory activity of MTX and COL, as a combination, in

the treatment of atherosclerosis. In *vivo studies* will be performed in order to assess the effect of MTX and Col as a combination in liposomes on the plaque progression, plaque composition, and vessel wall inflammation. For the quantification of plaque burden that is a good indicator of future coronary events, imaging techniques including magnetic resonance imaging (MRI) can be used. . Additionally, positron-emission tomography with 18F-fluorodeoxyglucose combined with computed tomography (^{18}F-FDG PET/CT) can be used to analyze the inflammatory activity within the atherosclerotic vessel (by monitoring the change of ^{18}F-FDG uptake). On the other hand, the histological density of macrophages can be used to confirm the infiltration of macrophages in an area characterized by more inflammation. In conclusion, the thesis provides important insights into the pathophysiology and progression of atherosclerosis and identified innovative ways of treating this challenging disease.

List of Publications

- **Di Francesco V**, Di Francesco M, Decuzzi P, Palomba R, Ferreira MFMM. “Synthesis of Two Methotrexate Prodrugs for Optimizing Drug Loading into Liposomes”. Pharmaceutics, 2021, 13.3: 332. doi.org/10.3390/pharmaceutics13030332.

- **Di Francesco V**, Gurgone D, Palomba R, Ferreira MFMM, Catelani T, Cervadoro A, Maffia P, Decuzzi P. “Modulating lipoprotein transcellular transport and atherosclerotic plaque formation in apoE -/- mice via nanoformulated lipid-methotrexate” ACS Appl Mater Interfaces. 2020 Jul 28. doi: 10.1021/acsami.0c12202.

- Ferreira M, Rizzuti IF, Palange AL, Barbato MG, **Di Francesco V**, Di Francesco M, Decuzzi P, “Optimizing the pharmacological properties of discoidal polymeric nanoconstructs against triple negative breast cancer cells”, Front Bioeng Biotechnol, 2020, doi: 10.3389/fbioe.2020.00005.

- Di Francesco M, Primavera R, Summa M, Pannuzzo M, **Di Francesco V**, Di Mascolo D, Bertorelli R, Decuzzi P,”Engineering shape-defined PLGA microPlates for the sustained release of anti-inflammatory molecules”, J Control Release, 2019; 319:201-212. doi: 10.1016/j.jconrel.2019.12.039.

Awards:

Best oral communication award at the 1st International Northern-Southern Europe Workshop in Nanomedicine, at the University of Chieti – Pescara “G. D’Annunzio” from January 15-17, 2020.

References

1. Abubakar, I., T. Tillmann, and A. Banerjee, *Global, regional, and national age-sex specific all-cause and cause-specific mortality for 240 causes of death, 1990-2013: a systematic analysis for the Global Burden of Disease Study 2013.* Lancet, 2015. **385**(9963): p. 117-171.
2. Mozaffarian, D., *Global scourge of cardiovascular disease: time for health care systems reform and precision population health*. 2017, American College of Cardiology Foundation Washington, DC.
3. Roth, G.A., et al., *Global, regional, and national burden of cardiovascular diseases for 10 causes, 1990 to 2015.* Journal of the American College of Cardiology, 2017. **70**(1): p. 1-25.
4. WHO. *About cardiovascular diseases. Geneva: World Health Organization.* November 6, 2019]; Available from: https://www.who.int/cardiovascular_diseases/about_cvd/en/.
5. Lnsis, A., *Atherosclenrosis.* Nature, 2000. **407**: p. 233-241.
6. Lusis, A.J., *Insight review articles.* Nature. Nat Publ Gr, 2000. **407**: p. 233-41.
7. Hossain, S.S., et al., *Magnetic resonance imaging-based computational modelling of blood flow and nanomedicine deposition in patients with peripheral arterial disease.* Journal of The Royal Society Interface, 2015. **12**(106): p. 20150001.
8. Davies, P.F., *Hemodynamic shear stress and the endothelium in cardiovascular pathophysiology.* Nature clinical practice Cardiovascular medicine, 2009. **6**(1): p. 16-26.
9. Gargiulo, S., M. Gramanzini, and M. Mancini, *Molecular imaging of vulnerable atherosclerotic plaques in animal models.* International journal of molecular sciences, 2016. **17**(9): p. 1511.
10. Cochain, C. and A. Zernecke, *Macrophages in vascular inflammation and atherosclerosis.* Pflügers Archiv-European Journal of Physiology, 2017. **469**(3-4): p. 485-499.
11. Skålén, K., et al., *Subendothelial retention of atherogenic lipoproteins in early atherosclerosis.* Nature, 2002. **417**(6890): p. 750-754.
12. Ley, K. and Y. Huo, *VCAM-1 is critical in atherosclerosis.* Journal of Clinical Investigation, 2001. **107**(10): p. 1209-1210.
13. Escate, R., T. Padro, and L. Badimon, *LDL accelerates monocyte to macrophage differentiation: effects on adhesion and anoikis.* Atherosclerosis, 2016. **246**: p. 177-186.
14. Rubic, T., M. Trottmann, and R.L. Lorenz, *Stimulation of CD36 and the key effector of reverse cholesterol transport ATP-binding cassette A1 in monocytoid cells by niacin.* Biochemical pharmacology, 2004. **67**(3): p. 411-419.
15. Jamkhande, P., et al., *Therapeutic approaches to drug targets in atherosclerosis, Saudi Pharm.* Saudi Pharmaceutical Journal, 2014.
16. Ross, S., et al., *Effect of bile acid sequestrants on the risk of cardiovascular events: a Mendelian randomization analysis.* Circulation: Cardiovascular Genetics, 2015. **8**(4): p. 618-627.
17. Naghavi, M., et al., *From vulnerable plaque to vulnerable patient: a call for new definitions and risk assessment strategies: Part I.* Circulation, 2003. **108**(14): p. 1664-1672.
18. Tarkin, J.M., et al., *Imaging atherosclerosis.* Circulation research, 2016. **118**(4): p. 750-769.
19. Kockx, M. and M. Knaapen, *Pathological changes in the coronary arteries in the acute coronary syndromes.* Heart, 2006. **92**(11): p. 1557-1558.
20. Rioufol, G., et al., *Multiple atherosclerotic plaque rupture in acute coronary syndrome: a three-vessel intravascular ultrasound study.* Circulation, 2002. **106**(7): p. 804-808.
21. Hansson, G.K., *Inflammation and atherosclerosis: the end of a controversy.* Circulation, 2017. **136**(20): p. 1875-1877.
22. Ross, R., *Atherosclerosis—an inflammatory disease.* New England journal of medicine, 1999. **340**(2): p. 115-126.

23. Palmer, R.D. and M. Vaccarezza, *New promises and challenges on inflammation and atherosclerosis: insights from CANTOS and CIRT Trials.* Frontiers in cardiovascular medicine, 2019. **6**: p. 90.
24. Riccioni, G. and V. Sblendorio, *Atherosclerosis: from biology to pharmacological treatment.* Journal of geriatric cardiology: JGC, 2012. **9**(3): p. 305.
25. Galván-Peña, S. and L.A. O'Neill, *Metabolic reprograming in macrophage polarization.* Frontiers in immunology, 2014. **5**: p. 420.
26. Hoeksema, M.A., J.L. Stöger, and M.P. de Winther, *Molecular pathways regulating macrophage polarization: implications for atherosclerosis.* Current atherosclerosis reports, 2012. **14**(3): p. 254-263.
27. Bi, Y., et al., *M2 macrophages as a potential target for antiatherosclerosis treatment.* Neural plasticity, 2019. **2019**.
28. Chan, E.S. and B.N. Cronstein, *Mechanisms of action of methotrexate.* Bulletin of the NYU Hospital for Joint Diseases, 2013. **71**(suppl 1): p. S5.
29. !!! INVALID CITATION !!! .
30. Chistiakov, D.A., et al., *Mechanisms of foam cell formation in atherosclerosis.* Journal of Molecular Medicine, 2017. **95**(11): p. 1153-1165.
31. Chistiakov, D.A., Y.V. Bobryshev, and A.N. Orekhov, *Macrophage-mediated cholesterol handling in atherosclerosis.* Journal of cellular and molecular medicine, 2016. **20**(1): p. 17-28.
32. De Vecchis, R., C. Baldi, and L. Palmisani, *Protective effects of methotrexate against ischemic cardiovascular disorders in patients treated for rheumatoid arthritis or psoriasis: novel therapeutic insights coming from a meta-analysis of the literature data.* Anatolian journal of cardiology, 2016. **16**(1): p. 2.
33. Bulgarelli, A., et al., *Treatment with methotrexate inhibits atherogenesis in cholesterol-fed rabbits.* Journal of cardiovascular pharmacology, 2012. **59**(4): p. 308-314.
34. Nishina, N., et al., *Reduction of plasma IL-6 but not TNF-α by methotrexate in patients with early rheumatoid arthritis: a potential biomarker for radiographic progression.* Clinical rheumatology, 2013. **32**(11): p. 1661-1666.
35. Singh, J.A., et al., *2012 update of the 2008 American College of Rheumatology recommendations for the use of disease-modifying antirheumatic drugs and biologic agents in the treatment of rheumatoid arthritis.* Arthritis care & research, 2012. **64**(5): p. 625-639.
36. Micha, R., et al., *Systematic review and meta-analysis of methotrexate use and risk of cardiovascular disease.* The American journal of cardiology, 2011. **108**(9): p. 1362-1370.
37. Gerards, A.H., et al., *Inhibition of cytokine production by methotrexate. Studies in healthy volunteers and patients with rheumatoid arthritis.* Rheumatology, 2003. **42**(10): p. 1189-1196.
38. Rho, Y.H., et al., *Drugs used in the treatment of rheumatoid arthritis: relationship between current use and cardiovascular risk factors.* Archives of drug information, 2009. **2**(2): p. 34-40.
39. Coomes, E., E.S. Chan, and A.B. Reiss, *Methotrexate in atherogenesis and cholesterol metabolism.* Cholesterol, 2011. **2011**.
40. Reiss, A.B., et al., *Adenosine A2A receptor occupancy stimulates expression of proteins involved in reverse cholesterol transport and inhibits foam cell formation in macrophages.* Journal of leukocyte biology, 2004. **76**(3): p. 727-734.
41. McPherson, J.A., et al., *Adenosine A2A receptor stimulation reduces inflammation and neointimal growth in a murine carotid ligation model.* Arteriosclerosis, thrombosis, and vascular biology, 2001. **21**(5): p. 791-796.
42. Ridker, P.M., et al., *Low-Dose Methotrexate for the Prevention of Atherosclerotic Events.* New England Journal of Medicine, 2019. **380**(8): p. 752-762.

43. Thornton, C., et al., *Methotrexate-mediated activation of an AMPK-CREB-dependent pathway: a novel mechanism for vascular protection in chronic systemic inflammation.* Annals of the Rheumatic Diseases, 2016. **75**(2): p. 439-448.
44. Ferrari, M., *Frontiers in cancer nanomedicine: directing mass transport through biological barriers.* Trends in Biotechnology, 2010. **28**(4): p. 181-188.
45. Agyare, E. and K. Kandimalla, *Delivery of polymeric nanoparticles to target vascular diseases.* Journal of biomolecular research & therapeutics, 2014. **3**(1).
46. Di Mascolo, D., et al., *Rosiglitazone-loaded nanospheres for modulating macrophage-specific inflammation in obesity.* Journal of Controlled Release, 2013. **170**(3): p. 460-468.
47. Stigliano, C., et al., *Methotraxate-Loaded Hybrid Nanoconstructs Target Vascular Lesions and Inhibit Atherosclerosis Progression in ApoE−/− Mice.* Advanced healthcare materials, 2017. **6**(13): p. 1601286.
48. Maranhão, R.C., et al., *Methotrexate Carried in Lipid Core Nanoparticles Reduces Myocardial Infarction Size and Improves Cardiac Function in Rats.* International journal of nanomedicine, 2017. **12**: p. 3767.
49. Gomes, F.L., et al., *Regression of atherosclerotic plaques of cholesterol-fed rabbits by combined chemotherapy with paclitaxel and methotrexate carried in lipid core nanoparticles.* Journal of cardiovascular pharmacology and therapeutics, 2018. **23**(6): p. 561-569.
50. Ridker, P.M., *Residual inflammatory risk: addressing the obverse side of the atherosclerosis prevention coin.* European heart journal, 2016. **37**(22): p. 1720-1722.
51. Westlake, S.L., et al., *The effect of methotrexate on cardiovascular disease in patients with rheumatoid arthritis: a systematic literature review.* Rheumatology, 2010. **49**(2): p. 295-307.
52. Choi, H.K., et al., *Methotrexate and mortality in patients with rheumatoid arthritis: a prospective study.* The Lancet, 2002. **359**(9313): p. 1173-1177.
53. Gridneva, G., et al., *Evaluation of methotrexate effect on the acute-phase response in rheumatoid arthritis after 12-week treatment.* Klinicheskaia meditsina, 2014. **92**(3): p. 59-63.
54. Bäck, M. and G.K. Hansson, *Anti-inflammatory therapies for atherosclerosis.* Nature reviews. Cardiology, 2015. **12**(4): p. 199.
55. Mach, F., et al., *Reduction of atherosclerosis in mice by inhibition of CD40 signalling.* Nature, 1998. **394**(6689): p. 200-203.
56. Hansson, G.K. and A. Hermansson, *The immune system in atherosclerosis.* Nature immunology, 2011. **12**(3): p. 204.
57. Schroder, K. and J. Tschopp, *The inflammasomes.* cell, 2010. **140**(6): p. 821-832.
58. Shi, X., et al., *Expression of the NLRP3 inflammasome in carotid atherosclerosis.* Journal of Stroke and Cerebrovascular Diseases, 2015. **24**(11): p. 2455-2466.
59. Whitman, S.C., P. Ravisankar, and A. Daugherty, *Interleukin-18 enhances atherosclerosis in apolipoprotein E−/− mice through release of interferon-γ.* Circulation research, 2002. **90**(2): p. e34-e38.
60. Merhi-Soussi, F., et al., *Interleukin-1 plays a major role in vascular inflammation and atherosclerosis in male apolipoprotein E-knockout mice.* Cardiovascular research, 2005. **66**(3): p. 583-593.
61. Galea, J., et al., *Interleukin-1β in coronary arteries of patients with ischemic heart disease.* Arteriosclerosis, thrombosis, and vascular biology, 1996. **16**(8): p. 1000-1006.
62. Mallat, Z., et al., *Expression of interleukin-18 in human atherosclerotic plaques and relation to plaque instability.* Circulation, 2001. **104**(14): p. 1598-1603.
63. Elhage, R., et al., *Reduced atherosclerosis in interleukin-18 deficient apolipoprotein E-knockout mice.* Cardiovascular research, 2003. **59**(1): p. 234-240.
64. Dinarello, C.A., *Interleukin-1 in the pathogenesis and treatment of inflammatory diseases.* Blood, The Journal of the American Society of Hematology, 2011. **117**(14): p. 3720-3732.

65. Libby, P., *Interleukin-1 beta as a target for atherosclerosis therapy: biological basis of CANTOS and beyond.* Journal of the American College of Cardiology, 2017. **70**(18): p. 2278-2289.
66. Jin, Y. and J. Fu, *Novel Insights Into the NLRP 3 Inflammasome in Atherosclerosis.* Journal of the American Heart Association, 2019. **8**(12): p. e012219.
67. Li, X., et al., *Activation of Nlrp3 inflammasomes enhances macrophage lipid-deposition and migration: implication of a novel role of inflammasome in atherogenesis.* PloS one, 2014. **9**(1).
68. Yüksel, Ş., L. Ayvazyan, and A.Y. Gasparyan, *Familial Mediterranean fever as an emerging clinical model of atherogenesis associated with low-grade inflammation.* The open cardiovascular medicine journal, 2010. **4**: p. 51.
69. Crittenden, D.B., et al., *Colchicine use is associated with decreased prevalence of myocardial infarction in patients with gout.* The Journal of rheumatology, 2012. **39**(7): p. 1458-1464.
70. Langevitz, P., et al., *Prevalence of ischemic heart disease in patients with familial Mediterranean fever.* The Israel Medical Association journal: IMAJ, 2001. **3**(1): p. 9-12.
71. Yang, L.P., *Oral colchicine (Colcrys [R]) in the treatment and prophylaxis of gouty: profile report.* Drugs & aging, 2010. **27**(10): p. 855-858.
72. Terkeltaub, R.A., et al., *High versus low dosing of oral colchicine for early acute gout flare: twenty-four–hour outcome of the first multicenter, randomized, double-blind, placebo-controlled, parallel-group, dose-comparison colchicine study.* Arthritis & Rheumatism, 2010. **62**(4): p. 1060-1068.
73. Nidorf, M. and P.L. Thompson, *Effect of colchicine (0.5 mg twice daily) on high-sensitivity C-reactive protein independent of aspirin and atorvastatin in patients with stable coronary artery disease.* The American journal of cardiology, 2007. **99**(6): p. 805-807.
74. Jordan, K.M., et al., *British Society for Rheumatology and British Health Professionals in Rheumatology guideline for the management of gout.* Rheumatology, 2007. **46**(8): p. 1372-1374.
75. Hentgen, V., et al. *Evidence-based recommendations for the practical management of Familial Mediterranean Fever*. in *Seminars in arthritis and rheumatism*. 2013. Elsevier.
76. Nidorf, S.M., et al., *Low-dose colchicine for secondary prevention of cardiovascular disease.* Journal of the American College of Cardiology, 2013. **61**(4): p. 404-410.
77. Naruko, T., et al., *Neutrophil infiltration of culprit lesions in acute coronary syndromes.* Circulation, 2002. **106**(23): p. 2894-2900.
78. Nidorf, S.M., et al., *The effect of low-dose colchicine in patients with stable coronary artery disease: The LoDoCo2 trial rationale, design, and baseline characteristics.* American heart journal, 2019. **218**: p. 46-56.
79. Demidowich, A.P., et al., *Effects of colchicine in adults with metabolic syndrome: A pilot randomized controlled trial.* Diabetes, Obesity and Metabolism, 2019. **21**(7): p. 1642-1651.
80. Imazio, M., et al., *Colchicine for prevention of postpericardiotomy syndrome and postoperative atrial fibrillation: the COPPS-2 randomized clinical trial.* Jama, 2014. **312**(10): p. 1016-1023.
81. Hennessy, T., et al., *The Low Dose Colchicine after Myocardial Infarction (LoDoCo-MI) study: A pilot randomized placebo controlled trial of colchicine following acute myocardial infarction.* American heart journal, 2019. **215**: p. 62-69.
82. Ridker, P.M., *From C-reactive protein to interleukin-6 to interleukin-1: moving upstream to identify novel targets for atheroprotection.* Circulation research, 2016. **118**(1): p. 145-156.
83. Tardif, J.-C., et al., *Efficacy and safety of low-dose colchicine after myocardial infarction.* New England Journal of Medicine, 2019. **381**(26): p. 2497-2505.
84. *Colchicine for Prevention of Vascular Inflammation in Non-cardio Embolic Stroke (CONVINCE)*. Available from: https://www.clinicaltrials.gov/ct2/show/NCT02898610.

85. *Colchicine and Spironolactone in Patients With STEMI/SYNERGY Stent Registry (CLEAR-SYNERGY)*. Available from: https://clinicaltrials.gov/ct2/show/NCT03048825?term=CLEAR-SYNERGY&draw=2&rank=2
86. Galkina, E. and K. Ley, *Immune and inflammatory mechanisms of atherosclerosis.* Annual review of immunology, 2009. **27**.
87. Gimbrone Jr, M.A. and G. García-Cardeña, *Endothelial cell dysfunction and the pathobiology of atherosclerosis.* Circulation research, 2016. **118**(4): p. 620-636.
88. *Inflammation and Coronary Endothelial Function*. Available from: https://clinicaltrials.gov/ct2/show/NCT02366091.
89. *Treatment of Patients With Atherosclerotic Disease With Methotrexate-associated to LDL Like Nanoparticles*. Available from: https://clinicaltrials.gov/ct2/show/NCT04616872.
90. Di Francesco, V., et al., *Modulating lipoprotein transcellular transport and atherosclerotic plaque formation in apoe-/-mice via nanoformulated lipid-methotrexate conjugates.* ACS Applied Materials & Interfaces, 2020.
91. Zoghebi, K.A., et al., *Design and Biological Evaluation of Colchicine-CD44-Targeted Peptide Conjugate in an In Vitro Model of Crystal Induced Inflammation.* Molecules, 2020. **25**(1): p. 46.
92. Chen, Y., et al., *An injectable thermosensitive hydrogel loaded with an ancient natural drug colchicine for myocardial repair after infarction.* Journal of Materials Chemistry B, 2020.
93. Purcell, W.T. and D.S. Ettinger, *Novel antifolate drugs.* Current Oncology Reports, 2003. **5**(2): p. 114-125.
94. Abolmaali, S.S., A.M. Tamaddon, and R. Dinarvand, *A review of therapeutic challenges and achievements of methotrexate delivery systems for treatment of cancer and rheumatoid arthritis.* Cancer chemotherapy and pharmacology, 2013. **71**(5): p. 1115-1130.
95. Kasim, N.A., et al., *Molecular Properties of WHO Essential Drugs and Provisional Biopharmaceutical Classification.* Molecular Pharmaceutics, 2004. **1**(1): p. 85-96.
96. Bedoui, Y., et al., *Methotrexate an old drug with new tricks.* International Journal of Molecular Sciences, 2019. **20**(20): p. 5023.
97. Genestier, L., et al., *Mechanisms of action of methotrexate.* Immunopharmacology, 2000. **47**(2-3): p. 247.
98. Oh, J.-M., et al., *Efficient delivery of anticancer drug MTX through MTX-LDH nanohybrid system.* Journal of Physics and Chemistry of Solids, 2006. **67**(5): p. 1024-1027.
99. Bailey, L.B. and J.F. Gregory, 3rd, *Folate metabolism and requirements.* J Nutr, 1999. **129**(4): p. 779-82.
100. van Roon, E.N. and M.A. van de Laar, *Methotrexate bioavailability.* Clin Exp Rheumatol, 2010. **28**(5 Suppl 61): p. S27-32.
101. Li, Y., et al., *Self-assembly of multifunctional integrated nanoparticles loaded with a methotrexate–phospholipid complex: combining simplicity and efficacy in both targeting and anticancer effects.* RSC advances, 2016. **6**(89): p. 86717-86727.
102. Chan, E.S. and B.N. Cronstein, *Methotrexate—how does it really work?* Nature Reviews Rheumatology, 2010. **6**(3): p. 175-178.
103. Iqbal, M.P., *Accumulation of methotrexate in human tissues following high-dose methotrexate therapy.* 1998.
104. Conway, R. and J.J. Carey, *Risk of liver disease in methotrexate treated patients.* World journal of hepatology, 2017. **9**(26): p. 1092.
105. Prey, S. and C. Paul, *Effect of folic or folinic acid supplementation on methotrexate-associated safety and efficacy in inflammatory disease: a systematic review.* British Journal of Dermatology, 2009. **160**(3): p. 622-628.
106. Romao, V.C., et al., *Three decades of low-dose methotrexate in rheumatoid arthritis: can we predict toxicity?* Immunologic research, 2014. **60**(2-3): p. 289-310.

107. Schnabel, A. and W.L. Gross. *Low-dose methotrexate in rheumatic diseases—efficacy, side effects, and risk factors for side effects*. in *Seminars in arthritis and rheumatism*. 1994. Elsevier.
108. Karasulu, H.Y., et al., *Controlled Release of Methotrexate from W/O Microemulsion and Its In Vitro Antitumor Activity.* Drug Delivery, 2007. **14**(4): p. 225-233.
109. Li, M.-H., et al., *Dendrimer-based multivalent methotrexates as dual acting nanoconjugates for cancer cell targeting.* European journal of medicinal chemistry, 2012. **47**(1): p. 560-572.
110. Nogueira, D.R., et al., *In vitro antitumor activity of methotrexate via pH-sensitive chitosan nanoparticles.* Biomaterials, 2013. **34**(11): p. 2758-72.
111. Sartori, T., et al., *Development and validation of a fast RP-HPLC method for determination of methotrexate entrapment efficiency in polymeric nanocapsules.* J Chromatogr Sci, 2008. **46**(6): p. 505-9.
112. Zhang, Y., T. Jin, and R.X. Zhuo, *Methotrexate-loaded biodegradable polymeric micelles: preparation, physicochemical properties and in vitro drug release.* Colloids Surf B Biointerfaces, 2005. **44**(2-3): p. 104-9.
113. Curcio, M., et al., *Facile synthesis of pH-responsive polymersomes based on lipidized PEG for intracellular co-delivery of curcumin and methotrexate.* Colloids and Surfaces B: Biointerfaces, 2018. **167**: p. 568-576.
114. Guimarães, D., et al., *Increased Encapsulation Efficiency of Methotrexate in Liposomes for Rheumatoid Arthritis Therapy.* Biomedicines, 2020. **8**(12): p. 630.
115. Celia, C., et al., *Nanoliposomes as Multidrug Carrier of Gemcitabine/Paclitaxel for the Effective Treatment of Metastatic Breast Cancer Disease: A Comparison with Gemzar and Taxol.* Advanced Therapeutics: p. 2000121.
116. Popa, M. and C.V. Uglea, *Polymeric Nanomedicines*. 2013: Bentham Science Publishers.
117. Sercombe, L., et al., *Advances and challenges of liposome assisted drug delivery.* Frontiers in pharmacology, 2015. **6**: p. 286.
118. Lamichhane, N., et al., *Liposomes: clinical applications and potential for image-guided drug delivery.* Molecules, 2018. **23**(2): p. 288.
119. Ferreira, M., et al., *Optimizing the Pharmacological Properties of Discoidal Polymeric Nanoconstructs Against Triple Negative Breast Cancer Cells* Frontiers in Bioengineering and Biotechnology, 2020. **8**: p. 5.
120. Tetko, I.V., et al., *Estimation of Aqueous Solubility of Chemical Compounds Using E-State Indices.* Journal of Chemical Information and Computer Sciences, 2001. **41**(6): p. 1488-1493.
121. Tetko, I.V., V.Y. Tanchuk, and A.E. Villa, *Prediction of n-octanol/water partition coefficients from PHYSPROP database using artificial neural networks and E-state indices.* J Chem Inf Comput Sci, 2001. **41**(5): p. 1407-21.
122. ACDLabs. *Partition Coefficient Calculation with ACD/LogP*. 2021; Available from: https://www.acdlabs.com/products/percepta/predictors/logp/index.php.
123. De Rose, R.F., et al., *PDE5 inhibitors-loaded nanovesicles: Physico-chemical properties and in vitro antiproliferative activity.* Nanomaterials, 2016. **6**(5): p. 92.
124. dos Santos, A.M., et al., *Computational and experimental approaches for development of methotrexate nanosuspensions by bottom-up nanoprecipitation.* International Journal of Pharmaceutics, 2017. **524**(1-2): p. 330-338.
125. Palanikumar, L., et al., *pH-responsive high stability polymeric nanoparticles for targeted delivery of anticancer therapeutics.* Communications biology, 2020. **3**(1): p. 1-17.
126. Aigner, T. and S. Söder, *Histopathological examination of joint degeneration: typing, grading and staging of osteoarthritis.* Der Pathologe, 2006. **27**(6): p. 431-438.
127. Rajamäki, K., et al., *Extracellular acidosis is a novel danger signal alerting innate immunity via the NLRP3 inflammasome.* Journal of Biological Chemistry, 2013. **288**(19): p. 13410-13419.

128. Di Francesco, M., et al., *Doxorubicin Hydrochloride-Loaded Nonionic Surfactant Vesicles to Treat Metastatic and Non-Metastatic Breast Cancer.* ACS Omega, 2021.
129. Mircioiu, C., et al., *Mathematical modeling of release kinetics from supramolecular drug delivery systems.* Pharmaceutics, 2019. **11**(3): p. 140.
130. Rigter, P. and N. Peppas, *A simple equation for description of solute relase I. Fickian and non-fickian release from non-swellable devices in the form of slabs, spherer, cylinders or discs.* J. Control. Release, 1987. **5**: p. 23-36.
131. Mohan, A., et al., *Novel resveratrol and 5-fluorouracil coencapsulated in PEGylated nanoliposomes improve chemotherapeutic efficacy of combination against head and neck squamous cell carcinoma.* BioMed research international, 2014. **2014**.
132. Er, Y., et al., *The encapsulation and release of guanosine from PEGylated liposomes.* Journal of liposome research, 2009. **19**(1): p. 29-36.
133. Jain, A. and S.K. Jain, *In vitro release kinetics model fitting of liposomes: An insight.* Chemistry and physics of lipids, 2016. **201**: p. 28-40.
134. Prakash, J.D., et al., *Formulation and In vitro Characterization of Ketoconazole Liposomal Gel for Transdermal Delivery.* Research Journal of Pharmacy and Technology, 2017. **10**(1): p. 205-215.
135. Tiwari, G., et al., *Development and Optimization of Liposomes Containing 5 Fluorouracil and Tretinoin for Skin Warts: 32 Experimental Design.* FABAD Journal of Pharmaceutical Sciences, 2019. **44**(1): p. 17-26.
136. Wei, Y., et al., *Preparation, pharmacokinetics and biodistribution of baicalin-loaded liposomes.* International journal of nanomedicine, 2014. **9**: p. 3623.
137. Zhang, T., et al., *Curcumin-and Cyclopamine-Loaded Liposomes to Enhance Therapeutic Efficacy Against Hepatic Fibrosis.* Drug Design, Development and Therapy, 2020. **14**: p. 5667.
138. Jeong, C., et al., *Self-Assembled Supramolecular Bilayer Nanoparticles Composed of Near-Infrared Dye as a Theranostic Nanoplatform To Encapsulate Hydrophilic Drugs Effectively.* ACS Biomaterials Science & Engineering, 2019. **6**(1): p. 474-484.
139. Cadinoiu, A.N., et al., *Aptamer-functionalized liposomes as a potential treatment for basal cell carcinoma.* Polymers, 2019. **11**(9): p. 1515.
140. Libby, P. and G.K. Hansson, *Taming Immune and Inflammatory Responses to Treat Atherosclerosis*. 2018, Journal of the American College of Cardiology.
141. Kim, Y., et al., *Probing Nanoparticle Translocation Across the Permeable Endothelium in Experimental Atherosclerosis.* Proceedings of the National Academy of Sciences, 2014. **111**(3): p. 1078-1083.
142. Moore, K.J. and I. Tabas, *Macrophages in the Pathogenesis of Atherosclerosis.* Cell, 2011. **145**(3): p. 341-355.
143. Welsh, P., et al., *Targeting Inflammation to Reduce Cardiovascular Disease Risk: a Realistic Clinical Prospect?* British journal of pharmacology, 2017. **174**(22): p. 3898-3913.
144. Ridker, P.M., et al., *Antiinflammatory Therapy with Canakinumab for Atherosclerotic Disease.* New England journal of medicine, 2017. **377**(12): p. 1119-1131.
145. Weber, C. and H. Noels, *Atherosclerosis: Current Pathogenesis and Therapeutic Options.* Nature medicine, 2011. **17**(11): p. 1410.
146. Cronstein, B.N., D. Naime, and E. Ostad, *The Antiinflammatory Mechanism of Methotrexate. Increased Adenosine Release at Inflamed Sites Diminishes Leukocyte Accumulation in an in Vivo Model of Inflammation.* The Journal of clinical investigation, 1993. **92**(6): p. 2675-2682.
147. Bălănescu, A.R., et al., *Cardiovascular Effects of Methotrexate in Immune-Mediated Inflammatory Diseases.* Experimental and Therapeutic Medicine, 2019. **17**(2): p. 1024-1029.
148. Kivity, S., et al., *Clinical Characteristics and Risk Factors for Low Dose Methotrexate Toxicity: a Cohort of 28 Patients.* Autoimmunity reviews, 2014. **13**(11): p. 1109-1113.

149. Chen, M., et al., *Folate Receptor-Targeting and Reactive Oxygen Species-Responsive Liposomal Formulation of Methotrexate for Treatment of Rheumatoid Arthritis.* Pharmaceutics, 2019. **11**(11): p. 582.
150. Alekseeva, A.A., et al., *Liposomal formulation of a methotrexate lipophilic prodrug: assessment in tumor cells and mouse T-cell leukemic lymphoma.* The International Journal of Nanomedicine, 2017. **12**: p. 3735.
151. Bulgarelli, A., et al., *Anti-Atherogenic Effects of Methotrexate Carried by a Lipid Nanoemulsion that Binds to LDL Receptors in Cholesterol-Fed Rabbits.* Cardiovascular drugs and therapy, 2013. **27**(6): p. 531-539.
152. Robbins, C.S., et al., *Local Proliferation Dominates Lesional Macrophage Accumulation in Atherosclerosis.* Nature medicine, 2013. **19**(9): p. 1166.
153. Beldman, T.J., et al., *Hyaluronan Nanoparticles Selectively Target Plaque-Associated Macrophages and Improve Plaque Stability in Atherosclerosis.* ACS nano, 2017. **11**(6): p. 5785-5799.
154. Zhang, L., et al., *Promoting the Delivery of Nanoparticles to Atherosclerotic Plaques by DNA Coating.* ACS applied materials & interfaces, 2018. **11**(15): p. 13888-13904.
155. Davies, P.F., *Hemodynamic Shear Stress and the Endothelium in Cardiovascular Pathophysiology.* Nature Reviews Cardiology, 2009. **6**(1): p. 16.
156. Taylor, C.A., T.J. Hughes, and C.K. Zarins, *Finite Element Modeling of Three-Dimensional Pulsatile Flow in the Abdominal Aorta: Relevance to Atherosclerosis.* Annals of biomedical engineering, 1998. **26**(6): p. 975-987.
157. Hossain, S.S., T.J. Hughes, and P. Decuzzi, *Vascular Deposition Patterns for Nanoparticles in an Inflamed Patient-Specific Arterial Tree.* Biomechanics and modeling in mechanobiology, 2014. **13**(3): p. 585-597.
158. Charoenphol, P., et al., *Targeting Therapeutics to the Vascular Wall in Atherosclerosis–Carrier Size Matters.* Atherosclerosis, 2011. **217**(2): p. 364-370.
159. Beldman, T.J., et al., *Nanoparticle-Aided Characterization of Arterial Endothelial Architecture during Atherosclerosis Progression and Metabolic Therapy.* ACS nano, 2019. **13**(12): p. 13759-13774.
160. Wei, X., et al., *Nanoparticle Functionalization with Platelet Membrane Enables Multifactored Biological Targeting and Detection of Atherosclerosis.* Acs Nano, 2018. **12**(1): p. 109-116.
161. Kheirolomoom, A., et al., *Multifunctional Nanoparticles Facilitate Molecular Targeting And miRNA Delivery to Inhibit Atherosclerosis in ApoE–/–Mice.* ACS nano, 2015. **9**(9): p. 8885-8897.
162. Ye, M., et al., *SR-A-Targeted Phase-Transition Nanoparticles for the Detection and Treatment of Atherosclerotic Vulnerable Plaques.* ACS applied materials & interfaces, 2019. **11**(10): p. 9702-9715.
163. Liu, Y., et al., *Assessment of Targeted Nanoparticle Assemblies for Atherosclerosis Imaging with Positron Emission Tomography and Potential for Clinical Translation.* ACS applied materials & interfaces, 2019. **11**(17): p. 15316-15321.
164. Nahrendorf, M., et al., *Nanoparticle PET-CT Imaging of Macrophages in Inflammatory Atherosclerosis.* Circulation, 2008. **117**(3): p. 379.
165. Flores, A.M., et al., *Pro-Efferocytic Nanoparticles are Specifically Taken Up by Lesional Macrophages and Prevent Atherosclerosis.* Nature Nanotechnology, 2020: p. 1-8.
166. Lee, A., et al., *Dexamethasone-Loaded Polymeric Nanoconstructs for Monitoring and Treating Inflammatory Bowel Disease.* Theranostics, 2017. **7**(15): p. 3653.
167. Di Francesco, M., et al., *Physicochemical Characterization of pH-Responsive and Fusogenic Self-Assembled Non-Phospholipid Vesicles for a Potential Multiple Targeting Therapy.* International journal of pharmaceutics, 2017. **528**(1-2): p. 18-32.
168. Shen, C.-M., et al., *Stimulation of Smooth Muscle Cell Proliferation by ox-LDL-and Acetyl LDL-Induced Macrophage-Derived Foam Cells.* Life sciences, 2001. **70**(4): p. 443-452.

169. Xu, S., et al., *Evaluation of Foam Cell Formation in Cultured Macrophages: an Improved Method with Oil Red O Staining and DiI-oxLDL Uptake.* Cytotechnology, 2010. **62**(5): p. 473-481.
170. Yan, P., et al., *Biological Characteristics of Foam Cell Formation in Smooth Muscle Cells Derived From Bone Marrow Stem Cells.* International journal of biological sciences, 2011. **7**(7): p. 937.
171. MacRitchie, N., et al., *Plasmacytoid Dendritic Cells Play a Key Role in Promoting Atherosclerosis in Apolipoprotein E–Deficient Mice.* Arteriosclerosis, thrombosis, and vascular biology, 2012. **32**(11): p. 2569-2579.
172. MacRitchie, N., et al., *The Aorta Can Act as Site of Naïve CD4+ T Cell Priming.* Cardiovascular research, 2019.
173. Moshikur, R.M., et al., *Ionic Liquids with Methotrexate Moieties as a Potential Anticancer Prodrug: Synthesis, Characterization and Solubility Evaluation.* Journal of Molecular Liquids, 2019. **278**: p. 226-233.
174. Tishler, M., et al., *Synovial and Serum Levels of Methotrexate During Methotrexate Therapy of Rheumatoid Arthritis.* Rheumatology, 1989. **28**(5): p. 422-423.
175. Lee, A., et al., *Spherical Polymeric Nanoconstructs for Combined Chemotherapeutic and Anti-Inflammatory Therapies.* Nanomedicine: Nanotechnology, Biology and Medicine, 2016. **12**(7): p. 2139-2147.
176. Santarella-Mellwig, R., et al., *Correlative Light Electron Microscopy (CLEM) for Tracking and Imaging Viral Protein Associated Structures in Cryo-immobilized Cells.* JoVE (Journal of Visualized Experiments), 2018(139): p. e58154.
177. Pulanco, M.C., et al., *Complement Protein C1q Enhances Macrophage Foam Cell Survival and Efferocytosis.* The Journal of Immunology, 2017. **198**(1): p. 472-480.
178. Yokode, M., et al., *Stimulated Arachidonate Metabolism During Foam Cell Transformation of Mouse Peritoneal Macrophages with Oxidized Low Density Lipoprotein.* The Journal of clinical investigation, 1988. **81**(3): p. 720-729.
179. Lu, S.M. and G.D. Fairn, *7-Ketocholesterol Impairs Phagocytosis and Efferocytosis Via Dysregulation of Phosphatidylinositol 4, 5-Bisphosphate.* Traffic, 2018. **19**(8): p. 591-604.
180. Reiss, A.B., et al., *Atheroprotective Effects of Methotrexate on Reverse Cholesterol Transport Proteins and Foam Cell Transformation in Human THP-1 Monocyte/Macrophages.* Arthritis & Rheumatism: Official Journal of the American College of Rheumatology, 2008. **58**(12): p. 3675-3683.
181. Nicholson, A.C. and D.P. Hajjar, *CD36, Oxidized LDL and PPAR Gamma: Pathological Interactions in Macrophages and Atherosclerosis.* Vascular Pharmacology, 2004. **41**(4-5): p. 139.
182. Conniot, J., et al., *Immunization with Mannosylated Nanovaccines and Inhibition of the Immune-Suppressing Microenvironment Sensitizes Melanoma to Immune Checkpoint Modulators.* Nature nanotechnology, 2019. **14**(9): p. 891-901.
183. Alaarg, A., et al., *A Systematic Comparison of Clinically Viable Nanomedicines Targeting HMG-CoA Reductase in Inflammatory Atherosclerosis.* J Control Release, 2017. **262**: p. 47-57.
184. Beldman, T.J., et al., *Hyaluronan Nanoparticles Selectively Target Plaque-Associated Macrophages and Improve Plaque Stability in Atherosclerosis.* ACS Nano, 2017. **11**(6): p. 5785-5799.
185. Tang, J., et al., *Immune Cell Screening of a Nanoparticle Library Improves Atherosclerosis Therapy.* Proc Natl Acad Sci U S A, 2016. **113**(44): p. E6731-E6740.
186. Han, J., et al., *Native and Modified Low Density Lipoproteins Increase the Functional Expression of the Macrophage Class B Scavenger Receptor, CD36.* Journal of Biological Chemistry, 1997. **272**(34): p. 21654-21659.
187. Volobueva, A., et al., *Foam Cell Formation and Cholesterol Trafficking and Metabolism Disturbances in Atherosclerosis.* Cor et Vasa, 2018.

188. Chen, D.-Y., et al., *Blood Lipid Profiles and Peripheral Blood Mononuclear Cell Cholesterol Metabolism Gene Expression in Patients With and Without Methotrexate Treatment.* BMC medicine, 2011. **9**(1): p. 4.
189. Nguyen, M.T., et al., *Inflammation as a therapeutic target in atherosclerosis.* Journal of clinical medicine, 2019. **8**(8): p. 1109.
190. Spagnoli, L.G., et al., *Role of inflammation in atherosclerosis.* Journal of nuclear medicine, 2007. **48**(11): p. 1800-1815.
191. Hansson, G.K., *Inflammation, atherosclerosis, and coronary artery disease.* New England Journal of Medicine, 2005. **352**(16): p. 1685-1695.
192. van der Wal, A.C., et al., *Site of intimal rupture or erosion of thrombosed coronary atherosclerotic plaques is characterized by an inflammatory process irrespective of the dominant plaque morphology.* Circulation, 1994. **89**(1): p. 36-44.
193. Malaviya, A.N., et al., *Low-dose and high-dose methotrexate are two different drugs in practical terms.* International journal of rheumatic diseases, 2010. **13**(4): p. 288-293.
194. Cutolo, M., et al., *Anti-inflammatory mechanisms of methotrexate in rheumatoid arthritis.* Annals of the rheumatic diseases, 2001. **60**(8): p. 729-735.
195. Martinon, F., et al., *Gout-associated uric acid crystals activate the NALP3 inflammasome.* Nature, 2006. **440**(7081): p. 237-241.
196. Leung, Y.Y., L.L.Y. Hui, and V.B. Kraus. *Colchicine—Update on mechanisms of action and therapeutic uses*. in *Seminars in arthritis and rheumatism*. 2015. Elsevier.
197. Ades, S., *Adjuvant chemotherapy for colon cancer in the elderly: moving from evidence to practice.* 2009.
198. Chen, Y., et al., *An injectable thermosensitive hydrogel loaded with an ancient natural drug colchicine for myocardial repair after infarction.* Journal of Materials Chemistry B, 2020. **8**(5): p. 980-992.
199. Singhvi, G. and M. Singh, *In-Vitro Drug Release Characterization Models.* Int J Pharm Stud Res, 2011. **2**(1): p. 77-84.
200. Abu-Fanne, R., et al., *α-Defensins induce a post-translational modification of low density lipoprotein (LDL) that promotes atherosclerosis at normal levels of plasma cholesterol.* Journal of Biological Chemistry, 2016. **291**(6): p. 2777-2786.
201. Yang, M., et al., *Colchicine alleviates cholesterol crystal-induced endothelial cell pyroptosis through activating AMPK/SIRT1 pathway.* Oxidative medicine and cellular longevity, 2020. **2020**.
202. Folkman, J. and A. Moscona, *Role of cell shape in growth control.* Nature, 1978. **273**(5661): p. 345-349.
203. Singh, R., et al., *Quantitative assessment of morphology and sub-cellular changes in macrophages and trophoblasts during inflammation.* Biomedical Optics Express, 2020. **11**(7): p. 3733-3752.
204. Kasim, N.A., et al., *Molecular properties of WHO essential drugs and provisional biopharmaceutical classification.* Molecular pharmaceutics, 2004. **1**(1): p. 85-96.